Role of Mitochondrial Dynamics and Cell Death in a Dihydrotestosterone-induced Rat Model of Polycystic Ovarian Syndrome, and its Regulation by Gonadotropin

Hannah Mazier

A thesis submitted to the
Faculty of Graduate and Postdoctoral Studies
in partial fulfillment of the requirements for the
MSc degree in Cellular and Molecular Medicine

Department of Cellular and Molecular Medicine
Faculty of Medicine
University of Ottawa

CONTRIBUTION OF COLLABORATORS

All studies were carried out under the supervision of Dr. Benjamin Tsang. All experimental work was conducted by Ms. Hannah Mazier except those noted below.

Figure 3.2: DHT-induced ovarian structural abnormalities were modulated by gonadotropin. Dr. Patricia Lima (a postdoctoral fellow in Dr. Tsang's laboratory) completed the majority of the slide preparations, performed H&E staining and obtained/arranged the image composition of the whole ovary.

Figure 3.3: DHT suppressed granulosa cell apoptosis, which was attenuated by gonadotropin. Dr. Patricia Lima completed the majority of the slide preparations, and Dr. Reza Salehi (a postdoctoral fellow in Dr. Tsang's laboratory) performed TUNEL assay and obtained the images using immunofluorescence microscopy.

Figure 3.4: DHT-induced circular and constricted mitochondrial appearance were reduced by gonadotropin. Dr. Arkadiy Reunov (University of Ottawa Heart Institute) was our collaborator for this study with transmission electron microscopy (TEM). Dr. Reunov fixed and prepared the ovaries for image capture via TEM, and evaluated mitochondrial morphology. Ms. Mazier arranged the data to perform statistical analysis.

Figure 3.16: Co-treatment of early antral granulosa cells with FSH and Chemerin did not alter LC3I/II or p62 autophagy markers. This experiment (excluding densitometric analysis) was performed by Ms. Arianna Fiocco, a visiting undergraduate summer student in Dr. Tsang's laboratory, under the direct supervision of Ms. Hannah Mazier.

ABSTRACT

Polycystic ovarian syndrome (PCOS) is a multi-factorial infertility disorder whose etiology and pathogenesis is not completely understood. Although there is an association between dysregulation of mitochondrial fission and fusion to cell death (apoptotic and autophagic) and the pathogenesis of various diseases, this had not been reported in the context of granulosa cell death, follicular growth arrest and PCOS. Follicle-stimulating hormone (FSH), a granulosa cell survival factor, is used during gonadotropin therapy to assist in follicular maturation and ovulation in women with PCOS. Whether FSH can modulate the possible dysregulation of granulosa cell mitochondrial dynamics and cell death in PCOS had not been elucidated. Chemerin is an adipokine that has been associated with PCOS and granulosa cell apoptosis in follicle cultures. Its role in cell death (apoptotic and autophagic) of primary granulosa cells had not been confirmed.

In this thesis, we investigated the dysregulation of granulosa cell mitochondrial dynamics in PCOS pathogenesis by using an androgenized rat model, and its modulation by exogenous gonadotropin. The mechanisms involved in gonadotropic regulation were investigated using primary granulosa cells. Our data suggest that increased mitochondrial fission leads to early antral granulosa cell death, follicular growth arrest and anovulation in women with PCOS. FSH can regulate the phosphorylation of mitochondrial fission protein Drp1, which may lead to its suppression of mitochondrial fission and apoptosis in PCOS. Finally, chemerin had no effect on cell death in granulosa cell cultures. These findings provide a greater understanding of the processes involved in PCOS pathogenesis and the regulatory role of FSH in granulosa cells, laying the foundation for future study into the development of potential biomarkers and new treatment strategies.

TABLE OF CONTENTS

LIST OF TABLES

LIST OF FIGURES

LIST OF ABBREVIATIONS

APAF1	Apoptotic Protease-Activating Factor 1
AMPK	5' AMP-activated protein Kinase
ANOVA	Analysis Of Variance
ASRM	American Society for Reproductive Medicine
Atg	Autophagy-related protein
ATP	Adenosine Triphosphate
AtyF	Atypical Follicle
BAD	Bcl-2-Associated Death promoter
Bak	Bcl-2 homologous antagonist/killer
Bax	Bcl-2-associated X protein
Bcl-2	B-cell lymphoma 2
BMI	Body Mass Index
BSA	Bovine Serum Albumin
Ca^{2+}	Calcium
CaMKIα	Calmodulin-dependent protein Kinase Iα
cAMP	cyclic Adenosine Monophosphate
CCRL2	Chemokine (C-C motif) Receptor Like 2
CDDP	Cisplatin
CDK1	Cyclin-Dependent Kinase 1
CL	Corpus Luteum
ClQ	Chloroquine
CMKLR1	Chemokine-Like Receptor 1

CO_2	Carbon Dioxide
CTL	Control
CYP17	Cytochrome P450c17
Cys	Cysteine
DAPI	4',6-Diamidino-2-Phenylindole
DHEA	Dehydroepiandrosterone
DHT	5α-Dihydrotestosterone
DMSO	Dimethyl Sulfoxide
DNA	Deoxyribonucleic Acid
Drp1	Dynamin-related protein 1
EAF	Early Antral Follicle
eCG	equine Chorionic Gonadotropin
ECL	Enhanced Chemiluminescence
EGTA	Ethylene Glycol-bis(β-aminoethyl ether)-N,N,N',N'-Tetraacetic Acid
EIA	Enzyme Immunoassay
EM	Electron Microscopy
ESHRE	European Society of Human Reproduction and Embryology
ER	Endoplasmic Reticulum
ERK	Extracellular signal-Regulated Kinase
EV	Estradiol Valerate
FasL	Fas Ligand
FBS	Fetal Bovine Serum
FC	Flow Cytometry

Fis1	Mitochondrial Fission 1
FM	Fluorescence microscopy
FSH	Follicle-stimulating hormone
FSHR	Follicle-stimulating hormone receptor
GAPDH	Glyceraldehyde-3-Phosphate Dehydrogenase
GDF-9	Growth Differentiation Factor-9
Gn	Gonadotropin
GPR-1	G-protein coupled receptor-1
GTP	Guanosine Triphosphate hydrolase
GWA	Genome-Wide Association
H&E	Hematoxylin and Eosin
HAEC	Human Aorta Endothelial Cell
hCG	human Chorionic Gonadotropin
HCl	Hydrochloric Acid
HEPES	4-(2-Hydroxyethyl)-1-Piperazineethanesulfonic acid
hsc70	heat shock protein 70
IB	Immunoblotting
IBMX	3-Isobutyl-1-Methylxanthine
IGF-1	Insulin-like Growth Factor-1
IHC	Immunohistochemistry
IL-6	Interleukin 6
IMM	Inner Mitochondrial Membrane
i.p.	intraperitoneal

IR	Isotope Release
IRGM	Immunity-related GTPase family M
KO	Knockout
LAF	Large Antral Follicle
LAMP1	Lysosomal-Associated Membrane Protein 1
LC3	microtubule-associated protein 1 Light Chain 3
LH	Luteinizing Hormone
LHCGR	Luteinizing Hormone/Choriogonadotropin receptor
LOX-1	Lectin-like Oxidized low-density lipoprotein receptor-1
M199	Medium 199
MAPK	Mitogen-Activated Protein Kinase
MAPL	Mitochondrial-Anchored Protein Ligase
MARCH5	Membrane-Associated Ring finger (C3HC4) 5
Mdivi-1	Mitochondrial division Inhibitor 1
Mff	Mitochondrial fission factor
Mfn1	Mitofusin-1
Mfn2	Mitofusin-2
$MgCl_2$	Magnesium Chloride
MiD49	Mitochondrial Dynamics protein of 49 kDa
MiD51	Mitochondrial Dynamics protein of 51 kDa
MOMP	Mitochondrial Outer Membrane Permeabilization
mTOR	mechanistic Target Of Rapamycin
MTT	Methylthiazolyldiphenyl-Tetrazolium bromide

NaCl	Sodium Chloride
NaN_3	Sodium Azide
NIH	National Institute of Health
O_2	Oxygen
Oma1	Overlapping activity with M-AAA protease 1
OMM	Outer Mitochondrial Membrane
Opa1	Optic atrophy 1
oxLDL	oxidated low-density lipoprotein
p450scc	p450 side-chain cleavage enzyme
PAF	Preantral Follicle
POvF	Preovulatory Follicle
PBS	Phosphate-Buffered Saline
PCO	Polycystic Ovaries
PCOS	Polycystic Ovarian Syndrome
PE	Phosphatidylethanolamine
PFA	Paraformaldehyde
PI3K	Phosphoinositide 3-Kinase
PINK1	PTEN-Induced putative Kinase 1
PKA	Protein Kinase A [cyclic AMP (cAMP)-dependent protein kinase]
POF	Premature Ovarian Failure
PS1	Presenilin 1
PtdIns3K	class III Phosphatidylinositol 3-Kinase
Raf1	Rapidly accelerated fibrosarcoma 1

RARRES2	Retinoic Acid Receptor Responder protein 2
Ras	Rat sarcoma
RBC	Red Blood Cell
ROS	Reactive oxidative species
RT	Room Temperature
SDS	Sodium Dodecyl Sulfate
SDS-PAGE	Sodium Dodecyl Sulfate Polyacrylamide Gel Electrophoresis
SEM	Standard Error of the Mean
Ser	Serine
SQSTM1	Sequestosome 1
T2DM	Type II Diabetes Mellitus
TBST	Tris-Buffered Saline plus Tween-20
TEM	Transmission electron microscopy
TIG2	Tazarotene-Induced Gene 2 protein
TNF-α	Tumour necrosis factor-α
TNFR1	Tumour necrosis factor receptor 1
TOM20	Translocase of Outer Membrane 20
TP	Testosterone Propionate
TUNEL	Terminal deoxynucleotidyl transferase dUTP Nick End Labeling
ULK1	Unc-51 Like autophagy activating Kinase 1
XIAP	X-linked Inhibitor of Apoptosis

ACKNOWLEDGEMENTS

I would first like to give special thanks to Dr. Benjamin Tsang for his patience and support throughout my training program. I am grateful for his mentorship, which has led me to become more confident in my abilities (both professionally and personally), improve my critical thinking skills and prepare for the next step in my professional life.

I would like to thank past and current members of the Tsang lab for their encouragement and assistance throughout my program. I am thankful and proud to be associated with this lab group, as their hard work has inspired me to become a better researcher. Special thanks are given to Drs. Qi Wang and Patricia Lima for their mentorship and friendshsip. I would also like to thank Drs. Arkadiy Reunov (University of Ottawa Heart Institute) and Ciro Isidoro (University of Eastern Piedmont Amedeo Avogadro). Their collaborations and advice have led me to achieve my research goals.

Thanks are given to past and present members of my thesis advisory committee, Drs. Barbara Vanderhyden, Shannon Bainbridge, and Andree Gruslin. Their support and advice has provided me with different perspectives on how to approach a problem.

Thanks are given to the University of Ottawa, CIHR-IHDCYH Training Program in Reproduction, Early Development and the Impact of Health (CIHR-REDIH), and the Queen Elizabeth II Graduate Scholarship for Science and Technology (provided by the Ontario government) for funding support during my training.

I would like to thank my friends, family, and my parents Dan and Leigh Mazier. Their love and lifelong support have allowed me many opportunities, and for that I will always be grateful. I dedicate this thesis to Cameron Wagner. His love, encouragement and patience have led me to this point, and I am thankful to have him in my life.

CHAPTER 1: INTRODUCTION

1.1 Ovarian Function and Folliculogenesis

1.1.1 The Ovary

The ovary is the female reproductive organ responsible for the production, maturation and release of female gametes. The functional unit of the ovary is the follicle, which consists of the oocyte, the surrounding granulosa cells and the outermost theca cell layer (Richards and Pangas, 2010; McGee and Hsueh, 2000). These three cell types are involved in an interactive cross-talk of regulatory factors to allow for the growth and maturation of the oocyte, starting from primordial stage through primary, secondary, preantral and antral stages, where dominant follicle selection occurs (Orisaka *et al*., 2009). Very few follicles survive atresia during this time to continue development through the preovulatory stage and eventually gonadotropin-induced ovulation (McGee and Hsueh, 2000). During ovulation, the oocyte is released from the ovary into the uterine tube in preparation for fertilization.

1.1.2 Follicular Development and Growth

Folliculogenesis is the term coined for the development, maturation and growth of the ovarian follicle from primordial to preovulatory stages. During human prenatal development at the start of human folliculogenesis, primordial follicles are formed containing an oocyte, basal lamina layer and pre-granulosa cells. These primordial follicles remain quiescent until initial recruitment after the onset of menstruation (McGee and Hsueh, 2000; Baerwald *et al*., 2012). A cohort of recruited follicles develop from primordial to primary follicular stage, which is characterized by granulosa cell

differentiation from flat to cuboidal structure in a single cell layer and zona pellucida formation, which separates the oocyte and the granulosa cells. Theca cells differentiate into theca interna and theca externa layers surrounding the basal lamina, the oocyte increases in size, and granulosa cells continue to proliferate at the secondary and preantral follicular stages. At the antral stage, the formation of the fluid-filled antrum and the proliferation of granulosa cells and theca interna cells increase follicular growth rate. It is here where cyclic recruitment takes place, and only the largest, healthiest dominant follicle will be selected to continue development. By the preovulatory stage, the antrum is fully formed and the granulosa cells are described as either cumulus granulosa cells surrounding the oocyte or mural granulosa cells surrounding the antrum (Richards and Pangas, 2010). A luteinizing hormone (LH) surge induces ovulation of the fully mature dominant follicle, and the oocyte is released into the uterine tube. The remnants of the follicle become luteinized and develop into the corpus luteum.

1.1.3 Follicular Atresia and Apoptosis

During human folliculogenesis, only the dominant follicle in a cohort of approximately 1000 is destined to ovulate during a typical menstrual cycle, while the remaining non-dominant follicles undergo atresia via granulosa cell apoptosis and follicle degeneration (Hussein, 2005). Apoptosis is a form of programmed cell death necessary for the purposes of quality control and self-sacrifice, with damaged or unwanted cells removed to maintain normal function in a system. In the case of follicular atresia, degenerated oocytes exhibit cytoplasmic blebbing, cell shrinkage and DNA fragmentation as seen in apoptosis. A retraction of granulosa cells and microvilli, nuclear

condensation, and granulosa cell apoptosis followed by oocyte segmentation and cytoplasmic vacuolization is also observed (Devine *et al*., 2000; Hussein, 2005).

The mechanisms of granulosa cell apoptosis involve both extrinsic and intrinsic death pathways. Activation of the extrinsic death receptor-mediated pathway is initiated by the binding of the death ligands such as tumour necrosis factor alpha (TNF-α) and Fas ligand (FasL) to their death receptors TNFR1 and Fas, respectively. This leads to stimulation of death domains and downstream activation of a cascade of caspases and the induction of apoptosis (Hussein, 2005; Hussein, 2003). Atretic follicles have upregulated FasL and Fas contents compared to dominant follicles (Porter *et* al, 2001; Lin and Rui, 2010). The intrinsic, mitochondria-mediated death pathway is initiated by death signals stimulating the pro-apoptotic protein family Bcl-2 (e.g. BAD, Bax) on the mitochondrial membrane for the release of death proteins (e.g. cytochrome C, APAF1), which binds to and activates pro-caspase-9 to activate caspase-3 and granulosa cell apoptosis (Hussein, 2005; Jiang *et al.,* 2003). A second intrinsic pathway involving the endoplasmic reticulum (ER) also regulates apoptosis through stress-induced disruption of calcium homeostasis, resulting in a release of Ca^{2+} ions from the ER which signal calpains to activate the caspase cascade, and sensitize mitochondria to the Bcl-2 protein family by increasing mitochondrial permeability (Breckenridge *et al*., 2003; Rizzuto *et al*., 2003). This pathway has also been associated with granulosa cell apoptosis during follicular atresia (Lin *et al*., 2012).

1.1.4 Gonadotropic Regulation of Ovarian Cell Fate

Ovarian follicle development in mammals is a tightly regulated process dictated by

cytokines, growth factors and gonadotropins (Craig *et al.,* 2007, Orisaka *et al*., 2009). Gonadotropins are glycoprotein polypeptide hormones produced in the anterior pituitary gland and include follicle-stimulating hormone (FSH) and LH (Pierce and Parsons, 1981). The exception is human chorionic gonadotropin (hCG), which is produced in the placenta during pregnancy and by trophoblast cells during embryogenesis (Cole, 2009; Gallego *et al*., 2010). By binding to their transmembrane G-protein coupled receptors FSHR and LHCGR respectively, FSH acts as a main regulator for follicular cell differentiation and follicle maturation and the LH surge initiates follicular rupture, ovulation and luteinization (Sprengel *et al.*, 1990).

A key aspect of gonadotropic regulation in folliculogenesis is the production of follicular steroid hormones (androgens and estrogens) in a process known as steroidogenesis. Follicular steroidogenesis involves the gonadotropic (FSH and LH) induction of cell-specific steroidogenic enzymes and requires the cooperation of both theca and granulosa cells in a process called the "two-cell two-gonadotropin hypothesis" (Liu and Hsueh, 1986; Hillier, Whitelaw and Smith, 1994). Briefly, the conversion of cholesterol to pregnenolone [via p450 side-chain cleavage enzyme (p450scc)], to progesterone (via 3β-hydroxysteroid dehydrogenase), to androgens such as androstenedione (via CYP17) and testosterone (via 17β-hydroxysteroid dehydrogenase) is completed in the theca cells (Wen *et al*., 2010; Liu and Hsueh, 1986; Hillier, Whitelaw and Smith, 1994). Although granulosa cells are capable of progesterone synthesis, they cannot convert androgens to estrogens as they lack the CYP17 enzyme (Simpson, 1979). The aromatase enzyme responsible for estrogen synthesis is exclusively expressed in the granulosa cells in response to FSH, thus thecal androgens must diffuse across the

basement membrane into the granulosa cells for conversion to estrogen such as estradiol (Liu and Hsueh, 1986).

FSH is an important regulator in folliculogenesis as follicles transition from the preantral gonadotropin-responsive stage to the gonadotropin-dependent antral stage (Orisaka *et al*., 2009; Craig *et al*., 2007). Cyclic recruitment takes place during this time, and a major factor differentiating the dominant follicle and follicles destined for atresia is responsiveness to FSH, a known survival factor. The dominant follicle will have a higher sensitivity to FSH correlated with a higher number of FSHR in the granulosa cells, allowing it to continue development past the decline in FSH (mediated by estradiol negative feedback) and avoid granulosa cell death and atresia (McGee and Hsueh, 2000). FSH acts as a survival factor by promoting granulosa cell proliferation via up-regulation of cell cycle protein cyclin D2, and suppressing granulosa cell apoptosis via up-regulation of X-linked inhibitor of apoptosis (XIAP) and down-regulation of Fas and FasL (Han, Xia and Tsang, 2013; Wang, Rippstein and Tsang, 2003; Kim *et al*., 1998). FSH is also known to up-regulate genes involved in granulosa cell differentiation (Wayne *et al*., 2007; Alam *et al*., 2004; Saxena *et al.*, 2007).

Multiple signaling pathways mediate the action of FSH including Akt/PI3K, MAPK/ERK, and cyclic AMP (cAMP)-dependent protein kinase (PKA) (Craig *et al*, 2007; Wayne *et al*., 2007; Gloaguen *et al*., 2011). In the case of PKA, the active G_s subunit detaches from FSHR after FSH activation and binds to adenylyl cyclase, catalyzing the conversion of ATP into cAMP and pyrophosphate (Gloaguen *et al*., 2011). Four cAMP molecules are needed to activate PKA by binding to its two regulatory subunits. This binding causes a conformational change that disassociates the two catalytic

subunits from the complex to phosphorylate the serine, tyrosine and threonine residues of downstream targets, leading to the regulation of various intracellular events including transcriptional regulation of steroidogenic enzymes and downstream estrogen and progesterone production as well as regulation of ovarian cell fate (Gloaguen *et al.*, 2011; Hsueh, McGee and Hayashi, 2000; Hsueh *et al*., 1984; Wayne *et al*., 2007).

1.1.5 Chemerin and Ovarian Cell Fate

Chemerin, also known as retinoic acid receptor responder protein 2 (RARRES2) or tazarotene-induced gene 2 protein (TIG2), is an adipokine commonly associated with inflammation and immune function, adipogenesis, insulin signaling, and steroidogenesis (Goralski *et al*., 2007; Roh *et al*; 2007; Wittamer *et al*., 2003; Bozaoglu *et al*., 2007; Chen *et al*., 2013; Wang *et al.*, 2012; Wang *et al*., 2013). Chemerin has three different G-protein coupled receptors: chemokine-like receptor 1 (CMKLR1), chemokine (C-C motif) receptor like 2 (CCRL2) and G-protein coupled receptor-1 (GPR-1), though many of its functions are mediated by CMKLR1 binding (Goralski *et al.*, 2007; Wittamer *et al.*, 2003; Zabel *et al.*, 2008). CMKLR1-bound chemerin can act as a chemoattractant for immune cells such as macrophages and dendritic cells and increase the expression of pro-inflammatory cytokines such as IL-6 and TNF-α (Berg *et al*., 2010). Chemerin also stimulates intracellular calcium release, induces phosphorylation of extracellular signal-regulated kinase-1 and -2 (ERK 1/2), and may inhibit cAMP accumulation in dendritic cells and macrophages (Wittamer *et al*., 2003). In terms of adipogenesis, serum chemerin levels are correlated with body mass index (BMI) in metabolic syndrome, and intracellular chemerin levels are higher in adipose tissues of obese and type II diabetes

mellitus (T2DM) patients (Bozaoglu *et al*., 2010; Roh *et al*; 2007). Knockout studies of chemerin and CMKLR1 indicate their regulatory roles in adipocyte differentiation, as well as a tissue-specific role of chemerin on insulin sensitivity (increased in skeletal muscles, decreased in the liver) (Goralski *et* al, 2007; Takahashi *et al*., 2011).

In terms of female reproduction, chemerin inhibited IGF-1-induced progesterone and estradiol synthesis involving decreased aromatase levels and phosphorylation of Akt, ERK 1/2, and the IGF-1Rβ tyrosine subunit in primary human granulosa cells (Reverchon *et al.*, 2012). Chemerin was found to up-regulate rat granulosa cell prohibitin content, which suppresses FSH-induced steroidogenic enzyme expression such as aromatase and p450scc and downstream progesterone and estradiol secretion via Akt/PI3K signaling (Wang *et al.*, 2012; Wang *et al*., 2013). Investigations of chemerin in early antral follicle cultures *in vitro* conclude that chemerin induced granulosa cell apoptosis, suppressed XIAP expression, and suppressed basal, FSH- and growth differentiation factor-9 (GDF9)-induced follicle growth (Kim *et al*., 2013). However, chemerin-induced granulosa cell apoptosis was not assessed in isolated primary granulosa cell cultures. To better understand the role of chemerin in granulosa cell death, we need to confirm if its apoptotic signaling occurs directly in the granulosa cells, or if it induces apoptosis via cross-talk with other ovarian cell types.

1.2 Dysregulation of Folliculogenesis and Polycystic Ovarian Syndrome

1.2.1 Polycystic Ovarian Syndrome and its Symptoms

Polycystic ovarian syndrome (PCOS) is a multi-factorial disorder associated with

both reproductive and metabolic factors (e.g. obesity), and is characterized by early antral follicle growth arrest, chronic anovulation, suppressed granulosa cell proliferation, hyperandrogenemia, and insulin resistance (Dunaif, 1997; Franks, Stark and Hardy, 2008). This condition affects up to 10% of women at reproductive age and accounts for 75% of anovulatory infertility (Dunaif, 1997; Franks, 1995). Common symptoms that concern women with PCOS are hirsutism, acne and/or oily skin, irregular bleeding and infertility. Patients with PCOS have increased risk of long-term morbidities including T2DM, hypertension, cardiovascular diseases and various cancers (Azziz *et al*., 2009).

1.2.2 Diagnostic Criteria for Polycystic Ovarian Syndrome

As PCOS is a broad-spectrum syndrome, a list of criteria had to be established for its diagnosis. In 1990, the National Institute of Heath (NIH) first proposed that patients must have both menstrual dysfunction and clinical and/or biochemical signs of hyperandrogenism (Azziz *et al.*, 2006). These guidelines were amended to include polycystic ovaries as a factor during the ESHRE/ASRM consensus workshop in Rotterdam in 2003, which recommends that patients must have at least two of the following characteristics identified: a) polycystic ovaries as determined by ultrasonography, b) clinical and/or biochemical signs of hyperandrogenism, and c) oligo- and/or anovulation, with exclusion of other related disorders (Rotterdam ESHRE/ASRM-sponsored PCOS consensus workshop group, 2004). Most recently, the Androgen Excess Society suggested a tightening of these diagnostic criteria for PCOS in 2006, stipulating that hyperandrogenism must be present with exclusion of other related disorders, as well as oligo-/anovulation and/or polycystic ovaries (Azziz *et al*., 2006).

1.2.3 Pathogenesis of Polycystic Ovarian Syndrome

As per current diagnostic criteria, hyperandrogenism is the key feature of PCOS. Circulating androgen levels and expression of thecal steroidogenic enzymes are increased in patients with PCOS, while granulosa cell aromatase expression and secretion of progesterone and estradiol are lowered (Jakimiuk *et al.*, 2001; Ehrmann, 2005; Jakimiuk *et al.*, 1998; Welt *et al.*, 2005). Although follicles of women with PCOS are hyper-responsive to FSH due to increased FSHR expression, elevations in circulating LH and increased LHR expression result in a higher LH:FSH ratio, leading to androgen excess (Mason *et* al., 1994; Catteau-Jonard *et al*., 2008; Jakimiuk *et al.*, 2001; Goodarzi *et al*., 2011). Insulin resistance and hyperinsulinemia, which affects 50-70% of women with PCOS, is also a contributing factor of hyperandrogenism (Goodarzi *et al*., 2011). Androgen excess is associated with a multitude of characteristics associated with PCOS, including hirsutism, acne, alopecia (resembling male-pattern hair loss) and antral follicle growth arrest leading to cycle irregularity, oligo-/anovulation and subfertility (Ehrmann, 2005; Goodarzi *et al*., 2011).

1.2.4 Treatment Strategies for Polycystic Ovarian Syndrome

Due to its complex and heterogeneous nature, a wide range of treatment strategies is available to support patients depending on their symptoms and diagnostic criteria. The first course-of-action is changes in lifestyle such as diet and exercise to reduce weight. Obesity is closely associated with insulin sensitivity and androgen production, and weight loss has been attributed to increased chances of ovulation and pregnancy (Vause and Cheung, 2010; Thessaloniki ESHRE/ASRM-sponsored PCOS consensus workshop

group, 2008). Oral contraceptives are given to aid in symptoms such as irregular bleeding, hirsutism and acne (Cheung, 2010; Goodarzi *et al*., 2011). A common treatment to induce ovulation in PCOS women is clomiphene citrate, which interferes with the negative feedback of estrogen on FSH to increase FSH release, follicular maturation and ovulation in up to 80% of PCOS patients (Homberg, 2005; Thessaloniki ESHRE/ASRM-sponsored PCOS consensus workshop group, 2008). For patients with insulin resistance, the anti-diabetic drug metformin can increase insulin sensitivity, reduce androgen synthesis and induce ovulation, with increased effectiveness if taken in combination with clomiphene citrate (Omran, 2007; Vause and Cheung, 2010). If a patient still struggles to conceive after these treatments, another alternative is closely monitored gonadotropin therapy using exogenous FSH and hCG for follicular maturation and ovulation respectively. To avoid the risk of ovarian hyperstimulation syndrome and multiple births, closely monitored low-level administration is recommended (Vause and Cheung, 2010; Thessaloniki ESHRE/ASRM-sponsored PCOS consensus workshop group, 2008). Patients who already require laparoscopy may also undergo ovarian drilling, where perforations in the ovary can reduce thecal androgen production and encourage ovulation (Thessaloniki ESHRE/ASRM-sponsored PCOS consensus workshop group, 2008).

1.2.5 Animal Models of Polycystic Ovarian Syndrome

A wide array of animal models is used to study the pathogenesis of PCOS. Rhesus macaques, sheep and rodents are all examples of species induced by various factors such as estradiol valerate (EV) or the aromatase inhibitor letrozole, or by androgenization from testosterone propionate (TP), dehydroepiandrosterone (DHEA) or 5α-dihydrotestosterone

(DHT) (Padmanabhan and Veiga-Lopez, 2013; Mannerås *et al*., 2007). Although no model to date completely recapitulates all phenotypes of PCOS, these models are good resources for understanding cellular and molecular mechanisms of PCOS and developing future treatment strategies.

Androgenized rodent models are frequently used due to low cost, appropriate size for *in vitro* and *in vivo* studies, and relative homogeneity compared to other species (Walters, Allan and Handelsman, 2012). As a non-aromatizing androgen, DHT is ideal for hyperandrogenic induction due to its inability to be converted into estrogens by aromatase (Padmanabhan and Veiga-Lopez, 2013; Mannerås *et al*., 2007). A DHT-induced rat model has been developed in the last decade involving the surgical implantation of a DHT-filled continuous release capsule (Mannerås *et al.*, 2007). Three-month DHT-implanted rats have shown consistency in many phenotypes that correspond to human PCOS including suppression of steroidogenic enzymes, estradiol and progesterone secretion from granulosa cells, granulosa cell death, follicular atresia, polycystic ovaries, cycle irregularity, anovulation, insulin resistance, and increased adipocyte size, body fat and weight (Mannerås *et al*., 2007; Wang *et* al., 2012; Kim *et al.*, 2013; Hossain *et al*., 2013). Unlike human PCOS, DHT-treated rats had a reduction in ovarian size and weight (Mannerås *et al*., 2007). Our laboratory recently determined that changes in phenotype associated with PCOS begin after one month of DHT induction such as cycle irregularity, though much is still unknown (Nivet *et al.*, unpublished).

1.2.6 Granulosa Cell Fate and Follicle Growth Arrest in Polycystic Ovarian Syndrome

As briefly mentioned in earlier sections, a characteristic of PCOS is antral follicle growth arrest (**Fig. 1.1**). This is associated with follicular degeneration and the accumulation of cyst-like ovarian structures classified as polycystic ovaries (PCO), which resemble "a string of pearls" when viewed under ultrasonography (Goodarzi *et al*., 2011; Erhmann, 2005). This failure to progress past the antral stage can lead to cycle irregularities, oligo-/anovulation and infertility seen in PCOS (Goodarzi *et al*., 2011). Differences in follicular cell fate have been observed in the antral follicles of women with PCOS, including increased theca cell proliferation, decreased granulosa cell proliferation and increased granulosa cell apoptosis (Franks, Stark and Hardy, 2008; Ding *et al*., 2016; Mikaeili *et al*., 2016). As antral follicle atresia/degeneration is mediated by granulosa cell apoptosis during normally functioning folliculogenesis, it is likely that a dysregulation in granulosa cell fate contributes to follicular degeneration and antral follicle growth arrest in PCOS (Kim *et al*., 2013).

In DHT-induced rat studies, granulosa cell death was observed prior to follicular degeneration and accumulation of small, irregular atypical follicles (Kim *et al*., 2013). These structures have no oocyte and are predominantly theca cells, similar to the cysts seen in women with PCOS. Granulosa cell death may be associated with increased levels of serum/ovarian chemerin and ovarian CMKLR1, as seen in both PCOS patients and the DHT-induced model (Kim *et* al., 2013; Wang *et al.,* 2012). Although the effects of gonadotropin on granulosa cell death were not assessed, eCG administration

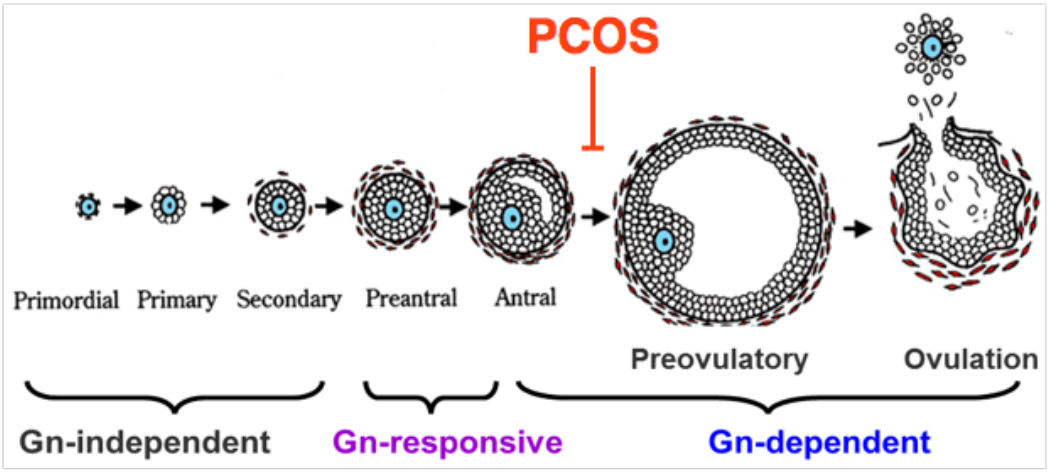

Figure 1.1: Polycystic ovarian syndrome arrests follicular growth at the early antral stage of folliculogenesis

The stages of folliculogenesis (primordial, primary, secondary, preantral, antral, preovulatory and ovulation) and their responsiveness to gonadotropin (Gn) are shown. In the case of polycystic ovarian syndrome, one of the main characteristics is antral follicle growth arrest. This dysregulation in folliculogenesis prevents dominant follicles to develop into fully mature follicles, leading to chronic anovulation and reduced fertility (modified from Craig *et al*., 2007).

was found to rescue ovarian length and reactivate folliculogenesis in the DHT-induced model (Hossain *et al*., 2013). These restorative characteristics suggest that gonadotropin (e.g. FSH) may prevent granulosa cell apoptosis in the DHT-induced rat model for PCOS.

Mechanisms leading to granulosa cell fate dysregulation in PCOS have not been fully elucidated. As studies from recent years show that dysfunctional regulatory mechanisms of cell death such as mitochondrial fission/fusion dynamics and autophagy are implicated in various disease pathogeneses, perhaps they also play a role in the pathogenesis of PCOS (Westermann, 2010; Archer, 2013; Nixon and Yang, 2012).

1.3 Mitochondrial Fission and Fusion Dynamics

1.3.1 Mitochondrial Function

Mitochondria are double membrane-bound organelles known first and foremost as "the powerhouse of the cell" due to their important role in cellular respiration by generating energy in the form of ATP through the citric acid cycle. However, mitochondria have a variety of other functions in cellular regulation involving cellular metabolism, calcium storage, and cell fate regulation, including proliferation and programmed cell death (Friedman and Nunnari, 2014; Nicholls, 2002; Westermann, 2010; McBride, Neuspiel and Wasiak, 2006). As mitochondria are highly dynamic, they constantly alter their morphology to fulfill these various regulatory processes in the cell.

1.3.2 Mitochondrial Fission and Fusion

Due to their dynamic nature, mitochondria constantly undergo division (fission)

and elongation (fusion) to form a network of important processes in cellular regulation and maintenance (Detmer and Chan, 2007; Youle and Karbowski, 2005). Fusion is important for the exchange of soluble and membranous components across mitochondria (Karbowski and Youle, 2003). During the S-phase of the cell cycle, mitochondria are hyperfused to increase the output of ATP, compensating for the energy required for DNA replication (Mitra *et al*., 2009). Meanwhile, mitochondrial fission is important for the segregation of mitochondrial DNA (mtDNA) and mitochondrial distribution during mitosis (Mishra and Chan, 2014; Westermann, 2010). Fission is also important for the purposes of quality control by isolating the damaged portions of mitochondria for autophagic degradation via mitophagy or by initiating the intrinsic apoptotic pathway (Detmer and Chan, 2007; Kluge, Fetterman and Vita, 2013).

Extensive mitochondrial fragmentation leads to a disruption in the inter-mitochondrial membrane space housing cytochrome C, likely due to cristae remodeling triggered by mitochondrial outer membrane permeabilization (MOMP). The release of cytochrome C initiates a downstream chain of events, including caspase-3 activation and apoptosis (Detmer and Chan, 2007; Lee *et al*; 2004). The inhibition of mitochondrial fragmentation reduces cytochrome C release and delays cell death and pro-apoptotic Bak and Bax deficient-cells have altered mitochondrial dynamics (Frank *et al*. 2001; Karbowski et al. 2006).

1.3.3 Regulation of Mitochondrial Fission and Fusion

A multitude of intracellular GTPase intermediates regulate both mitochondrial fission (Fis1, Drp1) and fusion (Opa1, Mfn1, Mfn2) (Lee *et al*, 2004; Youle and

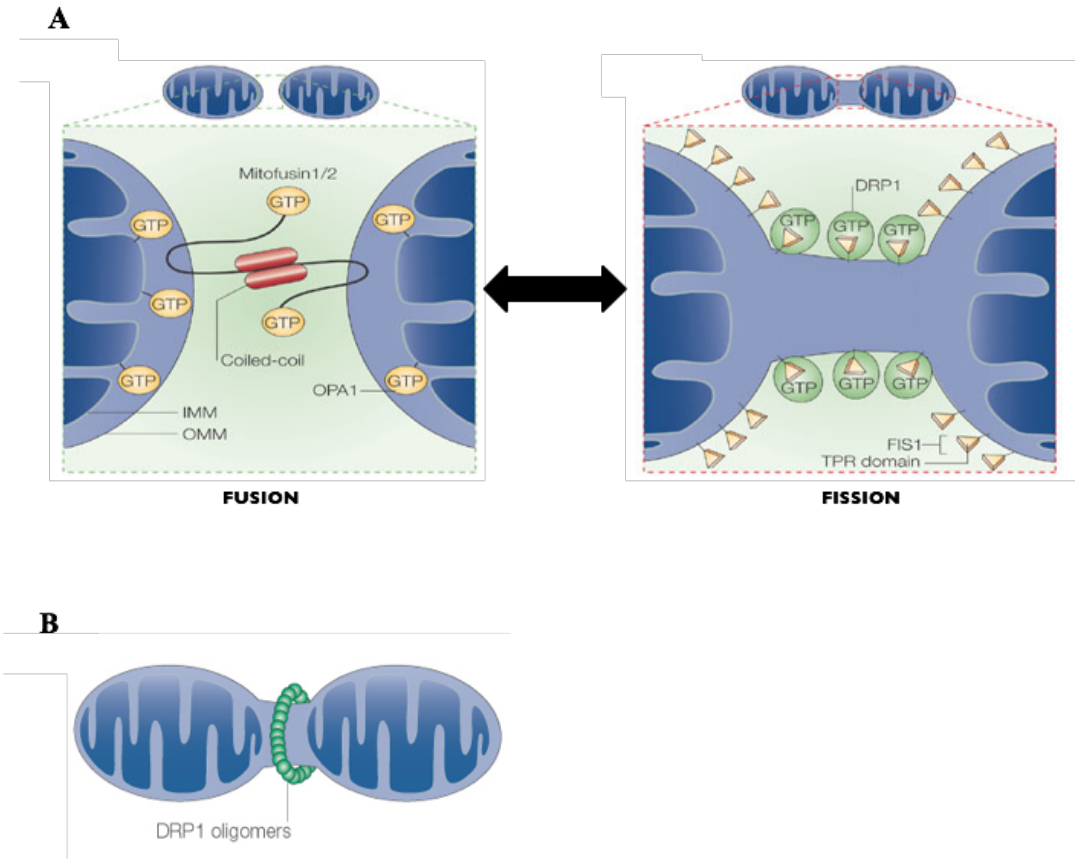

Figure 1.2: Intracellular proteins regulate mitochondrial fusion and fission dynamics

A: A number of intracellular intermediates regulate mitochondrial dynamics (fusion and fission). Mitofusin 1 and 2 are involved in outer mitochondrial membrane fusion while Opa1 regulates inner mitochondrial membrane fusion. During fission (division), Fis1 and Drp1 are involved.

B: Drp1 participates in mitochondrial fission by forming oligomers around the mitochondrion via GTP hydrolysis. These Drp1 oligomers coil around and constrict the mitochondrion, dividing it into two daughter mitochondria (Youle and Karbowski, 2005).

Karbowski, 2005; Detmer and Chan, 2007). As illustrated in **Fig. 1.2**, Mitofusin proteins Mfn1 and Mfn2 are GTPases involved in fusion of the outer mitochondrial membrane (OMM) by tethering homo- and hetero-oligomers to form an anti-parallel coiled coil (Youle and Karbowski, 2005). Meanwhile, Optical atrophy 1 (Opa1) is responsible for the fusion of the inner mitochondrial membrane (IMM), and the balance of its long and short forms ensure mitochondrial fusion by tethering of homo- and hetero-oligomers as well (Youle and Karbowski, 2005). However, apoptotic signaling can stimulate cleavage of the membrane-bound long-form Opa1 at its S1 cleavage site by Oma1, disrupting fusion and shifting the balance towards increased fission (Song *et al*., 2007). Mitochondrial Fission 1 (Fis1), along with recently discovered mitochondrial fission factor (Mff) and mitochondrial dynamics proteins of 49 and 51 kDa (MiD49 and MiD51), are among proteins on the outer mitochondrial membrane that facilitate the docking and oligomerization of dynamin-related protein 1 (Drp1) (Losón *et al*., 2013).

Drp1 is a cytoplasmic GTPase that functions as the key player in mitochondrial fission. During mitochondrial fission, Drp1 is recruited from the cytoplasm to the mitochondrial membrane. By GTP hydrolysis, Drp1 assembles an oligomer chain that coils and constricts around the mitochondrion until it divides into two daughter mitochondria (Youle and Karbowski, 2005; Chen and Chan, 2006). The activity of Drp1 is dependent on post-translational modifications, including ubiquitination, sumoylation, S-nitrosylation and phosphorylation (Chang and Blackstone, 2010; Detmer and Chan, 2007; Santel and Frank, 2008). When its Ser616 site (Ser635 in rats) is phosphorylated by the cyclin-dependent kinase 1 (CDK1)/cyclin B complex, mitochondrial fission is initiated as seen during mitosis. However, when its Ser637 site (Ser656 in rats) is

phosphorylated by PKA, Drp1 function is inhibited and inactive mitochondrial complexes accumulate, shifting mitochondrial dynamics towards mitochondrial fusion instead (Merrill *et al*., 2011; Chang and Blackstone, 2010). As cAMP accumulation is responsible for both the activation of PKA and the downstream inactivation of pro-apoptotic CDK1, it has been suggested that these two phosphorylation events (Ser616 and Ser637) are in opposition of one another (Li, Mao and Xia, 2012). Dephosphorylation of Ser637 by calcineurin allows Drp1 to change its conformation and perform its function during fission (Cereghetti *et al*; 2008). Recently, Ca^{2+}/calmodulin-dependent protein kinase Iα (CaMKIα) has also been shown to phosphorylate Ser637, initiated by an influx of Ca^{2+} into the neuronal cell. However, this study found that Fis1 affinity and subsequent mitochondrial fission increased with phosphorylation, in contradiction to other Ser637 studies (Han *et al.*, 2008).

Aside from phosphorylation, other post-translational modifications are capable of regulating Drp1 function. Bak/Bax-dependent sumoylation via E3 ligase MAPL allows Drp1 to protect itself from ubiquitination and facilitates localization, while nitrosylation of its Cys644 site by nitric oxide can promote fission (Braschi, Zunino and McBride, 2009; Cho et al, 2009). Ubiquitination by E3 ligase MARCH5 was originally believed to facilitate mitochondrial fusion, though recent studies indicate its role in trafficking and assembly/disassembly of Drp1 at the mitochondria to promote fission (Karbowski, Neutzner and Youle, 2007).

1.3.4 Dysregulation of Mitochondrial Dynamics and Associated Pathologies

Although mitochondria are highly dynamic by nature, fission and fusion must be

relatively well balanced in order to maintain a healthy cell. Dysregulation in mitochondrial dynamic proteins can shift this balance towards excessive fusion or fission, which can lead to cell death and disease pathogenesis. In recent years, a number of diseases have been linked to a dysregulation in mitochondrial fission and fusion dynamics, including neurodegenerative, cardiovascular, and renal disorders (Westermann, 2010; Archer *et al*., 2013; Shenouda *et al*., 2011). A mutation in Mfn2 is associated with Charcot-Marie-Tooth neuropathy, and a number of Opa1 mutations are involved in optic atrophy (Züchner *et al*., 2004; Olichon *et al*., 2006). In Huntington's disease, the mutated huntingtin protein binds to Drp1, increasing its activity and downstream mitochondrial fission and apoptosis (Song *et al*., 2011). A key protein associated with Alzheimer's disease, called β-amyloid protein, increases nitric oxide production and S-nitrosylation of Drp1, leading to mitochondrial fission and neuronal degeneration (Cho *et al*., 2009). Hypertension is associated with dysregulations in Mfn2, Opa1, and Ser616 phosphorylation of Drp1 (Ryan *et al*, 2013; Marsboom *et al*, 2012; Jin *et al*., 2011). The rapid accumulation of Drp1 during acute kidney injury can lead to mitochondrial fragmentation and impairment in ATP production, contributing to tissue dysfunction in chronic kidney disease (Zhan *et al*., 2013).

In the context of gynecological cancers, the functional food agent piceatannol enhanced the effects of cisplatin (CDDP) treatment on apoptosis induction by Drp1-mediated mitochondrial fragmentation in chemosensitive ovarian cancer cells (Farrand *et al*., 2013a). However, CDDP was unable to induce mitochondrial fragmentation and apoptosis in chemoresistant gynecological cancer cells due to an upstream inhibition of Opa1 processing (Kong *et al*., 2014). Dysregulation in mitochondrial dynamics is also

associated with cervical cancer, breast cancer, lung cancer, glioblastoma, neuroblastoma, colorectal cancer, pancreatic cancer and melanoma (Senft and Ronai, 2016).

1.3.5 Mitochondrial Dynamics in Ovarian Granulosa Cells

Recent studies on mitochondrial dynamics in the ovary suggest that fission and fusion homeostasis is crucial for maintaining healthy follicular development. In *Drosophila* sp., Drp1-null follicle cells had increased proliferation, resistance to apoptosis and developmental defects in ovarioles (Mitra *et al*., 2012; Tanner and McCall, 2011). An oocyte-specific Drp1 knockout (KO) mouse resulted in anovulation, follicle growth arrest, multi-organelle aggregations and mitochondrial deformations in the oocyte as well as decreased granulosa cell proliferation, while murine granulosa cells in response to cigarette smoke *in vivo* had down-regulated Mfn1 and Mfn2 contents (Udagawa *et al*., 2014; Gannon, Stämpfli, and Foster, 2013). Mitochondrial fragmentation and apoptosis were detected in the cumulus cells of a streptozotocin-induced type I diabetic Akita mouse model (Wang *et al*., 2010). In a cisplatin-induced mouse model for premature ovarian failure (POF), in which pathogenesis is associated with granulosa cell apoptosis and accelerated follicular atresia, Mfn2 and anti-apoptotic Bcl-2 levels were down-regulated while pro-apoptotic Bax levels were up-regulated. ATP levels were also decreased, and ultrastructural analysis of mitochondrial morphology via transmission electron microscopy (TEM) revealed mitochondrial membrane and cristae impairments (Chen *et al.*, 2015).

1.3.6 Mitochondrial Dysfunction and Polycystic Ovarian Syndrome

To date, the examination of mitochondrial fission and fusion dynamics in context to PCOS has not been reported, though the involvement of mitochondrial respiration in the pathogenesis of PCOS has been briefly examined. Oxidative stress occurring at mitochondrial complex I led to increased reactive oxygen species production and decreased mitochondrial O_2 consumption in polymononuclear leukocytes of PCOS patients (Victor *et al*., 2009). The occurrence of circulating markers of oxidative stress (e.g. homocysteine, malondialdehyde, dimethylarginine) was higher in PCOS patients regardless of obesity (Murri *et al*., 2013). As increased oxidative stress is associated with increased mitochondrial fission (Yu *et al*., 2008), overabundant mitochondrial fission may be seen in the pathophysiology of PCOS as well.

1.4 Autophagy

1.4.1 Overview of Autophagy

Autophagy, a name derived from the Greek words meaning "self eating", is a cell survival mechanism that involves the degradation of intracellular constituents. The three types of autophagy are macroautophagy, microautophagy and chaperone-mediated autophagy (Glick, Barth and Macleod, 2010; Mizushima, 2007). The main pathway of autophagy is macroautophagy, which involves the assembly of a double membrane-bound vesicle called the autophagosome to surround and degrade target proteins. The fusion of the autophagosome with the lysosome (forming a structure called the autolysosome) stimulates the breakdown and recycling of its cargo (He and Klionsky, 2009; Glick, Barth and Macleod, 2010; Mizushima, 2007). Macroautophagy can also

perform selective autophagy of organelles. An example of this is mitophagy, which involves the degradation of damaged mitochondria after undergoing fragmentation via mitochondrial fission (Kluge, Fetterman and Vita, 2013).

Neither microautophagy nor chaperone-mediated autophagy requires autophagosomes for degradation. Instead, microautophagy utilizes lysosomes directly via invagination, and chaperone-mediated autophagy uses an hsc70-containing chaperone to facilitate translocation into the lysosome (Lee, Giordano and Zhang, 2012; Sahu *et al*., 2011; Bejarano and Cuervo, 2010).

1.4.2 Mechanisms and the Autophagy Process

Macroautophagy (which will now be generalized as "autophagy") involves a vast number of players known as autophagy-related or Atg proteins whose main regulator is the mechanistic target of rapamycin (mTOR) (He and Klionsky, 2009; Mizushima, 2007; Glick, Barth and Macleod, 2010). mTOR is a serine/threonine kinase that suppresses autophagy via inhibitory phosphorylation of Unc-51 like autophagy activating kinase 1 (ULK1), another serine/threonine kinase (Wong *et* al., 2013). Insulin and growth factor signaling suppresses autophagy in basal conditions through various pathways (e.g. PI3K/Akt) upstream of mTOR and through inhibition of the mTOR-independent pathway (Raf1-MAPK-ERK1/2) (Martinez-Lopez and Singh, 2014; He and Klionsky, 2009).

Autophagy can be stimulated by a numbers of stressors such as nutrient deprivation and ATP depletion, ER stress, hypoxia and oxidative stress (He and Klionsky, 2009). These stressors can inactivate mTOR, which allows ULK1 activation and formation of the isolation membrane or phagophore (Wong *et* al., 2013). As illustrated in **Fig. 1.3**, the

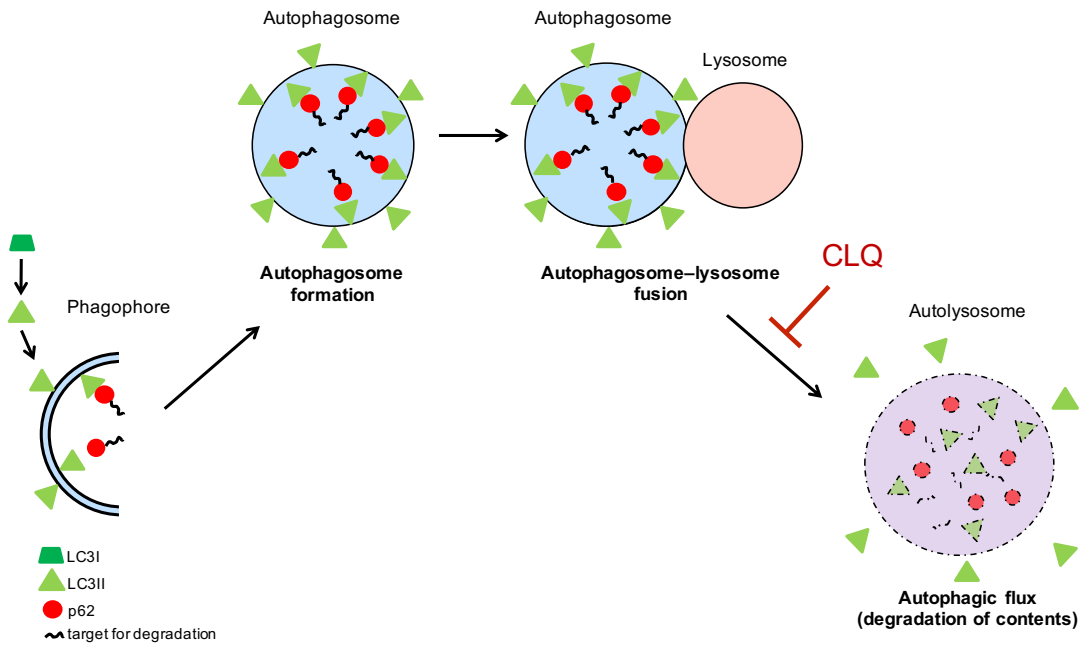

Figure 1.3: Autophagosome formation and degradation via lysosomal fusion

After autophagy is initiated by upstream regulators, the formation of the phagophore begins the sequestration of cargo by p62, which can selectively bind to ubiquitinated targets for degradation. LC3I becomes converted into LC3II and assembles along the phagophore during elongation to bind with its substrate p62. Once the autophagosome is fully formed, it fuses with the lysosome to form the autolysosome. Lysosomal enzymes degrade the cargo including p62 and interior-facing LC3II. In Western blot studies, the degradation of LC3II can complicate the interpretation of the data. The addition of a lysosomal inhibitor such as chloroquine (CLQ) can prevent degradation of the autophagosome contents to confirm if autophagic flux is occurring.

phagophore begins the sequestration of cargo, and proteins such as p62/sequestosome 1 (SQSTM1) can selectively target ubiquitinated cellular components for degradation (Bjørkøy *et al*., 2005). Nucleation and assembly of the phagophore involve many players including the class III phosphatidylinositol 3-kinase (PtdIns3K) complex containing Beclin-1 and various Atg proteins (Nobukuni et al. 2005; Mizushima, 2007). Phagophore elongation and autophagosome formation is mediated in part by microtubule-associated protein 1 light chain 3 (LC3). Cytoplasmic LC3, or LC3I, becomes conjugated to phosphatidylethanolamine (PE) via Atg12-Atg5-Atg16L and converts into LC3II (Fujita *et al*., 2008; Glick, Barth and Macleod, 2010). LC3II assembles along the phagophore both interiorly and exteriorly, and binds with its cargo-bound substrate p62 (Pankiv *et al*., 2007). Once the autophagosome is completely formed, it can fuse with the lysosome to form a structure called the autolysosome. Lysosomal enzymes degrade the cargo including p62 and interior-facing LC3II into monomeric units, which are recycled by the cell (Mizushima, 2007).

1.4.3 Methods of Studying Autophagy

A wide number of cellular and molecular assays can be utilized to study autophagy including TEM, fluorescence microscopy, Western blot, flow cytometry and isotopic labeling (**Fig. 1.4**; Mizushima, Yoshimori and Levine, 2010). However, it can be challenging to make accurate interpretations about an entire dynamic process when limited to assessing static measurements. This can be particularly difficult when trying to find the optimal time-of-action for autophagy during time-course studies. Great variability in the time-of-action across experimental replicates may complicate the intent to achieve a significant result after statistical analysis from a combined mean. Therefore,

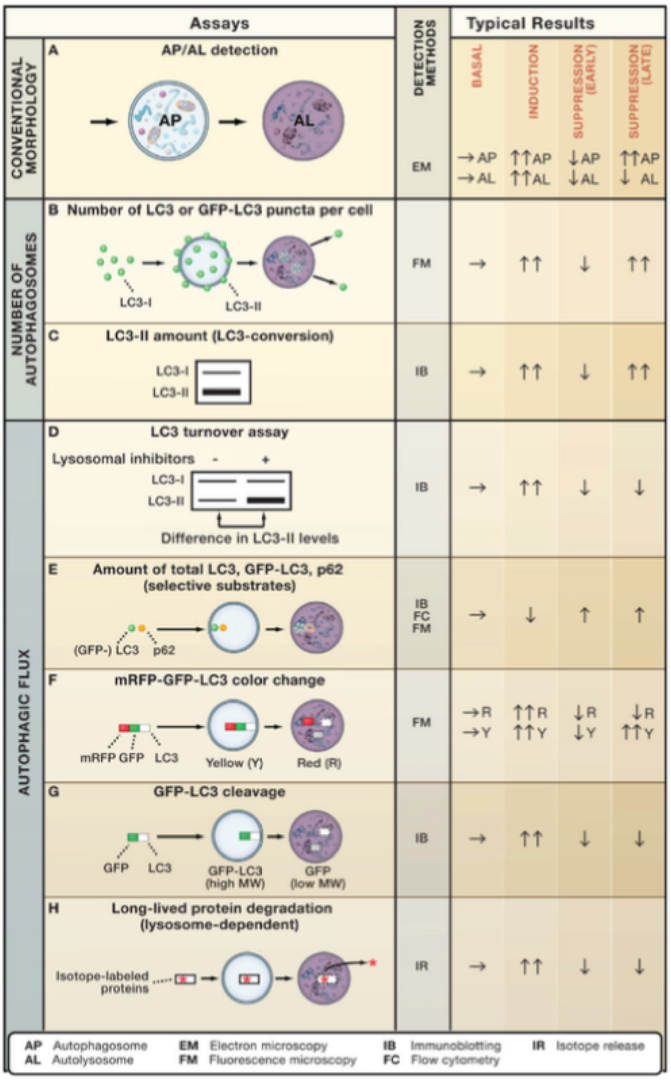

Figure 1.4: Overview of methods used to study autophagy

A: Electron microscopy (EM) can determine the presence of autophagosomes in a cell.

B-C: Fluorescence microscopy (FM), and immunoblotting (IB) without lysosomal inhibitors can indicate autophagosome formation, but not autophagic flux

D-H: FM, flow cytometry (FC), isotope release (IR), and IB with lysosomal inhibitors are methods used to determine autophagic flux. Chloroquine is an example of a lysosomal inhibitor, which inhibits fusion of the autophagosome and lysosome. (diagram taken from Mizushima, Yoshimori and Levine, 2010).

it is encouraged to carefully plan the methodological approach prior to experimentation, and to assess the data critically (Mizushima, Yoshimori and Levine, 2010). One of the most reliable yet classic methods in determining autophagy is ultrastructural identification of autophagic vacuoles (autophagosomes or autolysosomes) using TEM. By identifying their target components within the vacuole, organelle-specific autophagy such as mitophagy can be confirmed (Barth, Glick and Macleod, 2010; Gannon, Stämpfli and Foster, 2013).

The determination of autophagosome production is commonly studied by assessing LC3I to LC3II conversion as well as their relative amounts via fluorescence microscopy or Western blot (Mizushima, Yoshimori and Levine, 2010). In the case of Western blot analysis of LC3I/II, it is important to take precautions when interpreting the data. An increase in band intensity of LC3II indicates an increase in autophagosome production. Meanwhile, a decrease or no change in LC3II band intensity could indicate either one of two scenarios: a) autophagy is unable to be induced by the treatment; or b) autophagic flux has occurred and interior-facing LC3II has been degraded by the autolysosome (Mizushima and Yoshimori, 2007; Barth, Glick and Macleod, 2010). To reconcile this, it is now common to include a lysosomal inhibitor such as chloroquine to prevent fusion of the autophagosome and lysosome, resulting in an accumulation of autophagosomes (**Fig. 1.3**). Originally intended as a treatment for malaria, chloroquine is frequently used in autophagy studies as an inhibitor of lysosomal acidification, preventing fusion enzymes that require acidic conditions to function (Dunmore *et al*, 2013; Mizushima, Yoshimori and Levine, 2010). If the intensity of the band for LC3II is unchanged in chloroquine-free conditions but increased in chloroquine-containing conditions, this indicates that LC3II is

being degraded by the autolysosome and autophagic flux is occurring (Mizushima and Yoshimori, 2007; Barth, Glick and Macleod, 2010).

Another common marker to assess autophagic flux is p62. As p62 is contained within the interior of the autophagosome during autophagy, it will become degraded with the target contents after fusion with the lysosome. In Western blot studies, a decrease in p62 band intensity is generally indicative of autophagic flux, however recent studies suggest p62 expression may increase after prolonged starvation to compensate for the increased demand of autophagy (Sahani, Itakura and Mizushima, 2014; Mizushima and Yoshimori, 2007).

1.4.4 Autophagy-Mediated Cell Death and Dysregulation

Although autophagy is first and foremost a cell survival mechanism, chronic stress such as nutrient deprivation can stimulate autophagic cell death, another form of programmed cell death. Autophagic cell death is characterized by an overabundance of autophagic vacuoles and a loss in organelles without the nuclear fragmentation or membrane blebbing seen in apoptosis (Thorburn, 2008; Tsujimoto and Shimizu, 2005). Despite their distinctive morphological differences, there is extensive cross talk between autophagic cell death and apoptosis, which can occur simultaneously or independently of one another (Maiuri *et al*., 2007; Thorburn, 2008).

A dysregulation in autophagy leading to autophagic cell death has been linked to a number of pathological processes (Nixon and Yang, 2012). Neurons in Parkinson's disease have higher numbers of autophagic vacuoles caused by mutations in PINK1 and Parkin mitophagy proteins, while patients with amyotrophic lateral sclerosis have an

increased number of autophagosomes that may be associated with suppressed phospho-mTOR in neurons (Gasser, 2009; Sasaki, 2011; Morimoto et al. 2007). A mutation in presenilin 1 (PS1), a key factor of Alzheimer's disease, leads to defective lysosomal acidification required for autolysosome function (Lee *et al*., 2010). In Crohn's disease, a severe inflammatory bowel disorder, genome-wide association (GWA) scans indicate that genes critical for autophagy, Atg16L1 and IRGM, are implicated (Massey and Parkes, 2007).

1.4.5 Autophagy in Granulosa Cell Regulation, Follicular Atresia and PCOS

Although the occurrence of oocyte autophagic cell death during follicular atresia has been well established, the role of granulosa cell autophagy in follicular atresia has also recently been demonstrated (Escobar Sánchez, Echeverría Martínez and Vázquez-Nin, 2012; Devine *et al*., 2000). Studies on folliculogenesis and follicular atresia using eCG-primed rats indicated that autophagy induces apoptotic and non-apoptotic cell death in atretic follicles (Choi *et al*., 2010; Choi *et al*., 2011). Immunohistochemical (IHC) analysis showed increased LC3 and caspase-3 staining in the granulosa cells of atretic follicles (Choi *et al*., 2010; Choi *et al*., 2014). Gonadotropin treatment *in vivo* (via eCG) and *in vitro* (via FSH) suppressed autophagy by the Akt-mediated mTOR pathway, as seen by a reduction in both LC3II expression and autophagic vacuoles via TEM (Choi *et al*., 2014).

Studies relating granulosa autophagic cell death and follicle loss/degeneration have also been assessed. In response to cigarette smoke *in vivo*, murine granulosa cells had autophagic, but not apoptotic, cell death and follicle loss associated with up-regulated

LC3 and Beclin-1, and down-regulated Akt and mTOR protein contents as well as increases in autophagosome production and mitophagy when examined by TEM (Furlong *et al*., 2015; Gannon, Stämpfli and Foster, 2012; Gannon, Stämpfli and Foster, 2013). Ovaries obtained from women undergoing *in vitro* fertilization had lectin-like oxidized low-density lipoprotein receptor-1 (LOX-1), a receptor for oxidated low-density lipoprotein (oxLDL) associated with obesity, localized in regressed antral follicles (Duerrschmidt *et al*., 2006). oxLDL treatment of a human granulosa cell line showed an induction of apoptosis-independent autophagic cell death indicated by increased LCII:LC3I ratio and presence of autophagic vacuoles (Duerrschmidt *et al*., 2006; Schube *et al*., 2014).

As autophagy, mitophagy and autophagic cell death are found to induce granulosa cell death leading to follicular atresia or follicle loss, its dysregulation may also be associated with dysregulations in mitochondrial fission, granulosa cell death and follicular growth arrest in PCOS (Furlong *et al*., 2015; Choi *et al*., 2010). However, few studies using androgenized rodent models have attempted to determine the possible involvement of autophagy in the pathophysiology of PCOS. In DHEA-induced mice, there was no significant difference in mTOR or p-mTOR contents compared to control (Yaba and Demir; 2012). As this was assessed in pooled cells from the entire ovary, this lack of effect may be due to cell type-specific differences in autophagy. Myocardial tissue in DHT-implanted rats had disrupted autophagy as indicated by LC3II down-regulation and p62 up-regulation, though this was not assessed in the context of the ovary (Gao *et al*., 2016).

1.4.6 Chemerin and Autophagy

In recent years, chemerin has been established as an inducer of autophagy in various cell types. In human aorta endothelial cells (HAECs), chemerin-induced angiogenesis was associated with the induction of reactive oxidative species (ROS) generation and up-regulation of Beclin-1, Atg-7, Atg-12-Atg-5, and LC3II in chemerin-treated cells (Shen *et al*., 2013). These results were supported by an observed increase in autophagosome number in chemerin-treated cells, and the AMPK/mTOR pathway was confirmed to mediate chemerin's action on HAEC autophagy (Shen *et al*., 2013). Chemerin-induced autophagy was also recently investigated in skeletal muscle, with findings consistent to those found in HAECs (Xie *et al*., 2015). Chemerin increased levels of Beclin-1, Atg-5 and Atg-7 as well as the conversion of LC3I to LC3II via the Akt-Fox03α pathway upstream to mTOR (Xie *et al*., 2015; Mammucari, Schiaffino and Sandri, 2008). This was linked to a chemerin-induced up-regulation of mitochondrial fission proteins (Drp1 and Fis1) and down-regulation of mitochondrial fusion proteins (Mfn2 and Opa1), which led to mitochondrial dysfunction and ROS generation (Xie *et al*., 2015).

The above studies provide convincing evidence of chemerin-induced autophagy and the mechanisms involved in its regulatory effects. Although this has not yet been reported in the ovary, it is possible that chemerin-induced granulosa cell autophagy and autophagic cell death may be associated with chemerin-induced granulosa cell apoptosis demonstrated in ovarian follicles, due to the interactive cross-talk between apoptosis and autophagy (Kim *et al*., 2013; Maiuri *et al*., 2007; Thorburn, 2008).

1.5 Rationale

PCOS, a broad-spectrum disorder associated with dysregulated folliculogenesis, is characterized by increased granulosa apoptotic cell death, antral follicular growth arrest and anovulation. As mounting evidence links dysregulations in regulatory mechanisms of cell death, such as mitochondrial fission/fusion dynamics and autophagy, to the pathogenesis of various diseases, mitochondrial dynamics and autophagy may play significant roles in granulosa cell death associated with the pathogenesis of PCOS.

As FSH is known for its pro-survival regulatory roles in granulosa cells as well as its therapeutic use for induction of folliculogenesis and ovulation in PCOS, its potential modulatory role on mitochondrial dynamics and autophagy in the PCOS condition remains to be demonstrated. Possible mechanisms for its role in mitochondrial fission and fusion regulation may be related to post-translational modifications of Drp1. As cAMP is responsible for both the activation of anti-fission PKA and the inactivation of pro-fission CDK1 kinases for Drp1, it is possible that FSH regulates mitochondrial dynamics by suppressing the activity of Drp1 via phosphorylation sites Ser616 and Ser637, hence suppressing mitochondrial fission.

Lastly, the role of chemerin in the regulation of granulosa cell apoptosis needs to be confirmed. Previous findings suggest that chemerin inhibits FSH-induced granulosa cell steroidogenesis and induces apoptosis and follicular growth. As these apoptosis studies were completed in follicle cultures, its remains unclear whether chemerin acts directly on the granulosa cells and if it could induce apoptosis in isolated granulosa cell preparations. Its role in the regulation of mitochondrial dynamics, possibly resulting in granulosa cell apoptosis and autophagy, also remains a mystery.

1.6 Hypothesis

It is hypothesized that in PCOS, a dysregulated increase in mitochondrial fission leads to granulosa cell death (apoptotic and autophagic) and follicular growth arrest, responses that are attenuated by gonadotropin. FSH plays an important role in the regulation of granulosa cell mitochondrial dynamics by inhibiting the activity of mitochondrial fission proteins such as Drp1, leading to the suppression of mitochondrial fission and apoptosis. Chemerin induces cell death in granulosa cell cultures, possibly contributing to the pathogenesis of PCOS.

1.7 Overall and Specific Objectives

The overall objective of my research was to determine if the DHT-induced rat model exhibits dysregulation in mitochondrial dynamics and autophagy, and if these responses can be regulated by gonadotropin. These studies were accompanied by *in vitro* investigations of the mechanistic roles of FSH on mitochondrial fission/fusion and chemerin on granulosa cell death.

My specific objectives were:

1. To determine if PCOS is associated with dysregulation in mitochondrial fission/fusion and autophagy in a DHT-treated model, and if exogenous gonadotropin can modulate this dysregulation *in vivo*.
2. To determine if FSH can regulate mitochondrial fission/fusion proteins and morphology in granulosa cells from early antral follicles.
3. To determine if chemerin can induce programmed cell death in granulosa cells from early antral follicles.

CHAPTER 2: MATERIALS AND METHODS

2.1 Reagents and antibodies

Cell culture media (M199), fetal bovine serum (FBS), penicillin and streptomycin, fungizone, trypsin, Trypan blue and ProLong® Gold Antifade Mountant with DAPI were purchased from Life Technologies (Burlington, ON, Canada). Equine chorionic gonadotropin (eCG), 3-isobutyl-1-methylxanthine (IBMX), chloroquine diphosphate salt solid, methylthiazolyldiphenyl-tetrazolium bromide (MTT), dimethyl sulfoxide (DMSO), Hoechst 33258, anti-LC3 antibody and bovine serum albumin (BSA) were purchased from Sigma-Aldrich (Oakville, ON, Canada). Recombinant human FSH was supplied from the National Hormone and Peptide Program (Harbor-University of California, Los Angeles, Medical Center, Torrance, CA, USA). Recombinant mouse active chemerin was purchased from R&D (Minneapolis, MN, USA). Dihydrotestosterone (DHT) was provided from Steraloids Inc. (Newport, RI, USA). RBC lysis buffer was from eBiosciences (San Diego, CA, USA). Rabbit polyclonal anti-rat TOM20, rabbit polyclonal anti-rat Fis1, and mouse monoclonal anti-rat Drp1 antibodies were purchased from Santa Cruz (Dallas, TX, USA). Purified rabbit polyclonal isotype control antibody was from BioLegend (San Diego, CA, USA). Anti-rabbit Alexa Fluor® 488 secondary antibody was purchased from Invitrogen (Burlington, ON, Canada). Mouse monoclonal anti-rat Mitofusin1, mouse monoclonal anti-rat Mitofusin2, mouse monoclonal anti-rat β-actin, and mouse monoclonal anti-rat glyceraldehyde-3-phosphate dehydrogenase (GAPDH) antibodies were purchased from Abcam (Cambridge, MA, USA). Mouse monoclonal anti-rat Opa1 antibody was from BD Biosciences (Franklin, NJ, USA). Rabbit polyclonal anti-rat vinculin, rabbit polyclonal anti-rat p62, rabbit polyclonal anti-

rat phospho-Drp1 Ser637 and rabbit polyclonal anti-rat phospho-Drp1 Ser616 antibodies were obtained from Cell Signaling (Danvers, MA, USA). Horseradish peroxidase-conjugated secondary antibodies, reagents for DC™ Protein Assay and reagents for SDS-PAGE were purchased from Bio-Rad (Mississauga, ON, Canada). Enhanced chemiluminescence (ECL™) reagent, ECL Prime reagent and PageRuler™ Prestained Protein Ladder were purchased from Thermo Fisher Scientific (Burlington, ON, Canada). All other chemicals were of the highest analytical grade and were from Sigma-Aldrich.

2.2 Animal preparation

Female Sprague-Dawley rats (Charles River, Montréal, Canada) were maintained on 12-h light, 12-h dark cycles and given food and water *ad libitum*. All procedures were carried out in accordance with the Guidelines for the Care and Use of Laboratory Animals, Canadian Council on Animal Care, and were approved by the University of Ottawa Animal Care Committee.

2.3 DHT-filled SILASTIC® capsule preparation

The DHT-filled silicone capsules were prepared as previously described (Wang *et al*., 2013). SILASTIC® brand tubing (inner diameter 1.98 mm × outer diameter 3.18 mm; Dow Corning Corp., Midland, MI, USA) was cut to an appropriate length to achieve a surface area of 300 mm^2. The tubing was filled with DHT (purchase and use approved by Health Canada, authorization # 27438.02.12) via Pasteur pipette and sealed at both ends (3 mm) with adhesive, ensuring that no air bubbles were present. Control capsules were empty with sealant at both ends. After being left overnight for the sealant to dry, capsules

were submerged in 3% BSA in PBS with 0.1% NaN_3 solution for 1 d, washed three times in PBS for 5 min, then sterilized in 70% ethanol overnight. After sterilization, capsules were left to dry prior to use.

2.4 Animal surgery, DHT implantation and eCG injection

Rats at 21 d of age (reflective of the age of PCOS in humans) were implanted subcutaneously with either control (CTL) or DHT-filled continuous-release SILASTIC® capsules (83 μg/d) for 28 d to mimic the hyperandrogenic state in patients with PCOS (Sengupta, 2013; Bronstein *et al*, 2011). At 26 d post-implantation, half the rats with CTL implants and half the rats with DHT implants were injected with eCG (20 IU, i.p.) 48 h prior to sacrifice, resulting in a total of four treatment groups: CTL, DHT, eCG, or DHT + eCG.

2.5 Collection of ovaries from CTL, eCG, DHT and DHT + eCG rats

Rat ovaries were collected after euthanization via CO_2, with one ovary used for paraffin-embedded ovarian sections and the other ovary from the same rat used for TEM. The first ovary was fixed in 4% paraformaldehyde and ovarian weight/length were measured, followed by paraffin embedding, serial sectioning (4 μm) and mounting onto positively charged slides for hematoxylin and eosin (H&E) staining (to visualize ovarian structural features) or TUNEL assay (to determine granulosa cell apoptosis). The second ovary was fixed in 2.5% glutaraldehyde in 0.1 M cacodilate buffer for conventional TEM. Standard procedures for dehydration and Spurr's Low Viscosity embedding mixture (Electron Microscopy Sciences, Hatfield, PA, USA) were performed as per

manufacturer's instructions. Semi-thin and ultra-thin sections were contrasted with toluidine blue (Electron Microscopy Sciences) for follicle-stage selection, and micrographs were taken on a JEOL 1230 transmission electron microscope.

2.6 Primary culture of rat granulosa cells

Ovaries from rats at 21 d of age were collected in M199 medium supplemented with HEPES (10 mM, pH 7.4), streptomycin-penicillin (100 U/mL), and Fungizone (0.625 g/mL), and excised of excess fat and tissue prior to incubation with 6 mM EGTA for 15 min and 0.5 M sucrose for 5 min. Granulosa cells were selectively released from preantral/early antral stage follicles based on size via follicle puncture using a 26.5-gauge needle and filtered through a 40-μm nylon cell strainer (BD Biosciences) to remove cell clumps and oocytes. After wash and centrifugation (900 × g, 10 min), the viability of granulosa cells was determined by Trypan blue exclusion. Granulosa cells were plated (0.6×10^6 per well in a 6-well plate; 1×10^4 per well in a 8-well chamber slide) at 37ºC for 2 d in M199 containing 10% FBS in a humidified atmosphere of 95% air and 5% CO_2. Granulosa cells were starved overnight in M199 without FBS followed by treatment with FSH (0 - 200 ng/ml) and/or chemerin (0 - 200 ng/ml) for a designated time (0 – 48 h). IBMX (10 μM) was added 90 min prior to and during FSH treatments to prevent cAMP degradation.

2.7 Isolation of granulosa cells from CTL, DHT, eCG and DHT + eCG rats

Granulosa cells from CTL, DHT, eCG or DHT + eCG rats were collected using the same method as primary granulosa cell culture (carefully avoiding puncture of

preovulatory follicles and corpus lutea), stopping after the wash and centrifugation steps. Granulosa cells were then washed and centrifuged with PBS followed by RBC lysis buffer for 1 min. After wash and centrifugation with PBS again, cell pellets were immediately stored at -80 ºC until protein extraction.

2.8 Description of ovarian structural features and categorization of follicle stages

To classify follicles at different stages of development, we assessed the appearance of the antrum, the number of granulosa and theca cell layers, the presence of mural and cumulus granulosa cells, and relative follicle size. The presence of corpora lutea were also noted. Only follicles that had visible oocytes were considered for categorization. Primary and secondary follicles had a single- and double-layer of granulosa cells, respectively. Preantral follicles had a minimum of 3 layers of granulosa cells with no antrum. Early antral follicles had a small antrum, taking up less than half of the entire follicle size. Late antral follicles had a substantial antrum that took up at least half of the follicle. Preovulatory follicles had the largest antrum taking up most of the follicle, and had even layers of mural granulosa cells as well as cumulus granulosa cells surrounding the oocyte. Atypical follicles were small collapsed structures in which an oocyte was not detectable, and were predominantly composed of theca cells.

2.9 Determination of apoptosis in CTL, eCG, DHT and DHT + eCG rats

In situ TUNEL assay was carried out in ovarian sections using TUNEL enzyme (#11 767 305 001, Roche, Mississauga, ON, Canada) and fluorescent TUNEL label (#11 767 291 910, Roche, Mississauga, ON, Canada) as per the manufacturer's instructions.

Briefly, after deparaffinization and hydration (with xylene, 100% ethanol, 95% ethanol, 80% ethanol, 70% ethanol, and distilled water in that order), the sections were permeabilized in 0.1% sodium citrate solution containing 0.1% of Triton X-100 for 8 min on ice. The sections were incubated in a combined solution of TUNEL enzyme and TUNEL label (5:45 proportion, respectively) during 1 h at 37°C, washed with PBS and mounted using ProLong® Gold Antifade Mountant with DAPI. The positive control of the reaction was performed using DNAse (1000 U/ml) diluted in 0.05 M Tris-HCl buffer (pH 7.5) containing 0.010 M $MgCl_2$, while the negative control consisted of incubation with the TUNEL label without the TUNEL enzyme.

Images were obtained (× 20 objective) on a Zeiss® Axioplan 2 Imaging microscope, using Axiovision® Release 4.8.2 imaging software. Follicles with visible oocytes were classified as preantral, early antral, late antral and preovulatory stage, and TUNEL positivity was determined if $\geq$ 50% of the granulosa cells had positive staining. The distinction between TUNEL positive and TUNEL negative follicles was clear, as the vast majority of TUNEL negative follicles had no positive signal. TUNEL positivity was expressed per follicle stage as the mean number of TUNEL positive follicles over total follicles, obtained from the mean of three representative slides per rat (1 ovary per rat). The primary researcher was blinded to the treatment groups, with images obtained by a different researcher to avoid bias.

2.10 Mitochondrial morphology assessment of CTL, eCG, DHT and DHT + eCG rats

After whole ovaries were imaged by TEM, mitochondrial morphology in granulosa

cells from preantral/antral follicles was categorized as either: a) rod-shaped appearance; b) circular appearance; c) constricted appearance or d) connected appearance. Mitochondria with rod-shaped appearance are elongated and have greater length compared to width, but do not exceed 1500 nm in length. The membranes and inner cristae structures of these mitochondria are clear and well defined. Mitochondria with circular appearance have clearly outlined mitochondrial membranes, though the interior can have bright (unhealthy) areas and poorly defined inner cristae structures. Mitochondria with constricted appearance are "dumb-bell shaped", with an area of reduced width that appears constricted or "pinched in" (non-uniform width). The membrane is still intact and clear across this region of constriction, but interior structures including cristae structures are not well defined and bright areas are common. Mitochondria with connected appearance have at least one of the following characteristics: a) highly elongated with the length exceeding 1500 nm; b) mitochondria that appear "forked" or misshapen (non-rod); or c) mitochondria that interact either distally or laterally. The clarity of the membrane and interior structures of connected mitochondria is variable. Each category of mitochondria is expressed as a percentage of total mitochondria assessed per treatment group, and a minimum of 275 mitochondria was assessed per treatment group.

2.11 Protein extraction and Western blot

Protein extracts were obtained by directly adding 100 µl hot lysis buffer (10 mM Tris, pH 7.4; 1% sodium dodecyl sulfate [SDS], 1mM sodium orthovanadate) to each well in a 6-well plate followed by rapidly scraping and transferring to a microcentrifuge

tube. In CTL, DHT, eCG and DHT + eCG granulosa cells, hot lysis buffer was added directly to the microcentrifuge tube and the cell pellet was re-suspended. Extracts were then boiled for 5 min followed by sonication, centrifugation (12,000 × g, 5 min) and collection of the supernatant. Protein concentrations were determined by BioRad DC® protein assay kit. Whole cell lysates (20 µg) were subjected to SDS-PAGE and proteins were electrophoretically transferred to a nitrocellulose membrane (GE Healthcare Lifesciences, Mississauga, ON, Canada).

After blocking with 5% skim milk in TBST (0.05% Tween-20 in 10 mM Tris; 0.15 M NaCl, pH 7.4) at room temperature for 1 h, membranes were incubated overnight at 4º C with antibodies against Drp1 (1:1000), phospho-Drp1 Ser616 (1: 1000), phospho-Drp1 Ser637 (1:500), LC3 (1:1000), p62 (1:500), Opa1 (1:1000), Mitofusin1 (1:1000), Mitofusin2 (1:1000), and Fis1 (1:1000) in TBST with constant agitation. Membranes were then treated with 1:5000 horseradish peroxidase-conjugated rabbit or mouse secondary antibodies for 1 h at room temperature, washed three times with TBST, then visualized using enhanced chemiluminescence according to the manufacturer's instructions. The intensity of the immunoreactive bands obtained by both CL-Xposure film (Thermo Fisher Scientific) and VersaDoc® were determined by densitometry quantification using AlphaEaseFC (Alpha Innotech, San Leandro, CA, USA) and normalized to GAPDH (1:10 000), β-actin (1:10 000) or vinculin (1:10 000) loading controls depending on the molecular weight of the protein.

2.12 Cell viability assay

At the end of the culture period, granulosa cells attached to the culture plate were

trypsinized (0.05% trypsin; 1-2 min at 37º C) and pooled with floating cells, pelleted, re-suspended and counted. Using a 96-well plate, 100 µl containing 2×10^5 cells were added per well. MTT solution (5 mg/ml in PBS) was then added in each well (10 µl) and incubated at 37ºC for 4 h in a humidified chamber. To solubilize the converted formazan dye, 100 µl DMSO was added per well and agitated for 10 min in the dark. Absorbance was measured at a wavelength of 570 nm and cell viability was expressed as a percentage compared to untreated control.

2.13 Determination of apoptosis *in vitro*

Attached and floating cells, collected as described above, were pooled and re-suspended in 4% paraformaldehyde containing Hoechst 33528 (6.25 µg/ml; overnight at 4º C). Cells were then spotted onto slides and assessed for typical nuclear morphology of apoptosis (nuclear shrinkage, condensation and fragmentation) under fluorescence microscopy. Healthy and apoptotic cells were counted in blinded conditions, and apoptotic cells were expressed as a percentage of total cells. A minimum of 400 cells was counted per treatment group.

2.14 Immunofluorescence and mitochondrial morphology assessment *in vitro*

At the end of the culture period in an 8-well glass culture slide (BD Biosciences), granulosa cells were rinsed with PBS and fixed in 4% paraformaldehyde overnight at 4º C. Cells were permeabilized with 0.25% Triton X-100 in PBS, washed in 0.1% PBS-T (TWEEN® 20) and blocked with 3% BSA prior to application of rabbit polyclonal TOM20 antibody (1:200) and Alexa Fluor® 488 goat anti-rabbit secondary antibody

(1:500) for mitochondrial visualization. Images were obtained (× 40 objective) on a Zeiss® Axioplan 2 Imaging microscope using Axiovision® Release 4.8.2 imaging software. Mitochondrial phenotype of each cell was categorized as either tubular or fragmented. Tubular mitochondria appeared as highly connected, long and tube-like while fragmented mitochondria were distinguished by short, rounded, circular morphology. Cells containing at least 8 fragmented mitochondria were classified as fragmented (Farrand *et al*., 2013b), and were expressed as percentage of total cells. At least 300 cells were counted per treatment group with the researcher blinded during image acquisition and morphology assessment.

2.15 cAMP accumulation assay

At the end of the incubation period, spent medium was collected, centrifuged (900 × g, 2 min, 4ºC) and stored at -80ºC. cAMP concentration was determined using an enzyme immunoassay kit (EIA; Enzo Lifesciences, Farmingdale, NY, USA), as per the manufacturer's instructions. The detection limitation of cAMP was 0.30 pmol/ml, and the intra- and inter-assay coefficients of variation were 11% and 14%, respectively.

2.16 Statistical analysis

Data are presented as mean ± SEM of a minimum of three independent experiments and are indicated in the figure legends. Three-way ANOVA was performed using SigmaPlot 11.0 statistical software (San Jose, CA, USA), while all other statistical analyses were performed using GraphPad Prism® 6.0 statistical software (San Diego, CA, USA). One-way ANOVA was used to assess the effects of a single variable while

two-way ANOVA and three-way ANOVA were used to assess the effects and interactions of two or three variables respectively, and multiple comparisons were achieved by Bonferroni *post hoc* test. Significant difference was defined at $P < 0.05$ (* or #).

CHAPTER 3: RESULTS

It is well established that the three-month DHT-induced rat model for PCOS has a smaller ovarian size and a higher number of ovarian structural abnormalities than control rats (Mannerås *et al*., 2007; Hossain *et al.* 2013; Kim *et al.*, 2013). To examine the ovarian dysregulation and the possible regulatory mechanisms involved in PCOS with a shorter DHT treatment, a hyperandrogenized rat model (1-month DHT-implant), which exhibits many of the phenotypes of human PCOS (unpublished findings, Nivet *et al*), was investigated. Since controlled stimulation with gonadotropin is also known to ameliorate certain phenotypes of PCOS (Cheung *et al*, 2002; Hossain *et al.* 2013), we also examined the possible influence of equine chorionic gonadotropin (eCG, i.p., 48 h), on a number of morphological and biochemical parameters in both sham-control (CTL) and DHT-implanted rats in the following *in vivo* design: CTL, DHT, eCG and DHT + eCG.

Although *in vivo* studies using a DHT-induced rat model are important in recapitulating many phenotypes of a PCOS patient, there can be limitations when attempting to determine molecular mechanisms in such a chronic, confounding system. Therefore, *in vitro* studies using granulosa cells from early antral follicles from 21-day old rats were carried out to initially investigate the signaling pathways of gonadotropin (e.g. FSH) and other regulatory factors (e.g. chemerin).

3.1 Ovarian size and structural features were affected in a one-month DHT-induced rat model

To determine if ovarian size and morphology are affected by one-month DHT treatment, ovarian length and weight were measured (**Fig. 3.1**). In support of unpublished

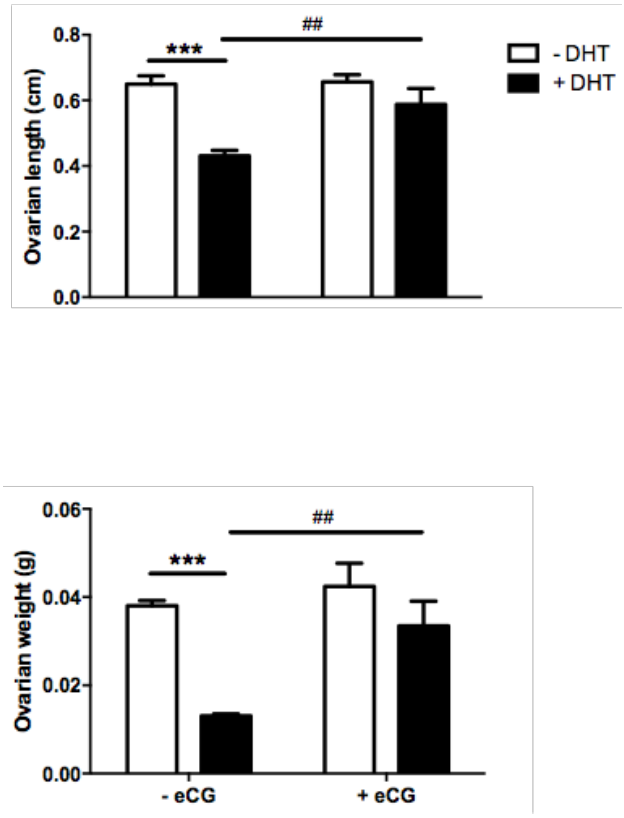

Figure 3.1: DHT reduced ovarian length and weight, which was attenuated by gonadotropin injection

Rats were surgically implanted with sham control capsule or DHT (83 μg/d) time-release capsules for 4 w and injected with eCG (20 IU i.p./rat) 48 h prior to sacrifice. Fresh ovaries from each rat were measured for length and weight. Data are presented as mean ± SEM of eight biological replicates, and analyzed by two-way ANOVA and Bonferroni *post hoc* test. ***, $P < 0.001$ vs. CTL. ##, $P < 0.01$ vs. DHT alone.

results from our own laboratory (Nivet *et al*., unpublished), DHT treatment significantly reduced both ovarian length (two-way ANOVA: DHT, $P < 0.001$) and weight (two-way ANOVA: DHT, $P < 0.001$) in our one-month DHT-treated rat model. The Bonferroni *post hoc* test indicated that the DHT group was significantly different than the CTL group for both length and weight (Bonferroni: $P < 0.001$ vs. CTL).

Next, whole ovarian sections were visualized following H&E staining to discern changes in structural features (as described in the Methods section) in our DHT-induced model (**Fig. 3.2**). Compared to the wide range of follicular stages and corpora lutea observed in the ovaries of control rats, the ovaries of DHT-treated rats had no corpora lutea and very few large follicles, presumably at late antral and/or preovulatory stages. Although the DHT ovary had high number of preantral and early antral follicles, its most distinctive feature was the accumulation of many atypical follicles, which are described as small structures predominantly composed of theca cells with no discernible oocyte (Kim *et al*., 2013).

3.2 Early antral granulosa cell apoptosis was induced in one-month DHT-treated rats

To determine the effects of one-month DHT treatment on rat granulosa cell apoptosis, whole ovarian sections were assessed using a fluorescent TUNEL stain. Follicle with observable oocytes were classified into preantral, early antral, late antral or preovulatory stages as described in the Methods section, and TUNEL positivity was determined if ≥ 50% of the granulosa cells had positive staining (**Fig 3.3A**; the number of follicles counted per group are indicated in **Table 3.1**).

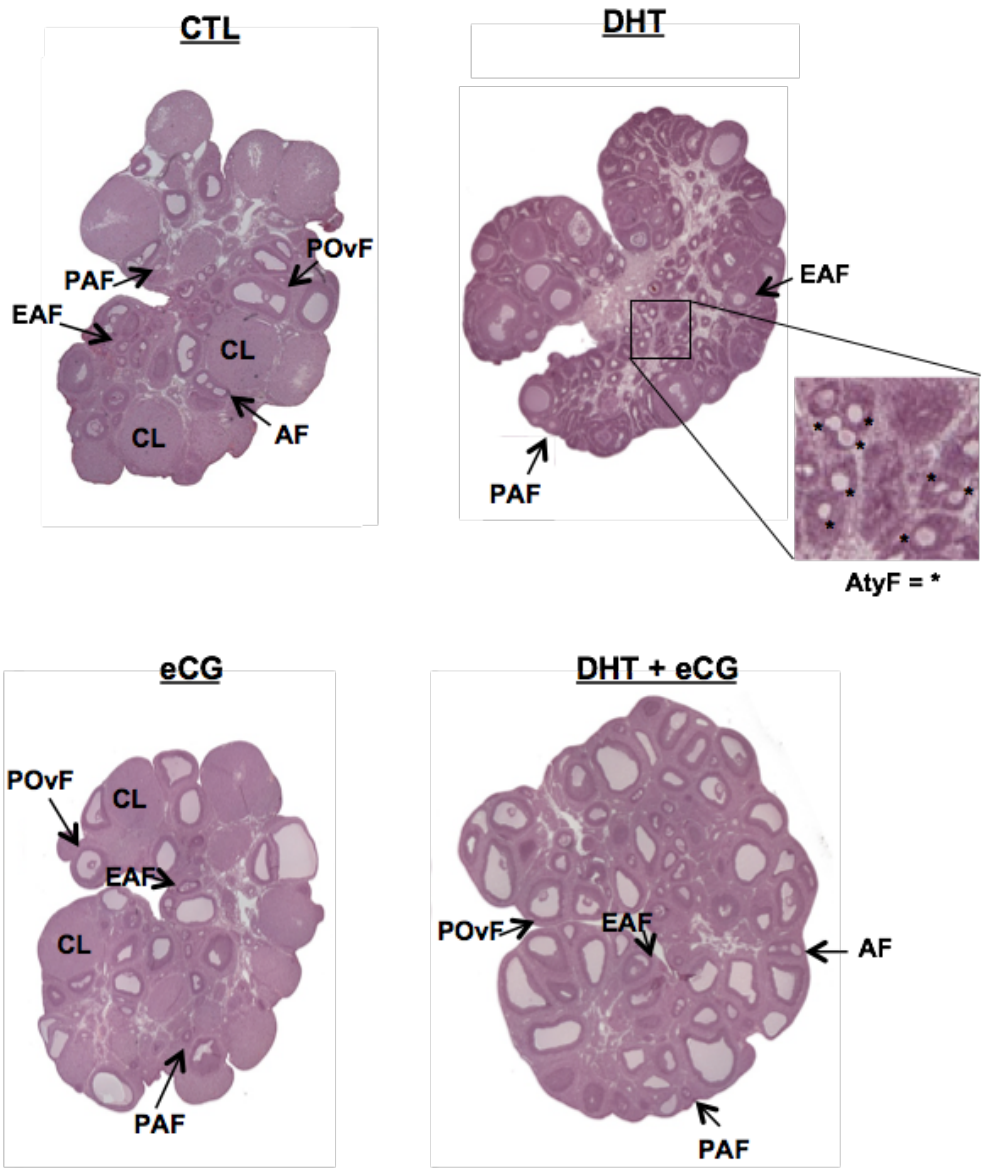

Figure 3.2: DHT-induced ovarian structural abnormalities were modulated by gonadotropin

After 1-month DHT implantation (83 μg/d) and eCG injection (20 IU/rat; i.p.) 48 h prior to sacrifice, representative sections of whole ovaries in each treatment group were visualized by H&E staining and variations in ovarian structural features were observed. PAF, preantral follicle; EAF, early antral follicle; POvF, preovulatory follicle; CL, corpus luteum; AtyF, atypical follicle.

As illustrated in **Fig. 3.3B**, DHT had a significant effect on granulosa cell apoptosis in early antral stage follicles (two-way ANOVA: DHT, $P = 0.001$), but not in follicles at preantral (two-way ANOVA: DHT, $P > 0.05$), late antral (two-way ANOVA: DHT, $P > 0.05$), or preovulatory stage (two-way ANOVA: DHT, $P > 0.05$). DHT rats were determined to be significantly different than CTL rats in early antral (Bonferroni: $P < 0.01$ vs. CTL) and late antral (Bonferroni: $P < 0.05$ vs. CTL) follicles.

3.3 Morphologic and molecular indicators demonstrated increased mitochondrial fission in granulosa cells of DHT-treated rats

Excessive mitochondrial fission can lead to the induction of apoptosis associated with disease pathogenesis (Westermann, 2010; Archer *et al*., 2013; Shenouda *et al*., 2011). To examine the morphologic characteristics of mitochondria in the androgenized rat model, the ultrastuctural morphology of granulosa cells in ovarian sections were examined by transmission electron microscopy (TEM). We categorized mitochondrial morphology in preantral/antral granulosa cells as having a rod-shaped, circular, constricted or connected appearance (**Fig. 3.4A**). Mitochondria with a rod-shaped appearance are elongated but do not exceed 1500 nm in length, and typify a normal, baseline state that does not undergo fission or fusion. Mitochondria that appear circular or constricted (dumb-bell shaped with "pinched in" membrane) can be morphologic indicators of mitochondrial fission post-fragmentation or mid-fragmentation, respectively. Mitochondria with a connected appearance must be at least exceed 1500 nm in length, have a forked or misshapen appearance and/or interact laterally/distally to each other, and are indicative of moments throughout the process of mitochondrial fusion.

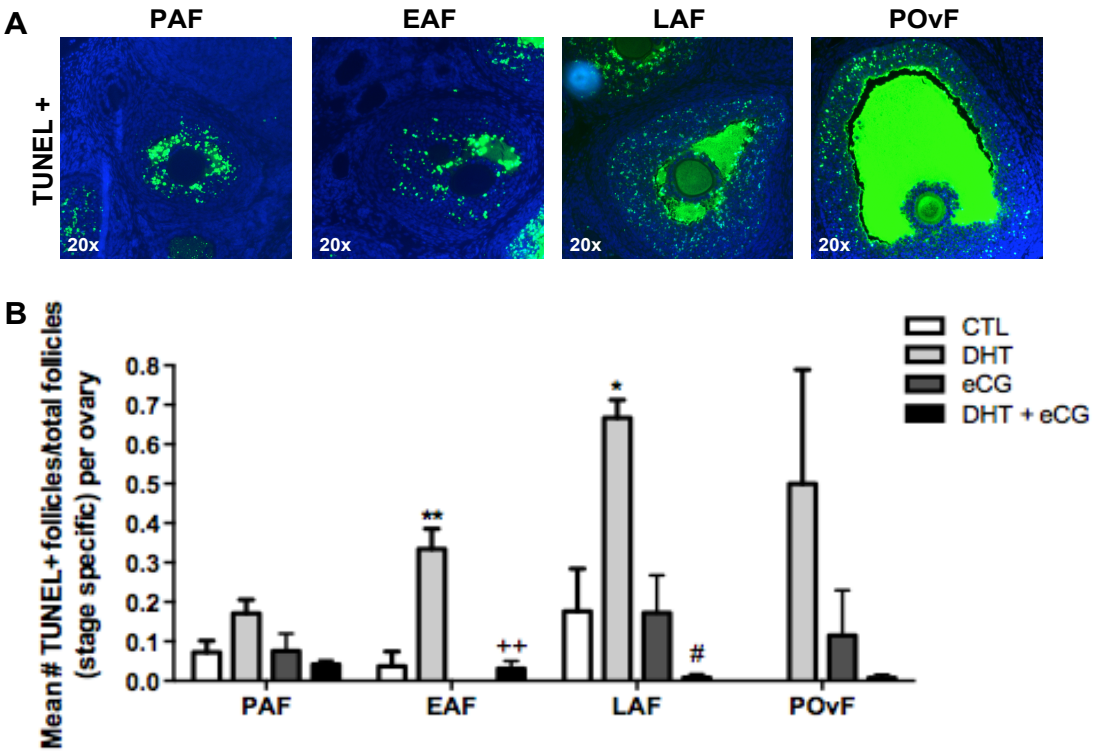

Figure 3.3: DHT induced granulosa cell apoptosis, which was attenuated by gonadotropin

(**A**) Representative images of TUNEL positive (+) preantral, early antral, late antral and preovulatory follicles from a 1-month DHT-induced rat ovary.

(**B**) After 1-month DHT implantation (83 µg/d) and 48 h after eCG injection (20 IU/rat), granulosa cell apoptosis was determined in PAF (preantral follicle), EAF (early antral follicle), LAF (late antral follicle) and POvF (preovulatory follicle) of whole ovarian sections (5 µm thick) by fluorescent TUNEL assay, and was expressed as a ratio of mean number of TUNEL+ follicles over total ovarian follicles per rat* (*Rat = 1 ovary per rat/ 3 representative slides from whole ovary/ 3 sections per slide; number of follicles/group indicated in **Table 3.1**). Data are presented as mean ± SEM of three biological replicates, and analyzed by two-way ANOVA and Bonferroni *post hoc* test. *, $P < 0.05$; **, $P < 0.01$ vs. CTL. #, $P < 0.05$ vs. DHT. ++, $P < 0.01$ vs. eCG.

Table 3.1: Number of follicles counted per group for Fig. 3.3

	CTL	DHT	eCG	DHT + eCG
PAF	10	24	9	9
EAF	9	14	9	15
LAF	5	8	6	12
POvF	2	1	5	8

As shown in **Fig. 3.4B**, two-way ANOVA indicates DHT significantly decreased the proportion of rod-shaped (DHT, $P = 0.001$) and connected mitochondria (DHT, $P < 0.001$), and increased the proportion of circular (DHT, $P < 0.001$) and constricted mitochondria (DHT, $P < 0.001$). Bonferroni analysis indicate that DHT rats had significantly less rod-shaped mitochondria ($P < 0.001$ vs. CTL) and significantly more circular ($P < 0.01$ vs. CTL) and constricted ($P < 0.001$ vs. CTL) mitochondria compared to CTL rats.

In addition to these mitochondrial morphology studies, we examined molecular indicators of mitochondrial fission in granulosa cells isolated from our *in vivo* treated rats. The activity of Drp1, a mediator of mitochondrial fission, is dependent on its phosphorylation status at its Ser616 (stimulates fission) and Ser637 (inhibits fission) sites (Cribbs and Strack, 2007). Therefore, we examined both the total and phosphorylated contents of Drp1 by Western blot analysis. As illustrated in **Fig. 3.5**, DHT significantly increased total Drp1 (DHT, $P = 0.001$) while phospho-Ser616 content remained unaffected (DHT, $P > 0.05$) relative to total Drp1 (two-way ANOVA). There were no observable bands for phospho-Drp1 Ser637. Bonferroni *post hoc* results were non-significant in phospho-Drp1 Ser616 and total Drp1.

3.4 DHT increased autophagosomal protein content

Although autophagy has been associated with granulosa cell death and follicular atresia during folliculogenesis, its dysregulation in the pathogenesis of PCOS has not been studied (Choi *et al*., 2010; Choi *et al*., 2011). In the present studies, we examined the autophagy markers LC3I, LC3II and p62 in isolated granulosa cells from our *in vivo*

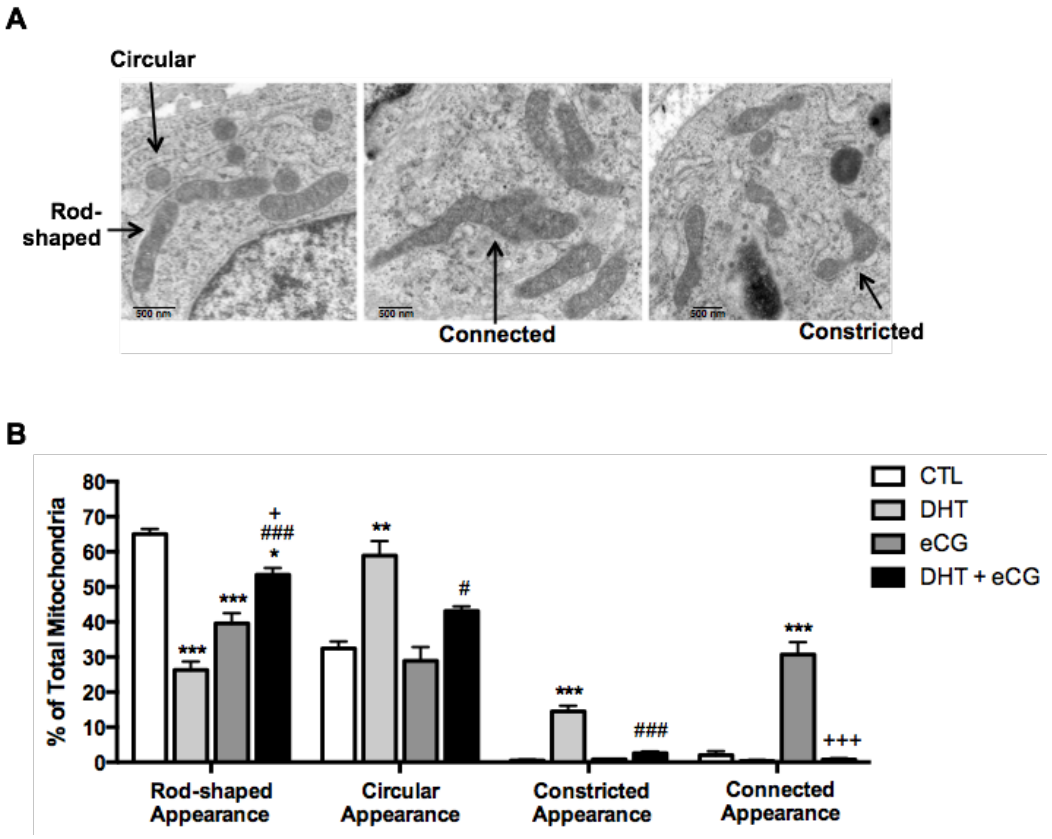

Figure 3.4: DHT-induced circular and constricted mitochondrial appearance were reduced by gonadotropin

(**A**) Representative examples of mitochondrial phenotypes (rod-shaped, circular, constricted or connected appearance) in transmission electron microscopy (TEM) images. (**B**) After 1-month DHT implantation (83 μg/d) and 48 h following eCG (20 IU/rat), TEM images of whole ovaries from each treatment group were captured and mitochondrial morphology was assessed. A minimum of 275 mitochondria was assessed per treatment group. Data are presented as mean ± SEM of three biological replicates, and analyzed by two-way ANOVA and Bonferroni *post hoc* test. *, $P < 0.05$, **, $P < 0.01$, ***, $P < 0.001$ vs. CTL; #, $P < 0.05$, ###, $P < 0.001$ vs. DHT; +, $P < 0.05$, +++, $P < 0.001$ vs. eCG. Scale bar = 500 nm.

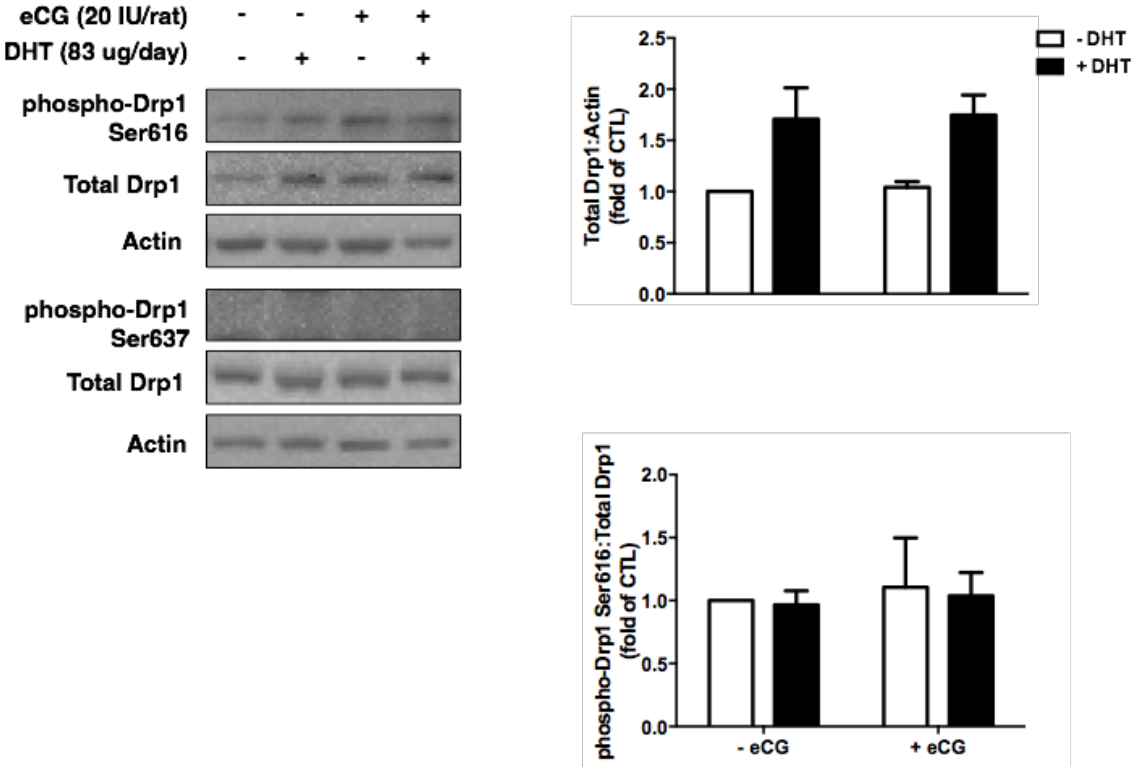

Figure 3.5: Granulosa cells in one-month DHT-induced rats exhibited increased total Drp1 content

After 1-month DHT implantation (83 μg/d) and 48 h after eCG (20 IU/rat), granulosa cells were isolated and protein contents of 53hosphor-Drp1 Ser616, 53hosphor-Drp1 Ser637 and total Drp1 were assessed by Western blot. Data are presented as mean ± SEM of six independent experiments, and analyzed by two-way ANOVA and Bonferroni *post hoc* test.

DHT-treated rats by Western blot (**Fig. 3.6**). DHT had no significant effect on LC3II:LC3I ratio (two-way ANOVA: DHT, $P > 0.05$) or p62 content (DHT, $P > 0.05$), but significantly increased LC3I content (DHT, $P = 0.047$) and trended towards increased LC3II content (DHT, $P = 0.060$), as indicated by two-way ANOVA. There were no significant Bonferroni *post hoc* results for this experiment ($P > 0.05$).

3.5 eCG modulated DHT-induced changes in ovarian morphology, granulosa cell apoptosis and mitochondrial morphology

In addition to studying the ovarian changes induced by DHT *in vivo*, we also investigated the possible modulatory role of gonadotropin on these ovarian responses. As shown in **Fig. 3.1**, two-way ANOVA indicate that eCG treatment alone and in combination with DHT had a significant effect on ovarian length (DHT, $P < 0.001$; eCG, $P = 0.013$; eCG × DHT, $P = 0.021$) and weight (DHT, $P < 0.001$; eCG, $P = 0.003$; eCG × DHT, $P = 0.048$). Bonferroni *post hoc* results also indicate that eCG mitigated the DHT-induced down-regulation of ovarian length ($P < 0.01$) and weight ($P < 0.01$). Ovaries exposed to eCG alone had a high number of corpus lutea and large follicles (late antral/preovulatory; **Fig. 3.2**), suggesting that these animals have ovulated. eCG also appeared capable of eliminating all atypical follicles and reactivating folliculogenesis in DHT-treated animals, as evident by the high number of late antral and preovulatory follicles. However, no corpus lutea were present in the DHT-treated rats following eCG injection. Statistical analyses of the DHT effects, eCG effects and eCG × DHT interaction on granulosa cell apoptosis by two-way ANOVA (assessing these parameters at different follicle stages in separate analyses) indicates the following: early antral

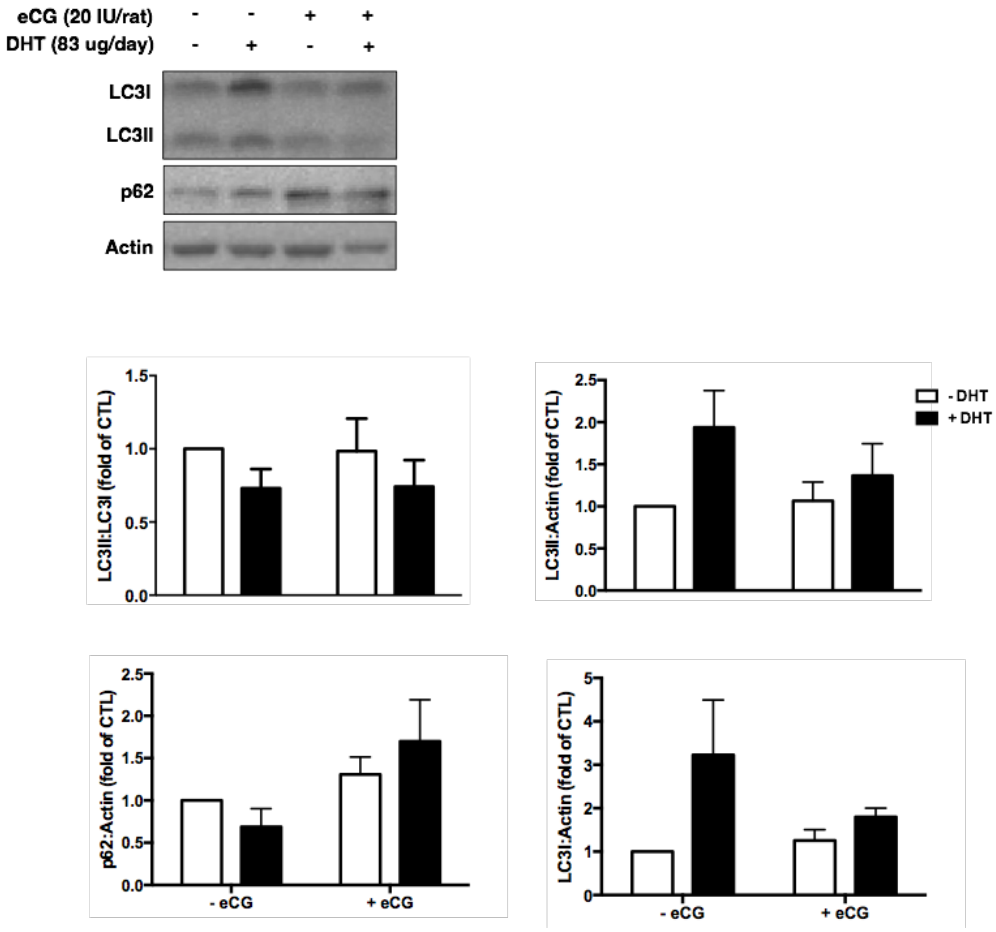

Figure 3.6: LC3II protein content was up-regulated by DHT treatment

After 1-month DHT implantation (83 μg/d) and eCG injection (20 IU/rat) 48 h prior to sacrifice, granulosa cells were isolated from rat ovaries and Western blots were performed to determine the protein contents of LC3I/II and p62 as well as LC3II:LC3I ratio. Data are presented as mean ± SEM of six independent experiments, and analyzed by two-way ANOVA and Bonferroni *post hoc* test.

(P = 0.001, P < 0.001, and P = 0.004, respectively), late antral (P > 0.05, P = 0.002, and P = 0.003, respectively), preantral (P > 0.05, P > 0.05, and P > 0.05, respectively) and preovulatory follicles (P > 0.05, P > 0.05, and P > 0.05) as seen in **Fig. 3.3B**. Specifically, DHT + eCG rats had increased granulosa cell apoptosis compared to eCG rats in early antral follicles (Bonferroni: P < 0.01 vs. eCG) and significantly decreased granulosa cell apoptosis compared to DHT rats in late antral follicles (Bonferroni: P < 0.05 vs. DHT).

The modulatory effects of eCG on DHT-induced changes in granulosa cell apoptosis appeared to be associated with its action on DHT-induced mitochondrial fission. Statistical analyses of the DHT effects, eCG effects and eCG × DHT interaction on mitochondrial appearance by two-way ANOVA **(Fig. 3.4B)** indicates the following: rod-shaped (P = 0.001, P > 0.05, and P < 0.001, respectively), circular (P < 0.001, P = 0.014, and P = 0.084, respectively) constricted (P < 0.001, P < 0.001, and P < 0.001, respectively) and connected mitochondria (P < 0.001, P < 0.001, and P < 0.001, respectively). Analysis by Bonferrroni *post hoc* test indicate a significantly higher proportion of connected mitochondria (P < 0.001 vs. CTL) in eCG compared to CTL rats, and significantly lower proportion of rod-shaped mitochondria (P < 0.001 vs. CTL). DHT + eCG rats had a significantly reduced proportion of circular (P < 0.05 vs. DHT) and constricted (P < 0.001 vs. DHT) mitochondria compared to DHT rats alone.

Despite these promising morphological results, Western blot analysis indicated that only DHT, but not eCG, had significant effects on the contents of total Drp1 (DHT, P = 0.001, eCG, P > 0.05; eCG × DHT P > 0.05) in granulosa cells (**Fig. 3.5**). Neither had a significant effect on phospho-Drp1 Ser616 (DHT, P > 0.05; eCG, P > 0.05; eCG × DHT

P > 0.05). There were no significant Bonferroni results (P > 0.05).

Autophagy markers were also assessed in these isolated granulosa cells, as shown in **Fig. 3.6**. Two-way ANOVA indicate that eCG, but not DHT, significantly increased granulosa cell p62 content (DHT, P > 0.05, eCG, P = 0.033; eCG × DHT P > 0.05). However, it had no significant influence on LC3II:LC3I ratio (DHT, P > 0.05, eCG, P > 0.05; eCG × DHT P > 0.05), LC3I content (DHT, P = 0.047, eCG, P > 0.05; eCG × DHT P > 0.05), or LC3II content (DHT, P = 0.06, eCG, P > 0.05; eCG × DHT P > 0.05). There were no significant effects indicated by the Bonferroni *post hoc* test.

3.6 FSH induced cell viability and cAMP production in granulosa cells *in vitro*

We first examined the role of FSH as a cell survival factor by assessing cell viability in an FSH concentration-response study of early antral granulosa cells incubated in the presence of the phosphodiesterase inhibitor isobutylmethylxanthine (IBMX; added 90 min prior to FSH), using the MTT assay. FSH significantly increased granulosa cell viability (**Fig. 3.7**; one-way ANOVA: P < 0.001), particularly at 50 ng/ml (P < 0.05 vs. 0 ng/ml) and 100 ng/ml (P < 0.001 vs. 0 ng/ml) [Bonferroni]. We also determined if FSH increases cAMP production in our early antral granulosa cell cultures by measuring cAMP concentration in spent medium by EIA, which is reflective of cellular cAMP concentration. As shown in **Fig. 3.8**, FSH significantly stimulated cAMP production in granulosa cells compared to basal levels (two-way ANOVA: FSH, P < 0.001; Time, P < 0.001; FSH × Time, P < 0.001). Bonferroni *post hoc* test shows significantly elevated cAMP concentration in FSH and FSH + chemerin rats compared to CTL rats at all time points (P < 0.001 vs. CTL) and compared to its treatment at 0.25 h (P < 0.001 vs. 0.25 h).

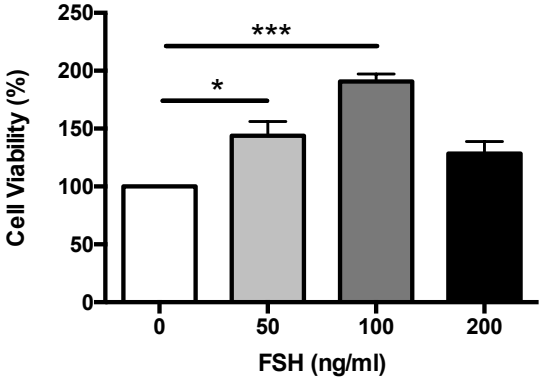

Figure 3.7: FSH increased granulosa cell viability *in vitro*

Early antral granulosa cell cultures obtained from 21-day old rats were pre-treated with IBMX (10 μM) 90 min prior to and during FSH treatment (0, 50, 100, 200 ng/ml) for 24 h. MTT assay was performed to assess cell viability. Data are presented as mean ± SEM of three independent experiments, and analyzed by one-way ANOVA and Bonferroni *post hoc* test. *, $P < 0.05$ vs. CTL; ***, $P < 0.001$ vs. untreated control (FSH = 0).

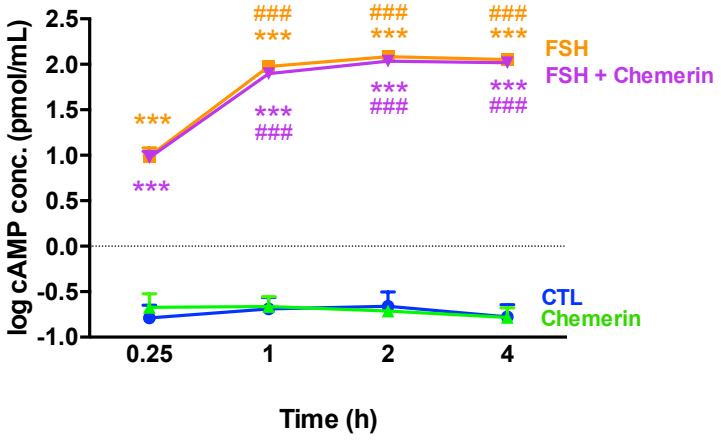

Figure 3.8: FSH markedly increased granulosa cell cAMP production *in vitro*

After pre-treating primary granulosa cell cultures with IBMX (10 μM) for 30 min, chemerin was added (100 ng/ml) for 1 h followed by FSH (100 ng/ml) in co-treatment for 0.25, 1, 2 and 4 h. EIA assay was performed to determine cAMP concentration in the spent medium. Data are log transformed and presented as mean ± SEM of three independent experiments, and analyzed by three-way ANOVA and Bonferroni *post hoc* test. ***, $P < 0.001$ vs. CTL. ###, $P < 0.001$ vs. 0.25 h.

3.7 FSH regulated Drp1 phosphorylation, but not Mfn1, Mfn2, Opa1, or Fis1 mitochondrial dynamic regulators *in vitro*

Although we failed to observe any significant effects of eCG on total or phosphorylated Drp1 contents *in vivo*, it is possible that the regulatory effects of eCG on Drp1 phosphorylation were missed as phosphorylation often occurs within a few hours. To determine if FSH had an effect on Drp1 phosphorylation *in vitro*, the contents of phospho-Drp1 Ser616 (**Fig. 3.9A)** and phospho-Drp1 Ser637 (**Fig. 3.9B)** were assessed by Western blot and densitometric analysis in a short time-course study. FSH significantly reduced phospho-Drp1 Ser616 content and increased phospho-Drp1 Ser637 content (three-way ANOVA results for **Fig. 3.9** are detailed in **Table 3.2)**. Our Bonferroni results for phospho-Drp1 Ser616 and Ser637 are described symbolically in **Fig. 3.9**.

A follow-up concentration-response study of FSH with IBMX was also performed without chemerin **(Fig. 3.10)** and FSH significantly increased phospho-Drp1 Ser637 ($P < 0.001$) and decreased phospho-Drp1 Ser616 ($P < 0.001$) as indicated by one-way ANOVA. These results are supported by the Bonferroni *post hoc* test described symbolically in **Fig. 3.10**. Total Drp1 content was unaffected by FSH treatment (one-way ANOVA: $P > 0.05$).

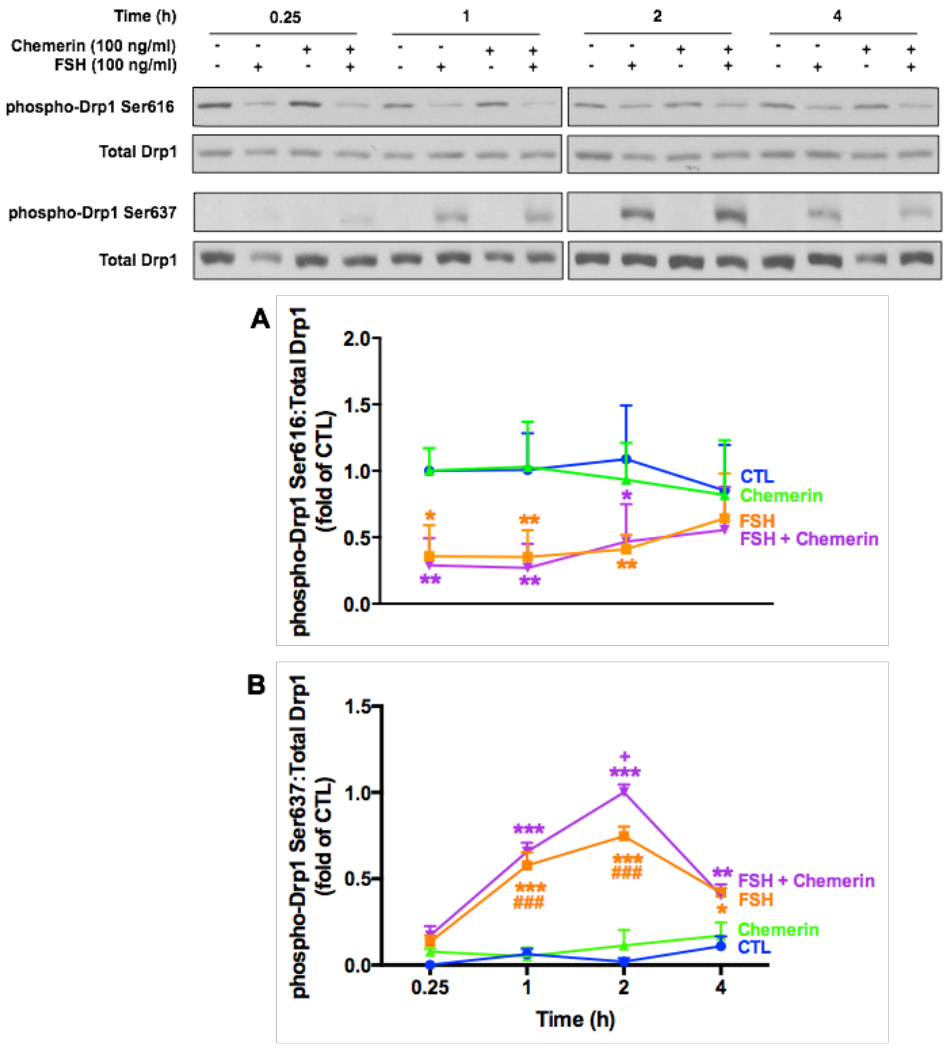

Figure 3.9: FSH regulated Drp1 phosphorylation at its stimulatory (Ser616) and inhibitory (Ser637) sites

Granulosa cell cultures were treated with IBMX (10 µM) 30 min prior and during to chemerin pre-treatment (0, 100 ng/ml; 1 h) and FSH treatment (0, 100 ng/ml; 0.25, 1, 2 and 4 h). Protein contents of phospho-Drp1 Ser616 (**A**) and phospho-Drp1 Ser637 (**B**) were determined by Western blot. Data are presented as mean ± SEM of three to four independent experiments, and analyzed by three-way ANOVA and Bonferroni *post hoc* test. (**A**) *, $P < 0.05$; **, $P < 0.01$ vs. CTL; (**B**) *, $P < 0.05$; **, $P < 0.01$; ***, $P < 0.001$ vs. CTL. ###, $P < 0.001$ vs. 0.25 h. +, $P < 0.05$ vs. FSH only group.

Table 3.2: Three-way ANOVA p-values for Fig. 3.9

	FSH	Time	FSH × Time	Chemerin	Chemerin × Time	Chemerin × FSH	Chemerin × FSH × Time
phospho-Drp1 Ser616:Total Drp1	< 0.001	> 0.05	0.034	> 0.05	> 0.05	> .0.05	> 0.05
phospho-Drp1 Ser637:Total Drp1	< 0.001	< 0.001	< 0.001	0.010	> 0.05	> 0.05	> 0.05

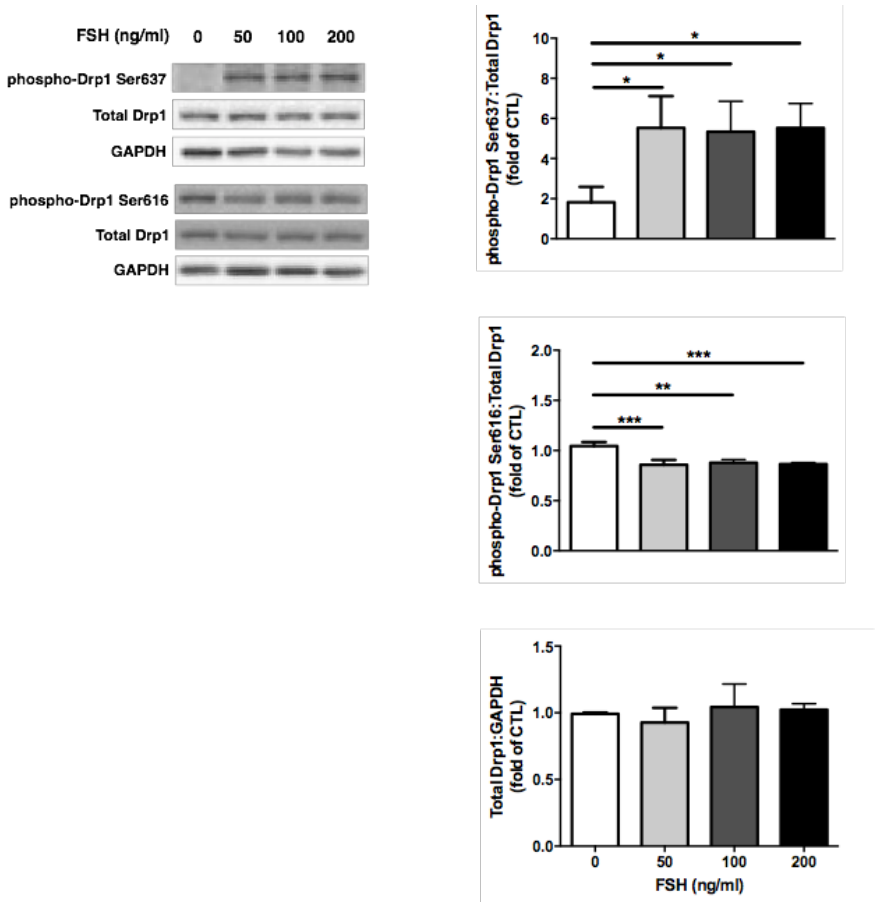

Figure 3.10: FSH regulated granulosa cell Drp1 phosphorylation by suppressing phospho-Drp1 Ser616 content and increasing phospho-Drp1 Ser637 content

Granulosa cells were pre-incubated with IBMX (10 μM; 90 min) and incubated with various concentrations of FSH (0, 50, 100 and 200 ng/ml; 2 h). Protein contents of phospho-Drp1 Ser616, phospho-Drp1 Ser637 and total Drp1 were determined by Western blot. Data are presented as mean ± SEM of three independent experiments, and analyzed by one-way ANOVA and Bonferroni *post hoc* test. *, $P < 0.05$; **, $P < 0.01$; ***, $P < 0.001$ vs. CTL.

To determine if FSH regulates mitochondrial fusion proteins, the total contents of Mfn1, Mfn2, and Opa1 were assessed by Western blot in a time-course study. As indicated in **Fig. 3.11** by two-way ANOVA, duration of incubation, but not FSH ($P > 0.05$), had a significant effect on the contents of Mfn1 ($P < 0.05$) and total Opa1 ($P = 0.006$) as they decrease over time with serum starvation. Mfn2 was not significantly affected by FSH or incubation duration ($P > 0.05$). We also assessed whether FSH can downregulate the protein content of the mitochondrial fission regulator Fis1 by Western blot in both time-course and concentration-response studies. Although FSH significantly decreased Fis1 content in the time-course study (**Fig. 3.12A**; two-way ANOVA: FSH, $P = 0.029$; Time, $P = 0.017$; FSH × Time, $P > 0.05$), particularly at 24 h (Bonferroni: $P < 0.05$ vs. CTL), no significant effect of FSH on Fis1 content was found in the follow-up FSH concentration-response study (**Fig. 3.12B**; one-way ANOVA: $P > 0.05$).

3.8 FSH did not suppress mitochondrial fragmentation in granulosa cells *in vitro*

Although FSH had been shown to regulate Drp1 phosphorylation and promote granulosa cell survival, its role on the suppression of mitochondrial fragmentation needed to be determined. The effect of FSH on mitochondrial morphology in granulosa cells was assessed by immunofluorescence (IF) microscopy of the mitochondrial marker TOM20. As presented in **Fig. 3.13A**, granulosa cells were categorized as either having tubular (long, highly-connected, tube-like) or fragmented (short, rounded, circular) mitochondria, indicative of mitochondrial fusion and fission, respectively. With the exception of incubation duration ($P < 0.001$), there had no significant effects of FSH in the absence and presence of IBMX ($P < 0.05$) indicated by two-way ANOVA (**Fig 3.13**).

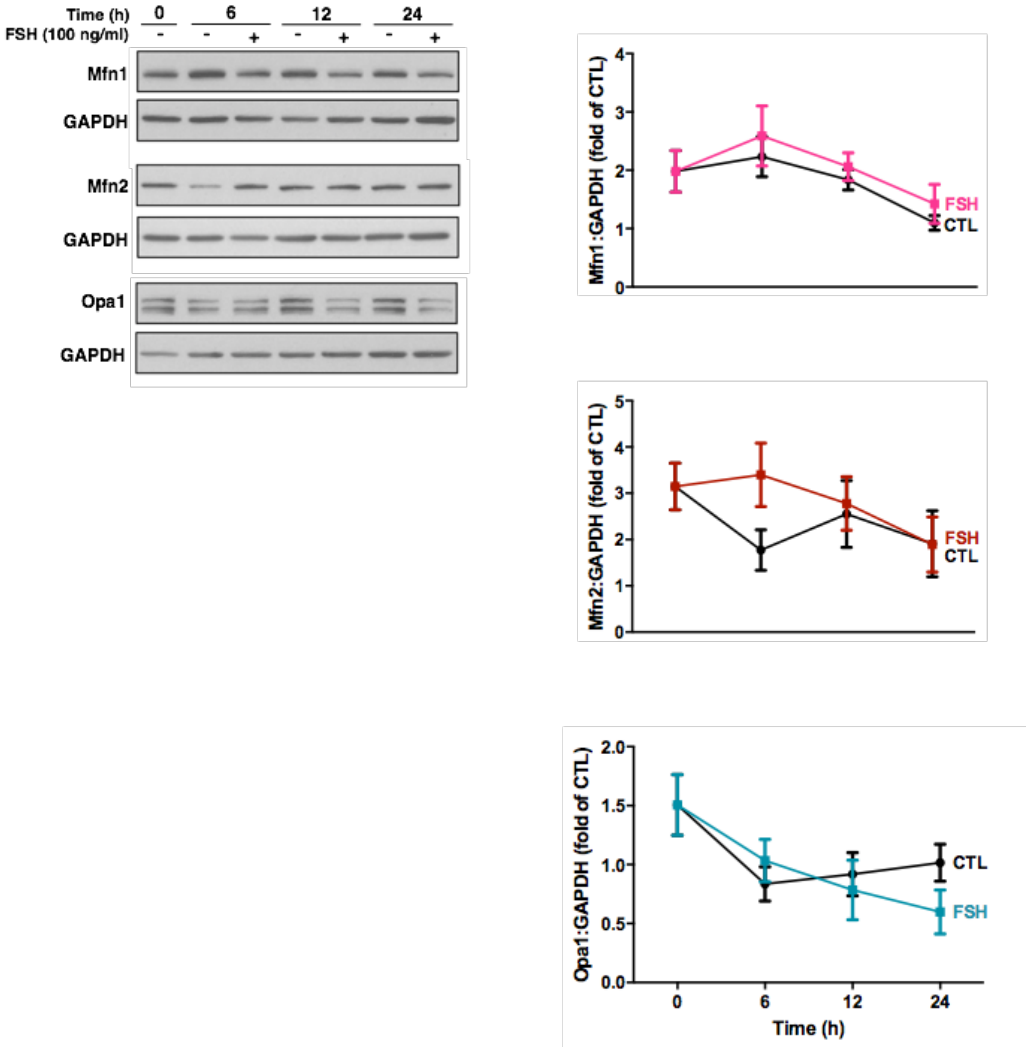

Figure 3.11: FSH had no effects on the contents of the mitochondrial fusion proteins Mfn1, Mfn2 and Opal

Granulosa cells were treated with FSH (100 ng/ml) for different culture durations (0, 6, 12 and 24 h), and protein contents of Mfn1, Mfn2 and Opal were determined by Western blot. Data are presented as mean ± SEM of five independent experiments, and analyzed by two-way ANOVA and Bonferroni *post hoc* test.

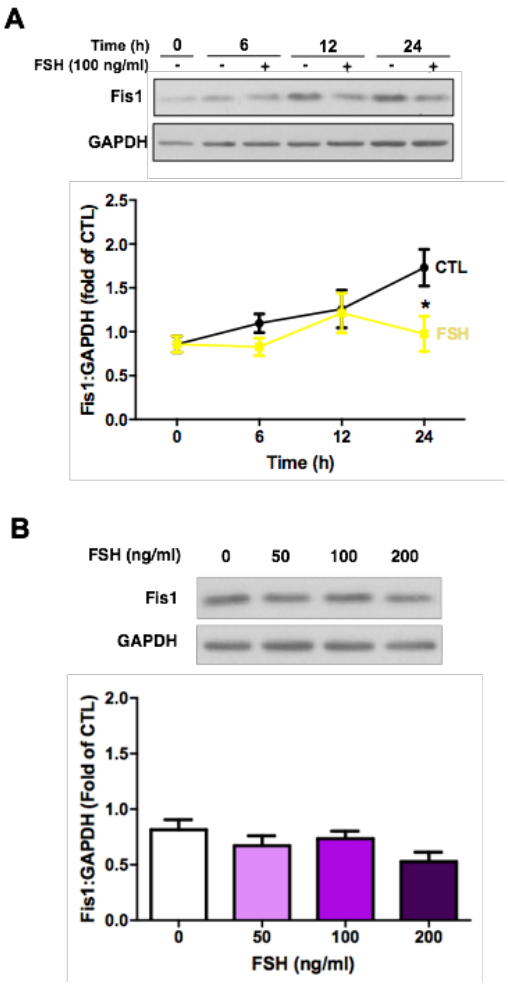

Figure 3.12: FSH had no effect on Fis1 protein content *in vitro*

(A) Granulosa cell were cultured for various durations (0, 6, 12 and 24 h ± FSH (100 ng/ml), and Fis1 content was assessed by Western blot. Data are presented as mean ± SEM of five independent experiments, and were analyzed by two-way ANOVA and Bonferroni *post hoc* test. *, $P < 0.05$ vs. CTL.

(B) Granulosa cell were cultured with various concentrations of FSH (0, 50, 100 and 200 ng/ml; 24 h), and Fis1 protein content was determined by Western blot. Data are presented as mean ± SEM of eight independent experiments, and analyzed by one-way ANOVA and Bonferroni *post hoc* test.

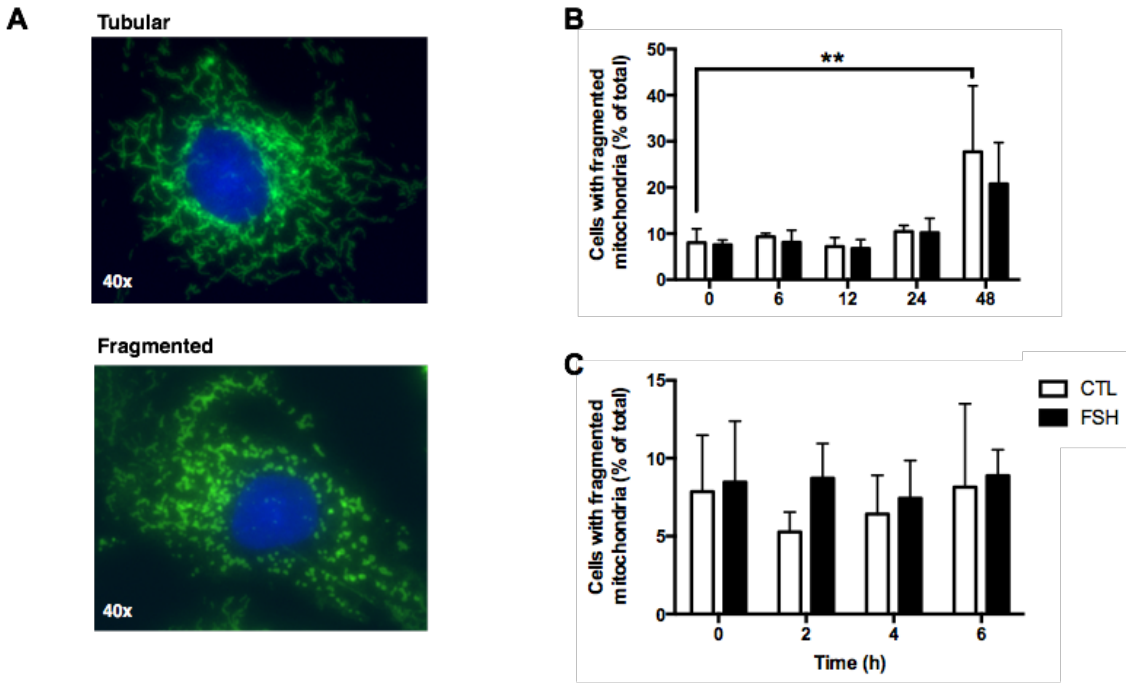

Figure 3.13: FSH did not suppress mitochondrial fragmentation in granulosa cells

(A) Representative examples of mitochondrial phenotypes (tubular and fragmented) in granulosa cells. Mitochondria were immuno-stained with TOM20 antibody and morphology was determined using immunofluorescence microscopy. Cells exhibiting ≥ 8 fragmented mitochondria (seen as shortened, circular bodies) were classified as "fragmented". At least 300 cells were assessed per treatment group in blinded studies.

(B) Granulosa cells were cultured with FSH (0, 100 ng/ml) for various duration (0, 6, 12, 24 and 48 h) in the absence of IBMX. Data are presented as mean ± SEM of four independent experiments, and analyzed by two-way ANOVA and Bonferroni *post hoc* test. **, $P < 0.01$ vs. CTL.

(C) Granulosa cells were pre-treated with IBMX (10 μM) for 90 min prior to and during FSH treatment (0, 100 ng/ml; 0, 2, 4, 6 h). Data are presented as mean ± SEM of five independent experiments, and analyzed by two-way ANOVA and Bonferroni *post hoc* test.

3.9 Chemerin had no significant effect on granulosa cell death, cAMP production or FSH-mediated Drp1 phosphorylation *in vitro*

Previous results have indicated that chemerin induces granulosa cell apoptosis in whole follicle cultures, though this was never examined in primary granulosa cells (Kim *et al*, 2013). In the present study, we assessed granulosa cell viability and apoptosis by the MTT assay and Hoechst nuclear staining, respectively. The addition of chemerin failed to alter cell viability (**Fig. 3.14A**; $P > 0.05$) or apoptosis (**Fig. 3.14B**; $P > 0.05$) as indicated by one-way ANOVA.

Despite these negative results, we completed our concurrent experiments on the possible effects of chemerin on FSH-mediated cAMP production and Drp1 phosphorylation as per the treatments described in **Fig. 3.8** and **Fig. 3.9**. Chemerin had no significant effect on basal and FSH-mediated cAMP accumulation (**Fig. 3.8**; three-way ANOVA: Chemerin, $P > 0.05$; FSH, $P < 0.001$; Time, $P < 0.001$; FSH × Chemerin, $P > 0.05$; Chemerin × Time, $P > 0.05$; FSH × Chemerin × Time, $P > 0.05$) or phospho-Drp1 Ser616 content (**Fig. 3.9A**; three-way ANOVA results are described in **Table 3.2**). Although chemerin had a statistically significant effect alone (ANOVA), it did not attenuate FSH-induced phospho-Drp1 Ser637 content (**Fig. 3.9B**; three-way ANOVA results are described in **Table 3.2**).

3.10 Chemerin did not alter the contents of autophagy markers in granulosa cells *in vitro*

Although chemerin-induced autophagy has been studied in skeletal muscle and human aorta endothelial cells (HAECs) (Xie *et al.*, 2015; Shen *et al.*, 2013), it has not yet

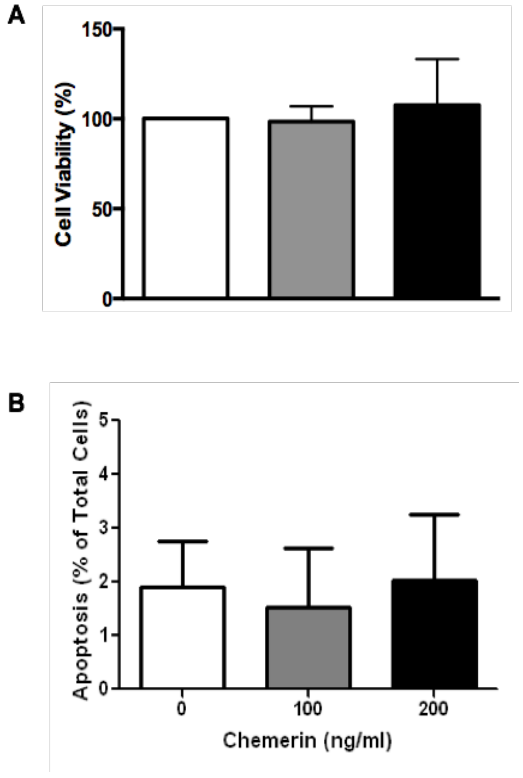

Figure 3.14: Chemerin did not reduce cell viability nor induce apoptosis in early antral granulosa cells *in vitro*

Granulosa cells were cultured with chemerin (0, 100, 200 ng/ml; 48 h) and cell viability **(A)** and apoptosis (**B**) were assessed by the MTT assay and Hoechst nuclear staining, respectively. Data are presented as mean ± SEM of three (**A**) or six (**B**) independent experiments, and analyzed by one-way ANOVA and Bonferroni *post hoc* test.

been reported in ovarian cells. To this end, the influence of chemerin on granulosa cell autophagy was examined in a time-course study (3, 6, 12 h), and contents of autophagy markers (LC3II:LC3I ratio or LC3I, LC3II and p62 contents) were assessed by Westernblot (**Fig. 3.15**). In both non-chloroquine and chloroquine-containing conditions, chemerin had no significant effect on LC3II:LC3I ratio or LC3I, LC3II and p62 contents in granulosa cells *in vitro* (two-way ANOVA: $P > 0.05$ for all endpoints studied**)**. In addition, neither FSH nor chemerin, alone or together, had any significant effects on these parameters in both non-chloroquine and chloroquine conditions (**Fig. 3.16**; two-way ANOVA: $P > 0.05$ for all endpoint studied**)**.

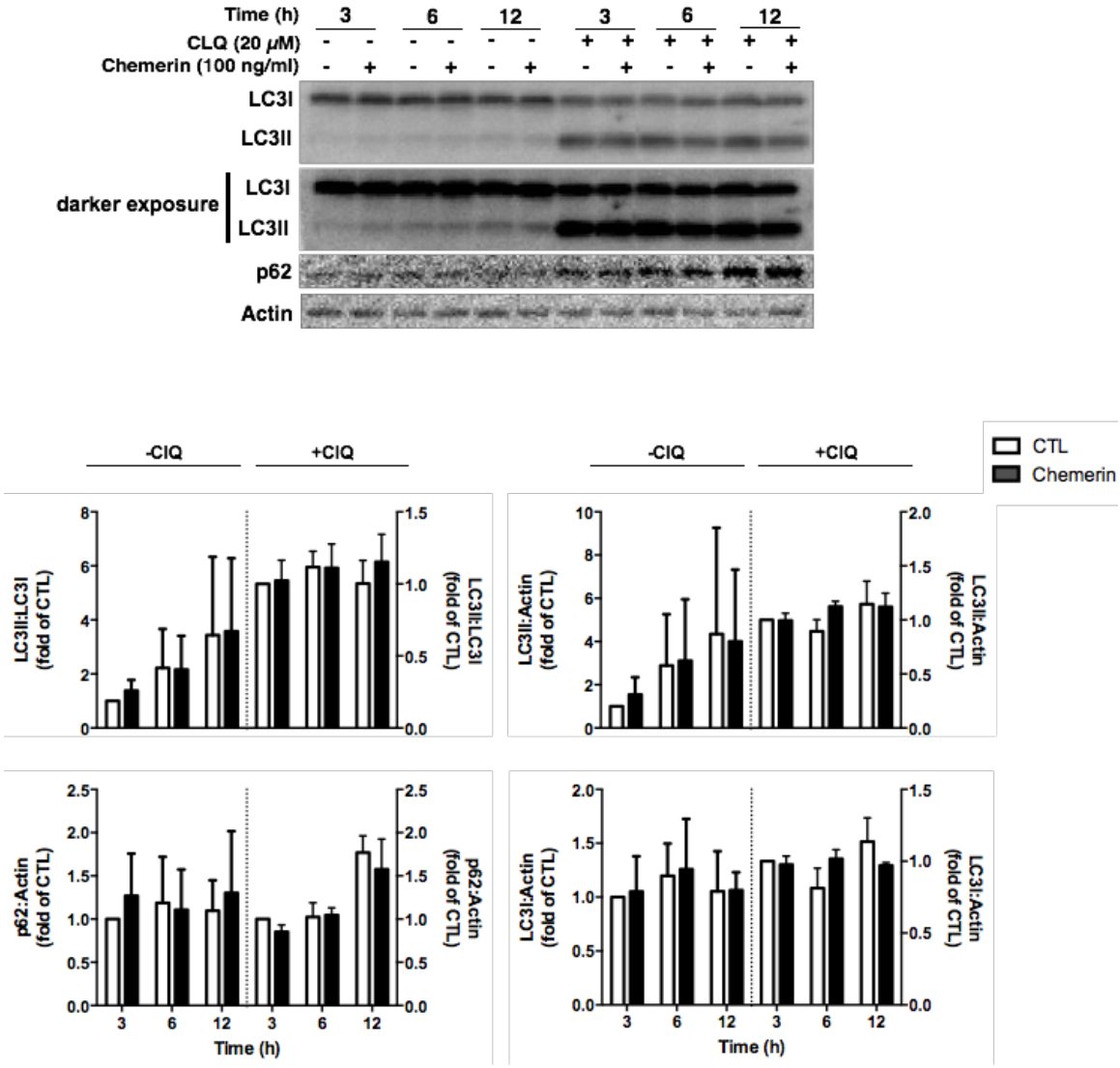

Figure 3.15: Chemerin did not affect granulosa cell autophagy markers LC3I/II or p62 *in vitro*

Granulosa cells were incubated with or without chemerin (100 ng/ml) for 3, 6 and 12 h in the presence and absence of chloroquine (CLQ; 20 μM). Protein contents of autophagy markers LC3I/II and p62 as well as LC3II:LC3I ratio were determined by Western blot analysis. Data are presented as mean ± SEM of three independent experiments, and analyzed by two-way ANOVA and Bonferroni *post hoc* test.

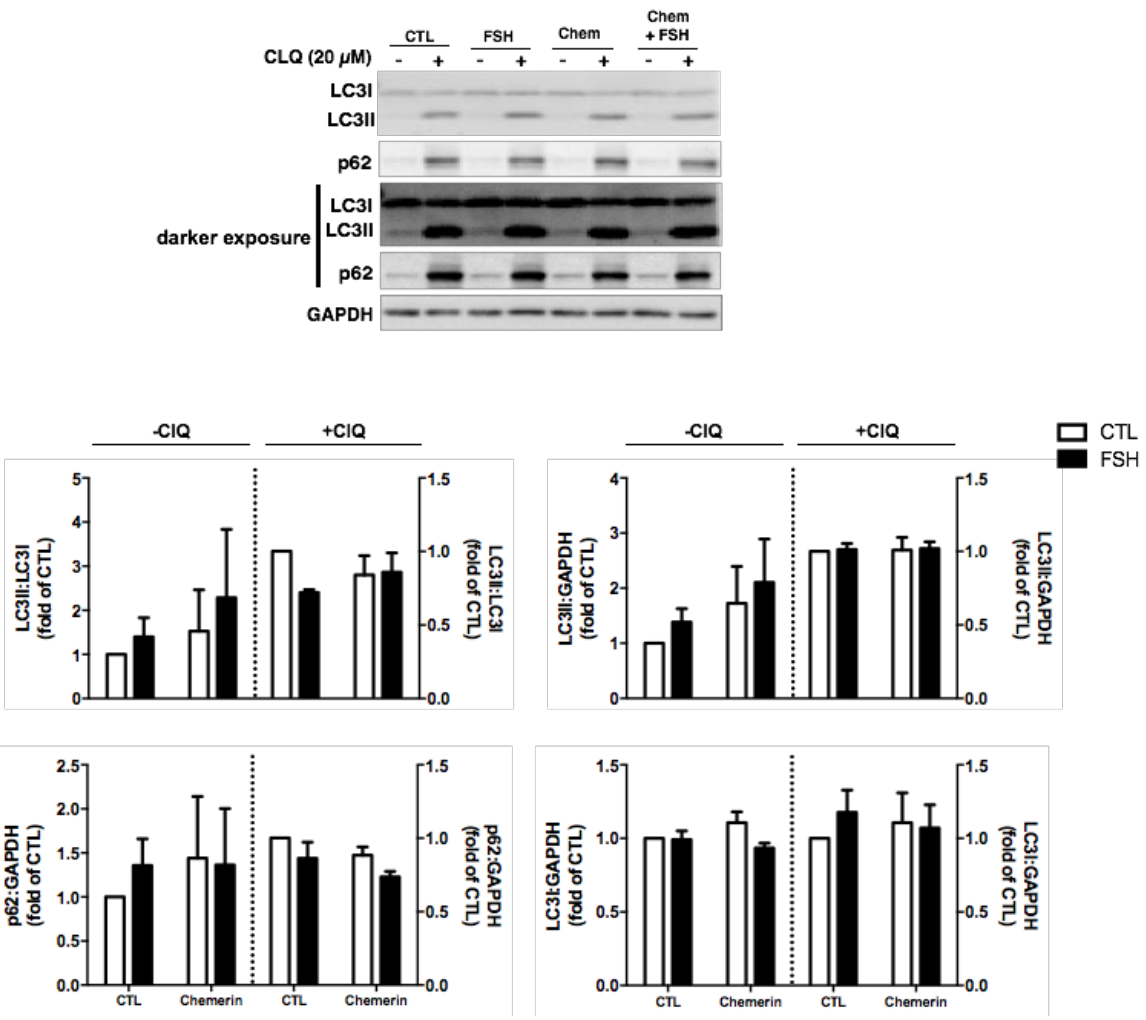

Figure 3.16: Co-treatment of early antral granulosa cells with FSH and Chemerin did not alter LC3I/II or p62 autophagy markers

Early antral granulosa cells were cultured with chemerin (0, 100 ng/ml) and FSH (0, 100 ng/ml), alone or together, for 12 h in conditions with and without chloroquine (CLQ; 20 μM). Protein contents of autophagy markers LC3I/II, p62 ad LC3II:LC3I ratio were determined via Western blot. Data are presented as mean ± SEM of three independent replicates, and analyzed by two-way ANOVA and Bonferroni *post hoc* test.

CHAPTER 4: DISCUSSION

4.1 Overview and contributions of research

Although the etiology of PCOS remains elusive due to its complex and heterogeneous nature, granulosa cell apoptosis has been suggested to play an important role in follicular growth arrest associated with the pathogenesis of PCOS (Ding *et al*., 2016; Mikaeili *et al*., 2016; Kim *et al*., 2013). However, important regulatory processes of granulosa cell death such as mitochondrial fission/fusion dynamics and autophagy had not been thoroughly studied in either a physiological or pathophysiological (e.g. PCOS) context, despite growing evidence of their dysregulation in various disease pathogeneses (Westermann, 2010; Archer *et al*., 2013; Shenouda *et al*., 2011; Nixon and Yang, 2012; Levine and Kroemer, 2008). Additionally, the role and mechanism of FSH as a granulosa cell survival factor in the regulation of mitochondrial dynamics had not been closely examined.

In the present study we demonstrated, for the first time, the dysregulation of mitochondrial fission and fusion dynamics and possibly autophagy in a DHT-induced rat model that recapitulates many phenotypes of PCOS. We also demonstrated the novel, modulatory role of gonadotropin (e.g. FSH) on granulosa cell mitochondrial dynamics in both physiological and pathophysiological conditions, as well as the mechanisms involved. These findings highlight the importance of mitochondrial dynamics in the granulosa cell, and how dysregulation in the regulatory processes of cell death may be involved in the pathogenesis of PCOS. They also improve our current understanding of the regulatory roles of FSH in granulosa cell fate decision and as a therapeutic for women with PCOS. Lastly, these findings provide the foundation for continued study on the

potential applications of mitochondrial dynamics proteins as diagnostic biomarkers or targets for treatment in PCOS.

4.2 One-month DHT-induced rats are a reliable model to study PCOS pathogenesis

A common approach in studying the cellular and molecular mechanisms of PCOS pathogenesis is the utilization of an androgenized rodent model (Padmanabhan and Veiga-Lopez, 2013; Walters, Allan, and Handelsman, 2012). Although no "perfect" animal model currently exists for human PCOS, the surgical implantation of a DHT-filled capsule for three months in rats has proven to be an effective model that mimics many phenotypes seen in PCOS (Mannerås *et al*., 2007; Wang *et* al., 2012; Kim *et al.*, 2013; Hossain *et al*., 2013). For the studies presented in this thesis, we used a DHT-induced rat model with a shorter (one month) duration of treatment and clarified its efficacy by examining ovarian size, ovarian structural features, and granulosa cell apoptosis. In accordance with both the three-month DHT-induced rat model and human PCOS, we found an induction of early antral granulosa cell apoptosis, follicular growth arrest, disrupted folliculogenesis and anovulation (Kim *et al.*, 2013; Ding *et al*., 2016; Mikaeili *et al*., 2016; Goodarzi *et al*., 2011). We also observed the accumulation of small atypical follicles and a reduction in ovarian length and width, features that are characteristic of the three-month DHT-induced model (Hossain *et al*., 2013l; Kim *et al.*, 2013). These results are consistent with unpublished findings from our lab, which include reproductive cycle irregularities and decreased ovarian length after one-month post-implantation of DHT (Nivet *et al*., unpublished). These initial studies confirmed that one-month DHT

induction provides a more convenient and less expensive model for studying PCOS, and that we may reliably use this model to perform novel studies pertaining to the pathogenesis of PCOS.

Of course, it is important to note that we can strengthen these conclusions by modifying our experiments to be less subjective in future studies. The differences in ovarian morphological features were described across treatment groups, though these were merely observations made in a single section of representative ovaries, which can be a confounding factor in the analysis. In fact, there is a discrepancy between the lack of late antral follicles in DHT rats seen by the H&E staining, and the relatively high number of late antral follicles in DHT rats as indicated in our TUNEL studies (which used 9 sections/rat). To improve upon these observations, an in-depth analysis on the proportion of ovarian structures in multiple rats across treatment groups can be determined (Kim *et al*., 2013). Our apoptosis studies using TUNEL can also be improved upon by using a more quantitative approach. Although the differences were very obvious between TUNEL negative follicles (which often showed zero positive signaling) and TUNEL positive follicles (which showed at least 50% positive signaling) during categorization, we can employ a more objective method of assessment by using a software program such as ImageJ to quantify the number of TUNEL positive cells as per total number of cells assessed within a selected area (i.e. granulosa cells as determined by DAPI staining) (Maidana *et al*., 2015).

4.3 Potential involvement of mitochondrial dynamics in PCOS pathogenesis

Dysregulated mitochondrial dynamics can lead to excessive mitochondrial fission and cell death in certain disease pathogeneses (Westermann, 2010; Archer *et al*., 2013; Shenouda *et al*., 2011). To assess the potential role of mitochondrial dynamics in PCOS, we evaluated morphological and molecular indicators of mitochondrial fission in our one-month DHT-induced rat model. Using TEM, we inferred the state of granulosa cell mitochondrial fission and fusion based on mitochondrial morphology and ultrastructural appearance. The reduction in rod-shaped mitochondria implied a disruption of the normal, baseline state of mitochondrial dynamics in our DHT-induced model, and suppression of connected mitochondria by DHT alluded to a reduction in mitochondrial fusion events (Wang *et al*., 2010; Picard *et al.*, 2013). Meanwhile, a higher proportion of circular and constricted morphologies suggested that excessive mitochondrial fission occurred in our DHT-induced model (Wang *et al*., 2010; Zhang *et al*., 2016; Picard *et al.*, 2013). Although circular morphology can also represent transverse sections of non-fragmented mitochondria, we assessed a high number of mitochondria per treatment group to ensure that any statistical differences were caused by DHT-induced fragmentation and not by random chance of transverse sections. Overall, these morphologic and ultrastructural findings suggest that a substantially high number of mitochondrial fission events occur in our DHT-induced rat model, which can lead to granulosa cell apoptosis, follicular growth arrest and anovulation as seen in PCOS.

To explore the biochemical mechanisms that regulate these changes in mitochondrial morphology, we assessed the contents of total and phosphorylated Drp1 by

Western blot in granulosa cells isolated from our *in vivo* model. The inclusion of phospho-Drp1 Ser637 and phospho-Drp1 Ser616 in our experiments is due to their respective roles in the suppression and stimulation of Drp1 activity (Merrill *et al*., 2011; Chang and Blackstone, 2010; Li, Mao and Xia, 2012). In support of our morphological findings, we saw a DHT-induced up-regulation of total Drp1 that likely compensates for the increased demand of mitochondrial fission in our chronic DHT-treated model. Meanwhile, the phosphorylated contents of Drp1 remained unaffected by DHT treatment. Initially, these results suggest that DHT regulates Drp1 exclusively through its modulation of total content and not by phosphorylation. However, another possibility is that DHT is capable of modulating Drp1 phosphorylation at a different time than our granulosa cell collection. Phosphorylation is a very rapid process that can occur within a few minutes, and it is possible we missed the optimal time-of-action in our chronic, DHT-induced model.

Regardless, our studies confirm that up-regulation of Drp1 can account for the increase in mitochondrial fission events seen in our DHT-induced rat model. It is possible that this excessive mitochondrial fission leads to granulosa cell apoptosis and follicular growth arrest in our DHT-induced rat model, consistent with its possible role in the pathogenesis of PCOS. These results are compatible with an androgen study performed in prostate cells, in which a synthetic androgen called methyl trienolone (R1881) increased both total and phospho-Ser616 Drp1 contents leading to enhanced mitochondrial fission and apoptosis (Choudhary *et al*., 2011).

4.4 Granulosa cell autophagy in PCOS

Autophagy acts first and foremost as a cell survival mechanism by recycling damaged intracellular contents and preventing cellular damage and death (He and Klionsky, 2009; Glick, Barth and Macleod, 2010; Mizushima, 2007). However, its dysregulation (associated with the induction of apoptosis and excessive mitochondrial fission via mitophagy) can lead to the pathogenesis of disease (Nixon and Yang, 2012; Levine and Kroemer, 2008; Kluge, Fetterman and Vita, 2013). As mitochondrial fission and apoptosis are implicated in our DHT-induced model, it is possible that granulosa cell autophagy is also involved in the pathogenesis of PCOS. In the present study, we assessed by Western blot the contents of autophagy markers LC3I, LC3II and p62 in granulosa cells isolated from our rat model, and found that DHT up-regulated LC3I and trended towards increased LC3II content. Due to the prolonged cellular stress caused by chronic DHT induction, the up-regulation of LC3 protein may compensate for the increased demand of autophagosome formation during autophagy (He and Klionsky, 2009; Mizushima, Yoshimori and Levine, 2010). However, we did not see LC3I to LC3II conversion to indicate autophagosome production or p62 degradation to indicate autophagic flux, which may lead to the conclusion that autophagic activity is not induced in our DHT-treated rat model (Mizushima and Yoshimori, 2007; Mizushima, Yoshimori and Levine, 2010).

A major challenge in assessing autophagy by molecular methods is its highly dynamic nature. Similar to the situation discussed earlier in our mitochondrial dynamics studies concerning Drp1 phosphorylation, it can be difficult to catch the appropriate time-of-action to see an effect when investigating a quick or dynamic process, and this is

especially true during *in vivo* studies with a chronic DHT-induced model (Mizushima and Yoshimori, 2007; Mizushima, Yoshimori and Levine, 2010). Additionally, the time-of-action for autophagy can greatly vary across biological and experimental replicates, and it may be difficult to obtain statistical significance from a combined mean. In terms of mitophagy, it may be helpful to use a mitochondrial turnover assay in granulosa cells, such as deuterium labelling and mass spectroscopy analysis of the half-lives of mitochondrial proteins, to determine an approximate time-of-effect (Kim *et al*., 2012). Regardless, it is generally recommended to perform multiple assays when studying autophagy to verify that the interpretations are correct (Mizushima, Yoshimori and Levine, 2010). The assessment of autophagosome number using TEM and/or immunofluorescence staining of autophagosomes and lysosomes in the whole ovary are future experiments that can confirm our findings in the current study. In the meantime, we can assume from our Western blot assessment that although autophagy was not active at the time of granulosa cell collection, LC3 protein is up-regulated in preparation for a higher number of autophagic events induced by DHT treatment, possibly reflecting the effects seen in PCOS.

4.5 Influence of gonadotropin on folliculogenesis and mitochondrial dynamics in PCOS

FSH, a key promoter of ovarian folliculogenesis, plays an important role in the growth of the dominant follicle due to its capabilities as a cell survival factor (Han, Xia and Tsang, 2013; Wang, Rippstein and Tsang, 2003; Kim *et al*., 1998; McGee and Hsueh, 2000). In the pathogenic state of PCOS, however, a dysregulated increase in the

ratio of LH:FSH can impair folliculogenesis and lead to antral follicle growth arrest and oligo-/anovulation (Ehrmann, 2005; Goodarzi *et al*., 2011). Controlled gonadotropin therapy with recombinant FSH and hCG, which can be combined with a GnRH agonist to suppress LH, is a treatment strategy to reactivate folliculogenesis and ovulation in women with PCOS (Vause and Cheung, 2010; Thessaloniki ESHRE/ASRM-sponsored PCOS consensus workshop group, 2008). However, the modulatory role of gonadotropin (e.g. FSH) in the context of our DHT-induced rat model is not completely understood.

To assess the influence of exogenous gonadotropin (eCG, with FSH- and LH-like activities) in an androgenized rat model for PCOS, we elaborated on previous findings from our lab that reported that eCG rescued ovarian length and reactivated ovulation in a three-month DHT-induced rat model (Popova *et al.*, 2002*;* Hossain *et al*., 2013). In our current studies using an androgenized rat model at a shorter duration of DHT induction (one month), we observed a restoration of ovarian length and width, as well as morphological changes in the whole ovary following eCG injection. In the absence of DHT, eCG failed to elicit a response on ovarian size. However, eCG had a significant effect that is dependent on the presence of DHT. This lack of response by eCG alone appear contrary to the observed increase in ovarian size in immature rats (21 days old), however they appear consistent with the lack of increased ovarian weight in more mature rats (111 days old) [Bell and Lunn, 1966; Hossain *et al*., 2013]. Whether age is a significant factor in the ovarian responsiveness to eCG remains to be determined.

The morphological changes induced by eCG in DHT-treated animals included an elimination of atypical follicles (the mechanism of which is yet unknown) and an increase in late antral and preovulatory follicles, which implies a reactivation of

folliculogenesis and follicular maturation. Although corpus lutea were not seen in our model to suggest the occurrence of ovulation, it is likely that the follicles were unresponsive to the LH-like capabilities of eCG and that the endogenous LH surge had not yet occurred (De la Lastra, Forcelledo and Serrano, 1972). Other than this discrepancy, our results appear to correspond with the findings seen in the three-month DHT-induced model, indicating that eCG can effectively modulate DHT-induced changes after only one month of implantation. Furthermore, we found that eCG attenuated DHT-induced granulosa cell apoptosis at the early antral follicular stage. Taken together, our findings suggest that gonadotropin is anti-apoptotic on granulosa cells in PCOS, leading to the reactivation of folliculogenesis and the restoration of ovarian size.

With our demonstration of DHT-induced mitochondrial fission and granulosa cell apoptosis in early antral follicles in the one-month DHT-treated rat model, we then investigated the potential modulatory effects of eCG on both morphological and molecular indicators of mitochondrial dynamics. Mitochondrial morphology studies demonstrated that eCG reduced the proportion of circular and constricted mitochondria in DHT-induced rats, and increased the proportion of rod-shaped (normal) mitochondria. The restoration of DHT-induced changes in mitochondrial dynamics offers new insight into the upstream modulatory role of eCG, leading to its attenuation of granulosa cell apoptosis and reactivation of folliculogenesis in PCOS. Despite these promising results, however, eCG did not have any effect on the total or phosphorylated contents of Drp1 in granulosa cells isolated from our *in vivo* model. These findings exclude the possible

involvement of other mitochondrial dynamics regulators (e.g. Fis1, Mfn1/2, Opa1), which will be the subject of future investigations.

As per our hypothesis regarding the regulation of Drp1 phosphorylation by FSH, we did not expect any eCG-induced effects on total Drp1 content. However, the inability of eCG to affect the phosphorylated contents of Drp1 *in vivo* was unanticipated. A likely reason for this may be due to the optimal time-of-action for phosphorylation, which can occur very rapidly and easily be missed. Phosphorylation studies are best examined in short-term, tightly controlled conditions *in vitro* rather than in a chronically treated model *in vivo*. The benefits of studying cell signaling *in vitro* is the ability to investigate mechanisms of a particular treatment without confounding factors in an appropriate time frame specific to the research objectives.

There are limitations to our assessment of eCG modulation on autophagy markers in our *in vivo* chronic DHT-rat model. With the exception of p62 up-regulation, eCG failed to significantly affect LC3I and LC3II contents or conversion of LC3I to LC3II (as determined by Western blot), the time-of-action for which might have been missed during our chronic treatment and assessment. It is possible that p62 up-regulation by eCG can indicate an inhibition of autophagic flux and a suppression of autophagy. However, assessment of autophagy by other experimental approaches and methodologies will determine if and how autophagy indeed plays role in the etiology of PCOS.

4.6 Role of FSH on mitochondrial fission protein Drp1

To better understand the molecular mechanisms of gonadotropic regulation on mitochondrial fission and fusion dynamics, we transitioned our focus to *in vitro* studies using primary granulosa cell cultures from early antral follicles of untreated rats. These

culture conditions eliminated any endogenous confounding factors that may influence the results, allowing us to determine FSH-specific changes in the granulosa cells. This includes a serum starvation period prior to treatment to ensure that any changes are due to the FSH alone, and not by interfering factors (e.g. growth factors) found in serum (Wang *et al.*, 2013; Twigg, Hardman and Baxter, 2000).

Due to the modulatory actions of eCG on mitochondrial morphology and granulosa cell apoptosis *in vivo*, we investigated whether recombinant FSH regulates proteins involved in mitochondrial fission (Drp1, Fis1) and fusion (Mfn1, Mfn2, Opa1) *in vitro*. Although FSH failed to up-regulate Mfn1, Mfn2 and Opa1 or suppress Fis1 and total Drp1 protein contents, it regulated Drp1 phosphorylation by decreasing phospho-Drp1 Ser616 (pro-fission site) content and increasing phospho-Drp1 Ser637 (anti-fission site) levels in both time-course and concentration-response studies. Although the precise signaling pathway involved had not been confirmed, it is likely that FSH-induced Drp1 phosphorylation is mediated by cAMP. Consistent with the literature, our current studies show substantial increase in cAMP production in response to FSH (Craig *et al*, 2007; Wayne *et al*., 2007; Gloaguen *et al*., 2011). Furthermore, cAMP-dependent protein kinase (PKA) phosphorylates Ser637 and is proposed to inhibit the Cdk1-CyclinB complex that phosphorylates Ser616 downstream (Merrill *et al*., 2011; Chang and Blackstone, 2010; Li, Mao and Xia, 2012). Nonetheless, these assumptions cannot be confirmed until PKA knockdown studies have been performed in future experiments.

As FSH modulated granulosa cell phospho-Drp1 content *in vitro*, it is possible that *in vivo* suppressive effects of eCG on DHT-induced mitochondrial fission could be due to its regulation of Drp1 phosphorylation, but its detection by Western blot was missed in

our chronic model. In an attempt to support our *in vivo* findings, we examined the effects of FSH on mitochondrial morphology *in vitro*. Contrary to our hypothesis, we did not see an FSH-induced suppression of fragmented mitochondria in both long- and short-term time-course studies. However, it is possible that an FSH-induced effect may be seen if we purposefully induce mitochondrial fragmentation first. As the time-of-action of FSH on Drp1 phosphorylation only occurs within a few minutes or hours, we would also expect to see FSH-mediated effects on mitochondrial morphology around this time period. However, the vast majority of mitochondria are healthy during this time and fragmentation is rarely observed, so the suppressive effects of FSH may not be significant if there is no mitochondrial fragmentation to suppress. By pre-treating our granulosa cells with a mitochondrial fission inducer (e.g. DHT) prior to FSH treatment, we may be able to see a significant effect of FSH-mediated suppression of fission. If the results of these future studies continue to prove that FSH has no effect on mitochondrial fission, then the study or the influence of FSH on other Drp1-mediated cell effects (e.g. peroxisome degradation and mitochondrial distribution) should be examined (Reddy *et al*; 2011; Koch *et al*., 2003).

The assessment of mitochondrial morphology by immunofluorescence staining *in vitro* is commonly used, though some drawbacks have been identified regarding the subjectivity of this approach (Kong *et al*., 2014; Ong *et al*., 2010; Farrand *et al*., 2013b). In particular, the variability of interpretation between observers can lead to different results. As recommended by Farrand *et al.*, we attempted to avoid this issue by employing an objective scoring system to determine mitochondrial fragmentation, with cut-off scores at different levels of stringency (Farrand *et al*., 2013b). In the present

study, as adopted by Farrand *et al*., we have chosen a cut-off score of at least eight mitochondria that exhibited a completely circular, punctate-like appearance to indicate a cell undergoing mitochondrial fragmentation (Farrand *et al*., 2013b). By setting a standard for our mitochondrial assessments, this can aid in the reproducibility of our results. Another possible issue is the aggregation of mitochondria in some cell types, which may mask the appearance of fragmented mitochondria due to their overlapping in a two-dimensional image. However, due to the spread out, epithelial-like nature of granulosa cells, mitochondria were well distributed and aggregation was hardly an issue (Roberts and Skinner, 1990).

4.7 Chemerin does not regulate cell death or mitochondrial dynamics in primary granulosa cells

The role of chemerin in the regulation of FSH- and forskolin-induced steroidogenesis has been described in primary granulosa cells (Wang *et al.*, 2012, Wang *et al*., 2013). As both FSH and forskolin are known to activate cAMP production, we determined if chemerin was also able to attenuate FSH-induced cAMP production and phospho-Drp1 contents, and whether this was associated with its induction of granulosa cell apoptosis seen in follicle cultures (Gloaguen *et al*., 2011; Hedin and Rosberg, 1983; Kim *et al*., 2013). Surprisingly, we failed to observe any notable changes in basal and FSH-stimulated granulosa cell cAMP production in the presence of chemerin, indicating that chemerin may not affect granulosa cell death via granulosa cell cAMP-mediated mitochondrial fission.

As the above results were being resolved, we performed concurrent studies of chemerin-induced granulosa cell apoptosis in primary granulosa cell cultures. We initially predicted that chemerin would induce granulosa cell apoptosis as this was already seen in the whole follicle cultures (Kim *et al*., 2013). However, chemerin did not affect cell viability or apoptotic cell death in the primary granulosa cell cultures. A recent study may support our findings, as granulosa cell apoptosis was unaffected in chemerin receptor CMKLR1-null mice (Tang *et al*., 2016). It is possible that the chemerin-induced granulosa cell death observed previously in follicle cultures involves the cross-talk of other cell types, as CMKLR1 is present on the oocyte, theca and granulosa cells in bovine and rat ovaries (Kim *et al*., 2013; Reverchon *et al*., 2014). Although the mechanisms involving chemerin signaling in the theca are unclear, chemerin is known to down-regulate GDF-9 expression in the oocyte. As GDF-9 is known to promote follicular growth by its suppression of granulosa cell apoptosis, it is possible that chemerin may attenuate GDF-9-induced granulosa cell survival (Orisaka *et al*., 2009; Kim *et al*., 2013).

Due to the inability of chemerin to suppress cell viability, it is unlikely that chemerin can induce autophagy to the point of autophagic cell death. Regardless, chemerin has been shown important role in various aspects of granulosa cell regulation, and this may include autophagy as evidenced by its effect on autophagy in other cell types (Kim *et al*., 2013; Wang *et al.*, 2012; Wang *et al*., 2013; Shen *et al.*, 2013, Xie *et al.*, 2015). We assessed the effects of chemerin on autophagy markers LC3I, LC3II and p62 via Western blot in serum-starved conditions with and without chloroquine in a time-course study and a co-treatment study with FSH, and noted that chemerin did not induce autophagy in either study.

As mentioned earlier, it is common to have a starvation period prior to treatment in granulosa cell studies as serum contains many growth factors that can mask the effects of treatment. However, the induction of cell starvation itself could stimulate autophagy as observed in our results (Mizushima and Yoshimori, 2007; Barth, Glick and Macleod, 2010). Although our treatments were compared to a control at all time points during our time course studies, it is possible that starvation-induced autophagy in the granulosa cells masked the effects of chemerin. Future studies of chemerin in both serum-free and serum-containing conditions will allow us to determine if chemerin can induce autophagy in non-starved conditions. Additionally, we should not completely rely on the results of just one method such as immunoblotting. Perhaps immunofluorescence studies involving LC3II, p62 and LAMP1 (which are indicators of autophagy during autophagosome formation and autolysosome fusion) would be helpful as a follow-up experiment to our Western blot studies (Mizushima and Yoshimori, 2007; Shuvayeva *et al*., 2014).

4.8 Conclusions and future directions

In this thesis, we investigated the involvement of mitochondrial dynamics in the pathogenesis of PCOS as well as its regulation by gonadotropin (e.g. FSH) using both *in vivo* and *in vitro* studies. We determined, for the first time, that up-regulation in Drp1 was associated with excessive mitochondrial fission and apoptosis in antral follicle stage granulosa cells in an androgenized rat model for PCOS. FSH, a known survival factor, increased phospho-Ser637 and decreased phospho-Ser616 contents of Drp1, and attenuated mitochondrial fission and apoptosis in the androgenized model for PCOS (**Fig. 4.1**). The adipokine chemerin was unable to induce apoptotic or autophagic cell death in

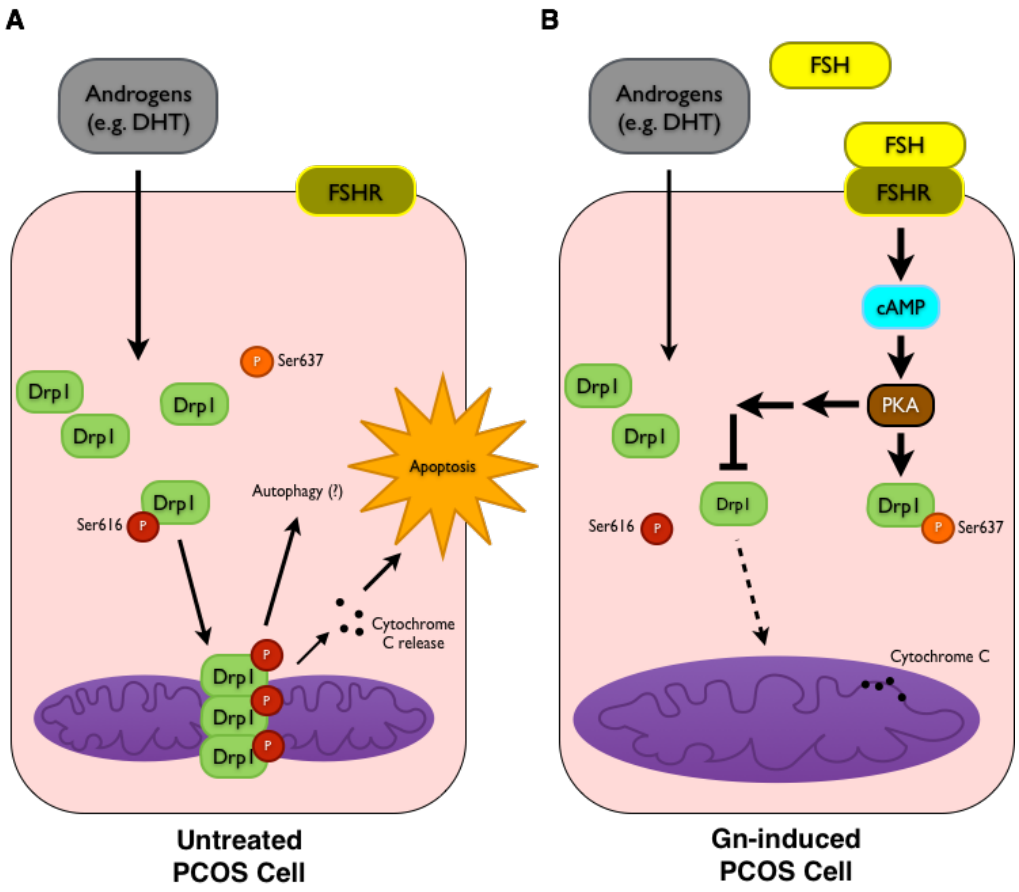

Figure 4.1: Hypothetical model of gonadotropin-induced modulation of mitochondrial dynamics in PCOS granulosa cells

(A) In PCOS, androgen excess results in the up-regulation of Drp1 leading to overabundant mitochondrial fission. This dysregulation in mitochondrial fission causes an increase in apoptosis and possibly autophagy, leading to early antral follicular growth arrest.

(B) During gonadotropin (Gn) stimulation, Drp1 is down-regulated by decreased phosphorylation of its stimulatory site (Ser616) and increased phosphorylation of its inhibitory site (Ser637). This contributes to its role as a suppressor of mitochondrial fission, apoptosis and follicular growth arrest in PCOS.

granulosa cells. These findings broaden our understanding of the mechanisms involved in PCOS pathogenesis and FSH-induced regulation, and provide novel insights into current treatment strategies of PCOS including gonadotropin therapy. They lay the groundwork for future studies involving the development of mitochondrial dynamics proteins as a biomarker for disease or as a target for future treatment strategies in PCOS.

As the one-month DHT-treated rat seems to be a likely candidate for future investigations concerning PCOS, our model could benefit from further studies that extend past the reproductive phenotypes of PCOS. Metabolic aspects of PCOS include its association to low-grade systemic inflammation involving leptin signaling, the binding of free steroid hormones and insulin resistance (Duleba *et al*., 2012; Houjeghani *et al*., 2012). Women with PCOS have elevated serum levels of the adipokines leptin and chemerin, which are correlated with the secretion of TNF-α and IL-6 inflammatory cytokines (Houjeghani *et al*. 2012, Ravishankar Ram *et al*., 2005; Berg *et al*., 2010). Elevated leptin can also cause leptin resistance in the hypothalamus, and a dysregulation of glucose homeostasis leading to insulin resistance as seen in PCOS (Koch *et al*., 2010). Insulin resistance is associated with high levels of active free steroids such as androgens, which is exacerbated by the suppression of sex hormone-binding globulin in women with PCOS (Houjeghani *et al*., 2012). One study has shown that hypothalamic leptin is unaffected in a three-month DHT-induced rat model, however the assessment of this inflammatory loop in relation to the metabolic aspects of PCOS still needs to be further elucidated (Nikolić *et al*., 2016).

Although our findings are promising with regards to the role of mitochondrial dynamics in PCOS, we need to extend our Drp1 studies and assess the possible

dysregulation of other mitochondrial dynamics proteins in our DHT-induced rat model. This would entail Western blot analysis of fission protein Fis1 and fusion proteins Mfn1, Mfn2 and Opa1. As Mfn1 and Mfn2 down-regulation has been associated with granulosa cell death and follicular degeneration in mice, the dysregulation of fusion proteins may also contribute to these phenotypes observed in our DHT-induced model (Gannon, Stämpfli, and Foster, 2013; Chen *et al.*, 2015). Regarding Drp1 and other mitochondrial dynamics proteins affected by DHT, an examination of the signaling pathways stimulated by DHT need to be elucidated by protein studies *in vitro.* Once the DHT-induced effects of mitochondrial fragmentation and mechanisms of these proteins have been confirmed *in vitro*, we can determine the outcomes of gene manipulation via ovary-specific conditional knockout of mitochondrial dynamics proteins (e.g. Drp1) in our DHT-induced model to demonstrate the importance of these proteins in PCOS pathogenesis (Huang *et al.*, 2013; Jeyasuria *et al.*, 2004; Pangas *et al.*, 2006). The use of a Drp1 inhibitor (e.g. mDivi-1, P110) provides promising results in animal studies as a potential treatment strategy for individuals with Huntington's disease (Guo *et al*., 2013; Manczak and Reddy, 2015; Reddy, 2014). By inhibiting Drp1 in our DHT-induced rat model, we can determine if PCOS pathogenesis is affected and if Drp1 is an ideal target for treatment. Additionally, its potential correlation with PCOS pathogenesis may allow Drp1 to be a candidate biomarker for the disease.

Although our studies in the DHT-induced rat model provide good insight into the pathogenesis of PCOS, it does not completely recapitulate all phenotypes of PCOS. Therefore, we must confirm if the biochemical and morphologic phenomenon observed in the current androgenized rat model could be validated in human PCOS patients. We

can determine if there is an associated dysregulation in mitochondrial dynamics proteins (e.g. Drp1) and mitochondrial morphology including fission and fusion in PCOS by assessing granulosa cells obtained from follicles from women with and without PCOS (Das *et al*., 2008; Mikaeili *et al*., 2016). To determine if gonadotropin therapy can modulate altered mitochondrial dynamics in PCOS, we can include "women with PCOS undergoing gonadotropin therapy" as a third treatment group to our studies.

CHAPTER 5: REFERENCES

Alam H, Maizels ET, Park Y, Ghaey S, Feiger ZJ, Chandel NS, Hunzicker-Dunn M. Follicle-stimulating hormone activation of hypoxia-inducible factor-1 by the phosphatidylinositol 3-kinase/AKT/Ras homolog enriched in brain (Rheb)/mammalian target of rapamycin (mTOR) pathway is necessary for induction of select protein markers of follicular differentiation. *J Biol Chem* 2004;279: 19431-19440.

Archer SL. Mitochondrial dynamics--mitochondrial fission and fusion in human diseases. *N Engl J Med* 2013;369: 2236-2251.

Azziz R, Carmina E, Dewailly D, Diamanti-Kandarakis E, Escobar-Morreale HF, Futterweit W, Janssen OE, Legro RS, Norman RJ, Taylor AE *et al.* Positions statement: criteria for defining polycystic ovary syndrome as a predominantly hyperandrogenic syndrome: an Androgen Excess Society guideline. *J Clin Endocrinol Metab* 2006;91: 4237-4245.

Azziz R, Carmina E, Dewailly D, Diamanti-Kandarakis E, Escobar-Morreale HF, Futterweit W, Janssen OE, Legro RS, Norman RJ, Taylor AE *et al.* The Androgen Excess and PCOS Society criteria for the polycystic ovary syndrome: the complete task force report. *Fertil Steril* 2009;91: 456-488.

Baerwald AR, Adams GP, Pierson RA. Ovarian antral folliculogenesis during the human menstrual cycle: a review. *Hum Reprod Update* 2012;18: 73-91.

Baker MJ, Lampe PA, Stojanovski D, Korwitz A, Anand R, Tatsuta T, Langer T. Stress-induced OMA1 activation and autocatalytic turnover regulate OPA1-dependent mitochondrial dynamics. *EMBO J* 2014;33: 578-593.

Barth S, Glick D, Macleod KF. Autophagy: assays and artifacts. *J Pathol* 2010;221: 117-124.

Bejarano E, Cuervo AM. Chaperone-mediated autophagy. *Proc Am Thorac Soc* 2010;7: 29-39.

Bell ET, Lunn SF. The effect of pregnant mare's serum gonadotropin and human chorionic gonadotropin on the wet and dry ovarian weight of immature rats. *J Reprod Fert* 1966;12: 453-459.

Berg V, Sveinbjörnsson B, Bendiksen S, Brox J, Meknas K, Figenschau Y. Human articular chondrocytes express ChemR23 and chemerin; ChemR23 promotes inflammatory signalling upon binding the ligand chemerin(21-157). *Arthritis Res Ther* 2010;12: R228.

Bjørkøy G, Lamark T, Brech A, Outzen H, Perander M, Overvatn A, Stenmark H, Johansen T. p62/SQSTM1 forms protein aggregates degraded by autophagy and has a protective effect on huntingtin-induced cell death. *J Cell Biol* 2005;171: 603-614.

Bozaoglu K, Bolton K, McMillan J, Zimmet P, Jowett J, Collier G, Walder K, Segal D. Chemerin is a novel adipokine associated with obesity and metabolic syndrome. *Endocrinology* 2007;148: 4687-4694.

Braschi E, Zunino R, McBride HM. MAPL is a new mitochondrial SUMO E3 ligase that regulates mitochondrial fission. *EMBO Rep* 2009;10: 748-754.

Breckenridge DG, Germain M, Mathai JP, Nguyen M, Shore GC. Regulation of apoptosis by endoplasmic reticulum pathways. *Oncogene* 2003;22: 8608-8618.

Bronstein J, Tawdekar S, Liu Y, Pawelczak M, David R, Shah B. Age of onset of polycystic ovarian syndrome in girls may be earlier than previously thought. *J Pediatr Adolesc Gynecol* 2011; 24: 15-20.

Catteau-Jonard S, Jamin SP, Leclerc A, Gonzalès J, Dewailly D, di Clemente N. Anti-Mullerian hormone, its receptor, FSH receptor, and androgen receptor genes are overexpressed by granulosa cells from stimulated follicles in women with polycystic ovary syndrome. *J Clin Endocrinol Metab* 2008;93: 4456-4461.

Cereghetti GM, Stangherlin A, Martins de Brito O, Chang CR, Blackstone C, Bernardi P, Scorrano L. Dephosphorylation by calcineurin regulates translocation of Drp1 to mitochondria. *Proc Natl Acad Sci U S A* 2008;105: 15803-15808.

Chang CR, Blackstone C. Dynamic regulation of mitochondrial fission through modification of the dynamin-related protein Drp1. *Ann N Y Acad Sci* 2010;1201: 34-39.

Chen W, Xu X, Wang L, Bai G, Xiang W. Low Expression of Mfn2 Is Associated with Mitochondrial Damage and Apoptosis of Ovarian Tissues in the Premature Ovarian Failure Model. *PLoS One* 2015;10: e0136421.

Chen X, Jia X, Qiao J, Guan Y, Kang J. Adipokines in reproductive function: a link between obesity and polycystic ovary syndrome. *J Mol Endocrinol* 2013;50: R21-37.

Cheung AP. Polycystic ovary syndrome: a contemporary view. *J Obstet Gynaecol Can* 2010;32: 423-425, 426-428.

Cho DH, Nakamura T, Fang J, Cieplak P, Godzik A, Gu Z, Lipton SA. S-nitrosylation of Drp1 mediates beta-amyloid-related mitochondrial fission and neuronal injury. *Science* 2009;324: 102-105.

Choi J, Jo M, Lee E, Choi D. Induction of apoptotic cell death via accumulation of autophagosomes in rat granulosa cells. *Fertil Steril* 2011;95: 1482-1486.

Choi J, Jo M, Lee E, Choi D. AKT is involved in granulosa cell autophagy regulation via mTOR signaling during rat follicular development and atresia. *Reproduction* 2014;147: 73-80.

Choi JY, Jo MW, Lee EY, Yoon BK, Choi DS. The role of autophagy in follicular development and atresia in rat granulosa cells. *Fertil Steril* 2010;93: 2532-2537.

Choudhary V, Kaddour-Djebbar I, Lakshmikanthan V, Ghazaly T, Thangjam GS, Sreekumar A, Lewis RW, Mills IG, Bollag WB, Kumar MV. Novel role of androgens in mitochondrial fission and apoptosis. *Mol Cancer Res* 2011;9: 1067-1077.

Cole LA. New discoveries on the biology and detection of human chorionic gonadotropin. *Reprod Biol Endocrinol* 2009;7: 8.

Craig J, Orisaka M, Wang H, Orisaka S, Thompson W, Zhu C, Kotsuji F, Tsang BK. Gonadotropin and intra-ovarian signals regulating follicle development and atresia: the delicate balance between life and death. *Front Biosci* 2007;12: 3628-3639.

Cribbs JT, Strack S. Reversible phosphorylation of Drp1 by cyclic AMP-dependent protein kinase and calcineurin regulates mitochondrial fission and cell death. *EMBO Rep* 2007;8: 939-944.

Das M, Djahanbakhch O, Hacihanefioglu B, Saridogan E, Ikram M, Ghali L, Raveendran M, Storey A. Granulosa cell survival and proliferation are altered in polycystic ovary syndrome. *J Clin Endocrinol Metab* 2008;93: 881-887.

De la Lastra M, Forcelledo ML, Serrano C. Influence of the hypophysis on pregnant mare's serum gonadotrophin-induced ovulation in immature rats. *J Reprod Fertil* 1972;31: 23-28.

Detmer SA, Chan DC. Functions and dysfunctions of mitochondrial dynamics. *Nat Rev Mol Cell Biol* 2007;8: 870-879.

Devine PJ, Payne CM, McCuskey MK, Hoyer PB. Ultrastructural evaluation of oocytes during atresia in rat ovarian follicles. *Biol Reprod* 2000;63: 1245-1252.

Ding L, Gao F, Zhang M, Yan W, Tang R, Zhang C, Chen ZJ. Higher PDCD4 expression is associated with obesity, insulin resistance, lipid metabolism disorders, and granulosa cell apoptosis in polycystic ovary syndrome. *Fertil Steril* 2016;105: 1330-1337.e1333.

Duerrschmidt N, Zabirnyk O, Nowicki M, Ricken A, Hmeidan FA, Blumenauer V, Borlak J, Spanel-Borowski K. Lectin-like oxidized low-density lipoprotein receptor-

1-mediated autophagy in human granulosa cells as an alternative of programmed cell death. *Endocrinology* 2006;147: 3851-3860.

Duleba AJ, Dokras A. Is PCOS an inflammatory process? *Fertil Steril* 2012;97: 7–12.

Dunaif A. Insulin resistance and the polycystic ovary syndrome: mechanism and implications for pathogenesis. *Endocr Rev* 1997;18: 774-800.

Dunmore BJ, Drake KM, Upton PD, Toshner MR, Aldred MA, Morrell NW. The lysosomal inhibitor, chloroquine, increases cell surface BMPR-II levels and restores BMP9 signalling in endothelial cells harbouring BMPR-II mutations. *Hum Mol Genet* 2013;22: 3667-3679.

Ehrmann DA. Polycystic ovary syndrome. *N Engl J Med* 2005;352: 1223-1236.

Escobar Sánchez ML, Echeverría Martínez OM, Vázquez-Nin GH. Immunohistochemical and ultrastructural visualization of different routes of oocyte elimination in adult rats. *Eur J Histochem* 2012;56: e17.

Farrand L, Byun S, Kim JY, Im-Aram A, Lee J, Lim S, Lee KW, Suh JY, Lee HJ, Tsang BK. Piceatannol enhances cisplatin sensitivity in ovarian cancer via modulation of p53, X-linked inhibitor of apoptosis protein (XIAP), and mitochondrial fission. *J Biol Chem* 2013;288: 23740-23750.

Farrand L, Kim JY, Im-Aram A, Suh JY, Lee HJ, Tsang BK. An improved quantitative approach for the assessment of mitochondrial fragmentation in chemoresistant ovarian cancer cells. *PLoS One* 2013;8: e74008.

Frank S, Gaume B, Bergmann-Leitner ES, Leitner WW, Robert EG, Catez F, Smith CL, Youle RJ. The role of dynamin-related protein 1, a mediator of mitochondrial fission, in apoptosis. *Dev Cell* 2001;1: 515-525.

Franks S. Polycystic ovary syndrome. *N Engl J Med* 1995;333: 853-861.

Franks S, Stark J, Hardy K. Follicle dynamics and anovulation in polycystic ovary syndrome. *Hum Reprod Update* 2008;14: 367-378.

Friedman JR, Nunnari J. Mitochondrial form and function. *Nature* 2014;505: 335-343.

Fujita N, Itoh T, Omori H, Fukuda M, Noda T, Yoshimori T. The Atg16L complex specifies the site of LC3 lipidation for membrane biogenesis in autophagy. *Mol Biol Cell* 2008;19: 2092-2100.

Furlong HC, Stämpfli MR, Gannon AM, Foster WG. Cigarette smoke exposure triggers the autophagic cascade via activation of the AMPK pathway in mice. *Biol Reprod* 2015;93: 93.

Gallego MJ, Porayette P, Kaltcheva MM, Bowen RL, Meethal SV, Atwood CS. The pregnancy hormones human chorionic gonadotropin and progesterone induce human embryonic stem cell proliferation and differentiation into neuroectodermal rosettes. *Stem Cell Res Ther* 2010;1: 28.

Gannon AM, Stämpfli MR, Foster WG. Cigarette smoke exposure leads to follicle loss via an alternative ovarian cell death pathway in a mouse model. *Toxicol Sci* 2012;125: 274-284.

Gannon AM, Stämpfli MR, Foster WG. Cigarette smoke exposure elicits increased autophagy and dysregulation of mitochondrial dynamics in murine granulosa cells. *Biol Reprod* 2013;88: 63.

Gao L, Cao JT, Liang Y, Zhao YC, Lin XH, Li XC, Tan YJ, Li JY, Zhou CL, Xu HY *et al.* Calcitriol attenuates cardiac remodeling and dysfunction in a murine model of polycystic ovary syndrome. *Endocrine* 2016;52: 363-373.

Gasser T. Molecular pathogenesis of Parkinson disease: insights from genetic studies. *Expert Rev Mol Med* 2009;11: e22.

Glick D, Barth S, Macleod KF. Autophagy: cellular and molecular mechanisms. *J Pathol* 2010;221: 3-12.

Gloaguen P, Crépieux P, Heitzler D, Poupon A, Reiter E. Mapping the follicle-stimulating hormone-induced signaling networks. *Front Endocrinol (Lausanne)* 2011;2: 45.

Goodarzi MO, Dumesic DA, Chazenbalk G, Azziz R. Polycystic ovary syndrome: etiology, pathogenesis and diagnosis. *Nat Rev Endocrinol* 2011;7: 219-231.

Goralski KB, McCarthy TC, Hanniman EA, Zabel BA, Butcher EC, Parlee SD, Muruganandan S, Sinal CJ. Chemerin, a novel adipokine that regulates adipogenesis and adipocyte metabolism. *J Biol Chem* 2007;282: 28175-28188.

Guo X, Disatnik MH, Monbureau M, Shamloo M, Mochly-Rosen D, Qi X. Inhibition of mitochondrial fragmentation diminishes Huntington's disease-associated neurodegeneration. *J Clin Invest* 2013;123: 5371-5388.

Han XJ, Lu YF, Li SA, Kaitsuka T, Sato Y, Tomizawa K, Nairn AC, Takei K, Matsui H, Matsushita M. CaM kinase I alpha-induced phosphorylation of Drp1 regulates mitochondrial morphology. *J Cell Biol* 2008;182: 573-585.

Han Y, Xia G, Tsang BK. Regulation of cyclin D2 expression and degradation by follicle-stimulating hormone during rat granulosa cell proliferation in vitro. *Biol Reprod* 2013;88: 57.

He C, Klionsky DJ. Regulation mechanisms and signaling pathways of autophagy. *Annu Rev Genet* 2009;43: 67-93.

Hedin L, Rosberg S. Forskolin effects on the cAMP system and steroidogenesis in the immature rat ovary. *Mol Cell Endocrinol* 1983;33: 69-80.

Hillier SG, Whitelaw PF, Smyth CD. Follicular oestrogen synthesis: the 'two-cell, two-gonadotrophin' model revisited. *Mol Cell Endocrinol* 1994;100: 51-54.

Homburg R. Clomiphene citrate--end of an era? A mini-review. *Hum Reprod* 2005;20: 2043-2051.

Hossain MM, Cao M, Wang Q, Kim JY, Schellander K, Tesfaye D, Tsang BK. Altered expression of miRNAs in a dihydrotestosterone-induced rat PCOS model. *J Ovarian Res* 2013;6: 36.

Houjeghani S, Pourghassem Gargari B, Farzadi L. Serum leptin and ghrelin levels in women with polycystic ovary syndrome: correlation with anthropometric, metabolic, and endocrine parameters. *Int J Fertil Steril* 2012;6: 117-126.

Hsueh AJ, Adashi EY, Jones PB, Welsh TH. Hormonal regulation of the differentiation of cultured ovarian granulosa cells. *Endocr Rev* 1984;5: 76-127.

Hsueh AJ, McGee EA, Hayashi M, Hsu SY. Hormonal regulation of early follicle development in the rat ovary. *Mol Cell Endocrinol* 2000;163: 95-100.

Huang L, Wang ZB, Jiang ZZ, Hu MW, Lin F, Zhang QH, Luo YB, Hou Y, Zhao Y, Fan HY *et al.* Specific disruption of Tsc1 in ovarian granulosa cells promotes ovulation and causes progressive accumulation of corpora lutea. *PLoS One* 2013;8: e54052.

Hussein MR. Apoptosis in the ovary: molecular mechanisms. *Hum Reprod Update* 2005;11: 162-177.

Hussein MR, Haemel AK, Wood GS. Apoptosis and melanoma: molecular mechanisms. *J Pathol* 2003;199: 275-288.

Jakimiuk AJ, Weitsman SR, Brzechffa PR, Magoffin DA. Aromatase mRNA expression in individual follicles from polycystic ovaries. *Mol Hum Reprod* 1998;4: 1-8.

Jakimiuk AJ, Weitsman SR, Navab A, Magoffin DA. Luteinizing hormone receptor, steroidogenesis acute regulatory protein, and steroidogenic enzyme messenger ribonucleic acids are overexpressed in thecal and granulosa cells from polycystic ovaries. *J Clin Endocrinol Metab* 2001;86: 1318-1323.

Jeyasuria P, Ikeda Y, Jamin SP, Zhao L, De Rooij DG, Themmen AP, Behringer RR, Parker KL. Cell-specific knockout of steroidogenic factor 1 reveals its essential roles in gonadal function. *Mol Endocrinol* 2004;18: 1610-1619.

Jiang MR, Li YC, Yang Y, Wu JR. c-Myc degradation induced by DNA damage results in apoptosis of CHO cells. *Oncogene* 2003;22: 3252-3259.

Jin HS, Sober S, Hong KW, Org E, Kim BY, Laan M, Oh B, Jeong SY. Age-dependent association of the polymorphisms in the mitochondria-shaping gene, OPA1, with blood pressure and hypertension in Korean population. *Am J Hypertens* 2011;24: 1127-1135.

Karbowski M, Neutzner A, Youle RJ. The mitochondrial E3 ubiquitin ligase MARCH5 is required for Drp1 dependent mitochondrial division. *J Cell Biol* 2007;178: 71-84.

Karbowski M, Norris KL, Cleland MM, Jeong SY, Youle RJ. Role of Bax and Bak in mitochondrial morphogenesis. *Nature* 2006;443: 658-662.

Karbowski M, Youle RJ. Dynamics of mitochondrial morphology in healthy cells and during apoptosis. *Cell Death Differ* 2003;10: 870-880.

Kim JM, Boone DL, Auyeung A, Tsang BK. Granulosa cell apoptosis induced at the penultimate stage of follicular development is associated with increased levels of Fas and Fas ligand in the rat ovary. *Biol Reprod* 1998;58: 1170-1176.

Kim TY, Wang D, Kim AK, Lau E, Lin AJ, Liem DA, Zhang J, Zong NC, Lam MPY, Ping P. Metabolic Labeling Reveals Proteome Dynamics of Mouse Mitochondria. *Mol Cell Proteomics* 2012;11: 1586-1594

Kim JY, Xue K, Cao M, Wang Q, Liu JY, Leader A, Han JY, Tsang BK. Chemerin suppresses ovarian follicular development and its potential involvement in follicular arrest in rats treated chronically with dihydrotestosterone. *Endocrinology* 2013;154: 2912-2923.

Kluge MA, Fetterman JL, Vita JA. Mitochondria and endothelial function. *Circ Res* 2013;112: 1171-1188.

Koch A, Thiemann M, Grabenbauer M, Yoon Y, McNiven MA, Schrader M. Dynamin-like protein 1 is involved in peroxisomal fission. *J Biol Chem* 2003;278: 8597-8605.

Koch C, Augustine RA, Steger J, Ganjam GK, Benzler J, Pracht C, Lowe C, Schwartz MW, Shepherd PR, Anderson GM, Grattan DR, Tups A. Leptin rapidly improves glucose homeostasis in obese mice by increasing hypothalamic insulin sensitivity. *J Neurosci* 2010;30: 16180–16187.

Kong B, Wang Q, Fung E, Xue K, Tsang BK. p53 is required for cisplatin-induced processing of the mitochondrial fusion protein L-Opa1 that is mediated by the mitochondrial metallopeptidase Oma1 in gynecologic cancers. *J Biol Chem* 2014;289: 27134-27145.

Lee J, Giordano S, Zhang J. Autophagy, mitochondria and oxidative stress: cross-talk and redox signalling. *Biochem J* 2012;441: 523-540.

Lee JH, Yu WH, Kumar A, Lee S, Mohan PS, Peterhoff CM, Wolfe DM, Martinez-Vicente M, Massey AC, Sovak G *et al.* Lysosomal proteolysis and autophagy require

presenilin 1 and are disrupted by Alzheimer-related PS1 mutations. *Cell* 2010;141: 1146-1158.

Lee YJ, Jeong SY, Karbowski M, Smith CL, Youle RJ. Roles of the mammalian mitochondrial fission and fusion mediators Fis1, Drp1, and Opa1 in apoptosis. *Mol Biol Cell* 2004;15: 5001-5011.

Levine B, Kroemer G. Autophagy in the pathogenesis of disease. *Cell* 2008;132: 27-42.

Li J, Mao G, Xia G. FSH modulates PKAI and GPR3 activities in mouse oocyte of COC in a gap junctional communication (GJC)-dependent manner to initiate meiotic resumption. *PLoS One* 2012;7: e37835.

Lin P, Rui R. Effects of follicular size and FSH on granulosa cell apoptosis and atresia in porcine antral follicles. *Mol Reprod Dev* 2010;77: 670-678.

Lin P, Yang Y, Li X, Chen F, Cui C, Hu L, Li Q, Liu W, Jin Y. Endoplasmic reticulum stress is involved in granulosa cell apoptosis during follicular atresia in goat ovaries. *Mol Reprod Dev* 2012;79: 423-432.

Liu YX, Hsueh AJ. Synergism between granulosa and theca-interstitial cells in estrogen biosynthesis by gonadotropin-treated rat ovaries: studies on the two-cell, two-gonadotropin hypothesis using steroid antisera. *Biol Reprod* 1986;35: 27-36.

Losón OC, Song Z, Chen H, Chan DC. Fis1, Mff, MiD49, and MiD51 mediate Drp1 recruitment in mitochondrial fission. *Mol Biol Cell* 2013;24: 659-667.

Maidana DE, Tsoka P, Tian B, Dib B, Matsumoto H, Kataoka K, Lin H, Miller JW, Vavvas DG. A Novel ImageJ Macro for Automated Cell Death Quantitation in the Retina. *Invest Ophthalmol Vis Sci* 2015;56: 6701-6708.

Maiuri MC, Zalckvar E, Kimchi A, Kroemer G. Self-eating and self-killing: crosstalk between autophagy and apoptosis. *Nat Rev Mol Cell Biol* 2007;8: 741-752.

Mammucari C, Schiaffino S, Sandri M. Downstream of Akt: FoxO3 and mTOR in the regulation of autophagy in skeletal muscle. *Autophagy* 2008;4: 524-526.

Manczak M, Reddy PH. Mitochondrial division inhibitor 1 protects against mutant huntingtin-induced abnormal mitochondrial dynamics and neuronal damage in Huntington's disease. *Hum Mol Genet* 2015;24: 7308-7325.

Mannerås L, Cajander S, Holmäng A, Seleskovic Z, Lystig T, Lönn M, Stener-Victorin E. A new rat model exhibiting both ovarian and metabolic characteristics of polycystic ovary syndrome. *Endocrinology* 2007;148: 3781-3791.

Marsboom G, Toth PT, Ryan JJ, Hong Z, Wu X, Fang YH, Thenappan T, Piao L, Zhang HJ, Pogoriler J *et al.* Dynamin-related protein 1-mediated mitochondrial mitotic

fission permits hyperproliferation of vascular smooth muscle cells and offers a novel therapeutic target in pulmonary hypertension. *Circ Res* 2012;110: 1484-1497.

Martinez-Lopez N, Singh R. ATGs: Scaffolds for MAPK/ERK signaling. *Autophagy* 2014;10: 535-537.

Mason HD, Willis DS, Beard RW, Winston RM, Margara R, Franks S. Estradiol production by granulosa cells of normal and polycystic ovaries: relationship to menstrual cycle history and concentrations of gonadotropins and sex steroids in follicular fluid. *J Clin Endocrinol Metab* 1994;79: 1355-1360.

Massey DC, Parkes M. Genome-wide association scanning highlights two autophagy genes, ATG16L1 and IRGM, as being significantly associated with Crohn's disease. *Autophagy* 2007;3: 649-651.

McBride HM, Neuspiel M, Wasiak S. Mitochondria: more than just a powerhouse. *Curr Biol* 2006;16: R551-560.

McGee EA, Hsueh AJ. Initial and cyclic recruitment of ovarian follicles. *Endocr Rev* 2000;21: 200-214.

Merrill RA, Dagda RK, Dickey AS, Cribbs JT, Green SH, Usachev YM, Strack S. Mechanism of neuroprotective mitochondrial remodeling by PKA/AKAP1. *PLoS Biol* 2011;9: e1000612.

Mikaeili S, Rashidi BH, Safa M, Najafi A, Sobhani A, Asadi E, Abbasi M. Altered FoxO3 expression and apoptosis in granulosa cells of women with polycystic ovary syndrome. *Arch Gynecol Obstet* 2016;294: 185-192.

Mishra P, Chan DC. Mitochondrial dynamics and inheritance during cell division, development and disease. *Nat Rev Mol Cell Biol* 2014;15: 634-646.

Mitra K, Rikhy R, Lilly M, Lippincott-Schwartz J. DRP1-dependent mitochondrial fission initiates follicle cell differentiation during Drosophila oogenesis. *J Cell Biol* 2012;197: 487-497.

Mitra K, Wunder C, Roysam B, Lin G, Lippincott-Schwartz J. A hyperfused mitochondrial state achieved at G1-S regulates cyclin E buildup and entry into S phase. *Proc Natl Acad Sci U S A* 2009;106: 11960-11965.

Mizushima N. Autophagy: process and function. *Genes Dev* 2007;21: 2861-2873.

Mizushima N, Yoshimori T. How to interpret LC3 immunoblotting. *Autophagy* 2007;3: 542-545.

Mizushima N, Yoshimori T, Levine B. Methods in mammalian autophagy research. *Cell* 2010;140: 313-326.

Morimoto N, Nagai M, Ohta Y, Miyazaki K, Kurata T, Morimoto M, Murakami T, Takehisa Y, Ikeda Y, Kamiya T *et al.* Increased autophagy in transgenic mice with a G93A mutant SOD1 gene. *Brain Res* 2007;1167: 112-117.

Murri M, Luque-Ramírez M, Insenser M, Ojeda-Ojeda M, Escobar-Morreale HF. Circulating markers of oxidative stress and polycystic ovary syndrome (PCOS): a systematic review and meta-analysis. *Hum Reprod Update* 2013;19: 268-288.

Nicholls DG. Mitochondrial function and dysfunction in the cell: its relevance to aging and aging-related disease. *Int J Biochem Cell Biol* 2002;34: 1372-1381.

Nikolić M, Veličković N, Djordjevic A, Bursać B, Macut D, Božić Antić I, Bjekić Macut J, Matić G, Vojnović Milutinović D. 5α-dihydrotestosterone treatment induces metabolic changes associated with polycystic ovary syndrome without interfering with hypothalamic leptin and glucocorticoid signaling. *Arch Biol Sci* 2016;68(3): 473-481

Nixon RA, Yang DS. Autophagy and neuronal cell death in neurological disorders. *Cold Spring Harb Perspect Biol* 2012;4.

Nobukuni T, Joaquin M, Roccio M, Dann SG, Kim SY, Gulati P, Byfield MP, Backer JM, Natt F, Bos JL *et al.* Amino acids mediate mTOR/raptor signaling through activation of class 3 phosphatidylinositol 3OH-kinase. *Proc Natl Acad Sci U S A* 2005;102: 14238-14243.

Olichon A, Guillou E, Delettre C, Landes T, Arnauné-Pelloquin L, Emorine LJ, Mils V, Daloyau M, Hamel C, Amati-Bonneau P *et al.* Mitochondrial dynamics and disease, OPA1. *Biochim Biophys Acta* 2006;1763: 500-509.

Omran MY. Metformin and polycystic ovary syndrome. *Int J Health Sci (Qassim)* 2007;1: 75-80.

Ong SB, Subrayan S, Lim SY, Yellon DM, Davidson SM, Hausenloy DJ. Inhibiting mitochondrial fission protects the heart against ischemia/reperfusion injury. *Circulation* 2010;121: 2012-2022.

Orisaka M, Tajima K, Tsang BK, Kotsuji F. Oocyte-granulosa-theca cell interactions during preantral follicular development. *J Ovarian Res* 2009;2: 9.

Padmanabhan V, Veiga-Lopez A. Animal models of the polycystic ovary syndrome phenotype. *Steroids* 2013;78: 734-740.

Pangas SA, Li X, Robertson EJ, Matzuk MM. Premature luteinization and cumulus cell defects in ovarian-specific Smad4 knockout mice. *Mol Endocrinol* 2006;20: 1406-1422.

Pankiv S, Clausen TH, Lamark T, Brech A, Bruun JA, Outzen H, Øvervatn A, Bjørkøy G, Johansen T. p62/SQSTM1 binds directly to Atg8/LC3 to facilitate degradation of ubiquitinated protein aggregates by autophagy. *J Biol Chem* 2007;282: 24131-24145.

Picard M, Gentil BJ, McManus MJ, White K, St Louis K, Gartside SE, Wallace DC, Turnbull DM. Acute exercise remodels mitochondrial membrane interactions in mouse skeletal muscle. *J Appl Physiol (1985)* 2013;115: 1562-1571.

Pierce JG, Parsons TF. Glycoprotein hormones: structure and function. *Annu Rev Biochem* 1981;50: 465-495.

Popova E, Krivokharchenko A, Ganten D, Bader M. Comparison between PMSG- and FSH-induced superovulation for the generation of transgenic rats. *Mol Reprod Dev* 2002;63: 177-182.

Porter DA, Harman RM, Cowan RG, Quirk SM. Relationship of Fas ligand expression and atresia during bovine follicle development. *Reproduction* 2001;121: 561-566.

Ravishankar Ram M, Gokulakrishnan Sundararaman P, Mahadevan S, Malathi R. Cytokines and leptin correlation in patients with polycystic ovary syndrome: biochemical evaluation in south Indian population. *Reprod Med Biol* 2005;**4**: 247–254.

Reddy PH. Increased mitochondrial fission and neuronal dysfunction in Huntington's disease: implications for molecular inhibitors of excessive mitochondrial fission. *Drug Discov Today* 2014;19: 951-955.

Reddy PH, Reddy TP, Manczak M, Calkins MJ, Shirendeb U, Mao P. Dynamin-related protein 1 and mitochondrial fragmentation in neurodegenerative diseases. *Brain Res Rev* 2011;67: 103-118.

Reddy PH, Reddy TP, Manczak M, Calkins MJ, Shirendeb U, Mao P. Dynamin-related protein 1 and mitochondrial fragmentation in neurodegenerative diseases. *Brain Res Rev* 2011;67: 103-118.

Reverchon M, Bertoldo MJ, Ramé C, Froment P, Dupont J. CHEMERIN (RARRES2) decreases in vitro granulosa cell steroidogenesis and blocks oocyte meiotic progression in bovine species. *Biol Reprod* 2014;90: 102.

Richards JS, Pangas SA. The ovary: basic biology and clinical implications. *J Clin Invest* 2010;120: 963-972.

Rizzuto R, Pinton P, Ferrari D, Chami M, Szabadkai G, Magalhães PJ, Di Virgilio F, Pozzan T. Calcium and apoptosis: facts and hypotheses. *Oncogene* 2003;22: 8619-8627.

Roberts AJ, Skinner MK. Mesenchymal-epithelial cell interactions in the ovary: estrogen-induced theca cell steroidogenesis. *Mol Cell Endocrinol* 1990;72: R1-5.

Roh SG, Song SH, Choi KC, Katoh K, Wittamer V, Parmentier M, Sasaki S. Chemerin--a new adipokine that modulates adipogenesis via its own receptor. *Biochem Biophys Res Commun* 2007;362: 1013-1018.

Rotterdam ESHRE/ASRM- sponsored PCOS consensus workshop. Revised 2003 consensus on diagnostic criteria and long-term health risks related to polycystic ovary syndrome. *Fertil Steril* 2004;81: 19-25.

Ryan JJ, Marsboom G, Fang YH, Toth PT, Morrow E, Luo N, Piao L, Hong Z, Ericson K, Zhang HJ *et al.* PGC1α-mediated mitofusin-2 deficiency in female rats and humans with pulmonary arterial hypertension. *Am J Respir Crit Care Med* 2013;187: 865-878.

Sahani MH, Itakura E, Mizushima N. Expression of the autophagy substrate SQSTM1/p62 is restored during prolonged starvation depending on transcriptional upregulation and autophagy-derived amino acids. *Autophagy* 2014;10: 431-441.

Sahu R, Kaushik S, Clement CC, Cannizzo ES, Scharf B, Follenzi A, Potolicchio I, Nieves E, Cuervo AM, Santambrogio L. Microautophagy of cytosolic proteins by late endosomes. *Dev Cell* 2011;20: 131-139.

Santel A, Frank S. Shaping mitochondria: The complex posttranslational regulation of the mitochondrial fission protein DRP1. *IUBMB Life* 2008;60: 448-455.

Sasaki S. Autophagy in spinal cord motor neurons in sporadic amyotrophic lateral sclerosis. *J Neuropathol Exp Neurol* 2011;70: 349-359.

Saxena D, Escamilla-Hernandez R, Little-Ihrig L, Zeleznik AJ. Liver receptor homolog-1 and steroidogenic factor-1 have similar actions on rat granulosa cell steroidogenesis. *Endocrinology* 2007;148: 726-734.

Schube U, Nowicki M, Jogschies P, Blumenauer V, Bechmann I, Serke H. Resveratrol and desferoxamine protect human OxLDL-treated granulosa cell subtypes from degeneration. *J Clin Endocrinol Metab* 2014;99: 229-239.

Senft D, Ronai ZA. Regulators of mitochondrial dynamics in cancer. *Curr Opin Cell Biol* 2016;39: 43-52.

Sengupta P. The laboratory rat: Relating its age with human's. *Int J Prev Med* 2013;4: 624-30.

Shen W, Tian C, Chen H, Yang Y, Zhu D, Gao P, Liu J. Oxidative stress mediates chemerin-induced autophagy in endothelial cells. *Free Radic Biol Med* 2013;55: 73-82.

Shenouda SM, Widlansky ME, Chen K, Xu G, Holbrook M, Tabit CE, Hamburg NM, Frame AA, Caiano TL, Kluge MA *et al.* Altered mitochondrial dynamics contributes to endothelial dysfunction in diabetes mellitus. *Circulation* 2011;124: 444-453.

Shuvayeva G, Bobak Y, Igumentseva N, Titone R, Morani F, Stasyk O, Isidoro C. Single amino acid arginine deprivation triggers prosurvival autophagic response in ovarian carcinoma SKOV3. *Biomed Res Int* 2014;2014: 505041.

Simpson ER. Cholesterol side-chain cleavage, cytochrome P450, and the control of steroidogenesis. *Mol Cell Endocrinol* 1979;13: 213-227.

Song W, Chen J, Petrilli A, Liot G, Klinglmayr E, Zhou Y, Poquiz P, Tjong J, Pouladi MA, Hayden MR *et al.* Mutant huntingtin binds the mitochondrial fission GTPase dynamin-related protein-1 and increases its enzymatic activity. *Nat Med* 2011;17: 377-382.

Song Z, Chen H, Fiket M, Alexander C, Chan DC. OPA1 processing controls mitochondrial fusion and is regulated by mRNA splicing, membrane potential, and Yme1L. *J Cell Biol* 2007;178: 749-755.

Sprengel R, Braun T, Nikolics K, Segaloff DL, Seeburg PH. The testicular receptor for follicle stimulating hormone: structure and functional expression of cloned cDNA. *Mol Endocrinol* 1990;4: 525-530.

Takahashi M, Okimura Y, Iguchi G, Nishizawa H, Yamamoto M, Suda K, Kitazawa R, Fujimoto W, Takahashi K, Zolotaryov FN *et al.* Chemerin regulates β-cell function in mice. *Sci Rep* 2011;1: 123.

Tang M, Huang C, Wang YF, Ren PG, Chen L, Xiao TX, Wang BB, Pan YF, Tsang BK, Zabel BA *et al.* CMKLR1 deficiency maintains ovarian steroid production in mice treated chronically with dihydrotestosterone. *Sci Rep* 2016;6: 21328.

Tanner EA, McCall K. Mitochondrial regulation of cell death in the Drosophila ovary. *Autophagy* 2011;7: 793-794.

Thessaloniki ESHRE/ASRM-sponsored PCOS consensus workshop group. Consensus on infertility treatment related to polycystic ovary syndrome. *Hum Reprod* 2008;23: 462-477.

Thorburn A. Apoptosis and autophagy: regulatory connections between two supposedly different processes. *Apoptosis* 2008;13: 1-9.

Tsujimoto Y, Shimizu S. Another way to die: autophagic programmed cell death. *Cell Death Differ* 2005;12 Suppl 2: 1528-1534.

Twigg SM, Hardman KV, Baxter RC. A purified bovine serum albumin preparation contains an insulin-like growth factor (IGF) binding protein-3 fragment that forms ternary complexes selectively with IGF-II and the acid-labile subunit. *Growth Horm IGF Res* 2000;10: 215-223.

Udagawa O, Ishihara T, Maeda M, Matsunaga Y, Tsukamoto S, Kawano N, Miyado K, Shitara H, Yokota S, Nomura M *et al.* Mitochondrial fission factor Drp1 maintains

oocyte quality via dynamic rearrangement of multiple organelles. *Curr Biol* 2014;24: 2451-2458.

Vause TD, Cheung AP, Sierra S, Claman P, Graham J, Guillemin JA, Lapensée L, Stewart S, Steward S, Wong BC *et al.* Ovulation induction in polycystic ovary syndrome. *J Obstet Gynaecol Can* 2010;32: 495-502.

Victor VM, Rocha M, Bañuls C, Alvarez A, de Pablo C, Sanchez-Serrano M, Gomez M, Hernandez-Mijares A. Induction of oxidative stress and human leukocyte/endothelial cell interactions in polycystic ovary syndrome patients with insulin resistance. *J Clin Endocrinol Metab* 2011;96: 3115-3122.

Walters KA, Allan CM, Handelsman DJ. Rodent models for human polycystic ovary syndrome. *Biol Reprod* 2012;86: 149, 141-112.

Wang Q, Frolova AI, Purcell S, Adastra K, Schoeller E, Chi MM, Schedl T, Moley KH. Mitochondrial dysfunction and apoptosis in cumulus cells of type I diabetic mice. *PLoS One* 2010;5: e15901.

Wang Q, Kim JY, Xue K, Liu JY, Leader A, Tsang BK. Chemerin, a novel regulator of follicular steroidogenesis and its potential involvement in polycystic ovarian syndrome. *Endocrinology* 2012;153: 5600-5611.

Wang Q, Leader A, Tsang BK. Inhibitory roles of prohibitin and chemerin in FSH-induced rat granulosa cell steroidogenesis. *Endocrinology* 2013;154: 956-967.

Wang Y, Rippstein PU, Tsang BK. Role and gonadotrophic regulation of X-linked inhibitor of apoptosis protein expression during rat ovarian follicular development in vitro. *Biol Reprod* 2003;68: 610-619.

Wayne CM, Fan HY, Cheng X, Richards JS. Follicle-stimulating hormone induces multiple signaling cascades: evidence that activation of Rous sarcoma oncogene, RAS, and the epidermal growth factor receptor are critical for granulosa cell differentiation. *Mol Endocrinol* 2007;21: 1940-1957.

Welt CK, Taylor AE, Fox J, Messerlian GM, Adams JM, Schneyer AL. Follicular arrest in polycystic ovary syndrome is associated with deficient inhibin A and B biosynthesis. *J Clin Endocrinol Metab* 2005;90: 5582-5587.

Wen X, Li D, Tozer AJ, Docherty SM, Iles RK. Estradiol, progesterone, testosterone profiles in human follicular fluid and cultured granulosa cells from luteinized pre-ovulatory follicles. *Reprod Biol Endocrinol* 2010;8: 117.

Westermann B. Mitochondrial fusion and fission in cell life and death. *Nat Rev Mol Cell Biol* 2010;11: 872-884.

Wittamer V, Franssen JD, Vulcano M, Mirjolet JF, Le Poul E, Migeotte I, Brézillon S, Tyldesley R, Blanpain C, Detheux M *et al.* Specific recruitment of antigen-

presenting cells by chemerin, a novel processed ligand from human inflammatory fluids. *J Exp Med* 2003;198: 977-985.

Wong PM, Puente C, Ganley IG, Jiang X. The ULK1 complex: sensing nutrient signals for autophagy activation. *Autophagy* 2013;9: 124-137.

Xie Q, Deng Y, Huang C, Liu P, Yang Y, Shen W, Gao P. Chemerin-induced mitochondrial dysfunction in skeletal muscle. *J Cell Mol Med* 2015;19: 986-995.

Yaba A, Demir N. The mechanism of mTOR (mammalian target of rapamycin) in a mouse model of polycystic ovary syndrome (PCOS). *J Ovarian Res* 2012;5: 38.

Youle RJ, Karbowski M. Mitochondrial fission in apoptosis. *Nat Rev Mol Cell Biol* 2005;6: 657-663.

Yu T, Sheu SS, Robotham JL, Yoon Y. Mitochondrial fission mediates high glucose-induced cell death through elevated production of reactive oxygen species. *Cardiovasc Res* 2008;79: 341-351.

Zabel BA, Nakae S, Zúñiga L, Kim JY, Ohyama T, Alt C, Pan J, Suto H, Soler D, Allen SJ *et al.* Mast cell-expressed orphan receptor CCRL2 binds chemerin and is required for optimal induction of IgE-mediated passive cutaneous anaphylaxis. *J Exp Med* 2008;205: 2207-2220.

Zhan M, Brooks C, Liu F, Sun L, Dong Z. Mitochondrial dynamics: regulatory mechanisms and emerging role in renal pathophysiology. *Kidney Int* 2013;83: 568-581.

Zhang L, Trushin S, Christensen TA, Bachmeier BV, Gateno B, Schroeder A, Yao J, Itoh K, Sesaki H, Poon WW *et al.* Altered brain energetics induces mitochondrial fission arrest in Alzheimer's Disease. *Sci Rep* 2016;6: 18725.

Züchner S, Mersiyanova IV, Muglia M, Bissar-Tadmouri N, Rochelle J, Dadali EL, Zappia M, Nelis E, Patitucci A, Senderek J *et al.* Mutations in the mitochondrial GTPase mitofusin 2 cause Charcot-Marie-Tooth neuropathy type 2A. *Nat Genet* 2004;36: 449-451.